Composite
Materials and Structures Program

Rensselaer Polytechnic Institute
Troy, N.Y. 12180-3590

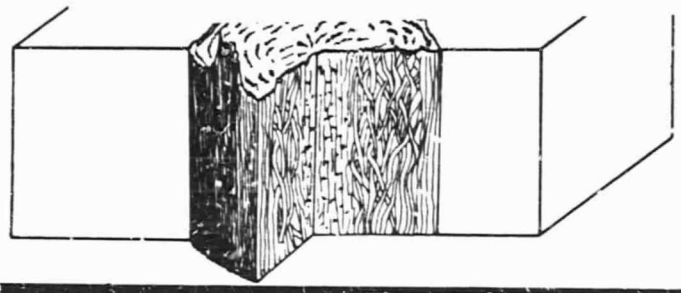

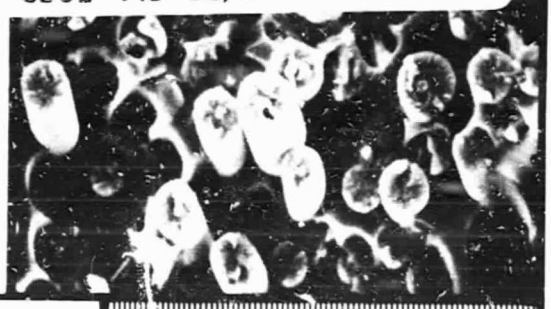

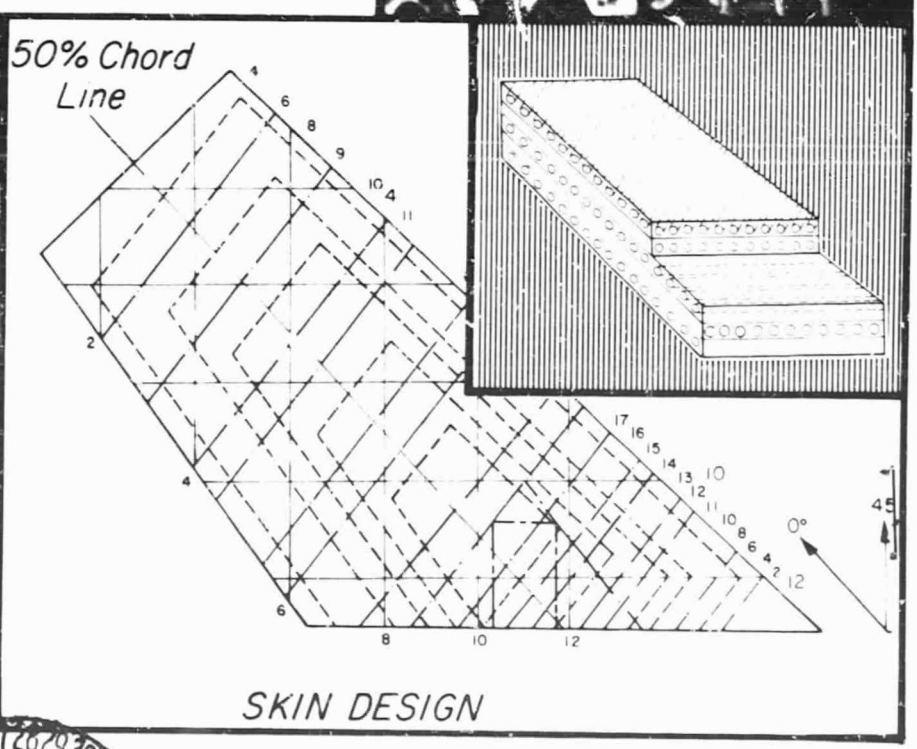

SKIN DESIGN

Sponsored by
NASA/AFOSR

Semi-Annual Progress Report
April 30, 1983 through September 30, 1983

COMPOSITE STRUCTURAL MATERIALS

Air Force Office of Scientific Research
and
National Aeronautics and Space Administration
Grant No. NGL 33-018-003

Co-Principal Investigators:

George S. Ansell
Dean, School of Engineering

Robert G. Loewy
Institute Professor

and

Stephen E. Wiberley
Professor of Chemistry

Rensselaer Polytechnic Institute
Troy, New York 12181

NASA Technical Officer
Michael A. Greenfield
Materials and Structures Division
NASA Headquarters

CONTENTS

	Page
LIST OF TABLES	v
LIST OF FIGURES	vi
PART I. INTRODUCTION	1
PART II. CONSTITUENT MATERIALS	7
II-A MECHANICAL PROPERTIES OF HIGH PERFORMANCE CARBON FIBERS (R. J. Diefendorf)	9
1. Introduction	9
2. Status	10
3. Progress During Report Period	12
4. Plans for Upcoming Period	26
5. References	27
6. Current Publications or Presentations by Professor Diefendorf on this Subject	29
PART III. COMPOSITE MATERIALS	31
III-A FATIGUE IN COMPOSITE MATERIALS (E. Krempl)	33
1. Introduction	33
2. Status	33
3. Progress During Report Period	33
4. Plans for Upcoming Period	34
5. Current Publications or Presentations by Professor Krempl on this Subject	34
III-B EXPERIMENTAL STUDIES OF MOISTURE AND TEMPERATURE EFFECTS ON THE MECHANICAL PROPERTIES OF GRAPHITE/EPOXY LAMINATES (S. S. Sternstein)	35
1. Introduction	35
2. Status	35
3. Progress During Report Period	35
4. Plans for Upcoming Period	48
5. Current Publications or Presentations by Professor Sternstein on this Subject	49

		Page
III-C	THEORY OF INHOMOGENEOUS SWELLING IN EPOXY RESIN (S. S. Sternstein)	51
1.	Introduction	51
2.	Status	51
3.	Progress During Report Period	52
4.	Plans for Upcoming Period	59
5.	Current Publications or Presentations by Professor Sternstein on this Subject	59
III-D	NUMERICAL INVESTIGATION OF THE MICROMECHANICS OF COMPOSITE FRACTURE (M. S. Shephard)	61
1.	Introduction	61
2.	Status	61
3.	Progress During Report Period	62
a.	The Fracture Criteria for Crack Propagation	62
b.	Debonding at Bimaterial Interface	71
c.	Automatic Meshing in the Presence of Crack Growth	73
4.	Plans for Upcoming Period	76
5.	References	76
6.	Current Publications or Presentations by Professor Shephard on this Subject	77
III-E	FREE-EDGE FAILURES OF COMPOSITE LAMINATES (T. L. Sham)	79
1.	Introduction	79
2.	Status	80
3.	Progress During Report Period	81
4.	Plans for Upcoming Period	82
5.	References	82
III-F	ANALYSIS OF UNBALANCED LAMINATES (E. G. Brunelle)	85
1.	Introduction	85
2.	Status	85
3.	Progress During Report Period	86
4.	Plans for Upcoming Period	89

Page

PART IV. GENERIC STRUCTURAL ELEMENTS 91

IV-A COMPACT LUG DESIGN (D. B. Goetschel) 93

1. Introduction 93

2. Status 94

3. Progress During Report Period 95

a. Literature Survey 95

b. Failure Theory 96

i) The minimum-gradient fiber strain criterion 107

c. Conclusions 110

4. Plans for Upcoming Period 112

5. References 112

IV-B QUANTIFICATION OF SAINT-VENANT'S PRINCIPLE FOR A GENERAL PRISMATIC MEMBER (D. B. Goetschel) .. 119

1. Introduction 119

2. Status 123

3. Progress During Report Period 128

4. Plans for Upcoming Period 135

5. References 136

PART V. PROCESSING SCIENCE AND TECHNOLOGY 139

V-A VARIATION OF RESIN PROPERTIES THROUGH THE THICKNESS OF CURED SAMPLES (B. Wunderlich) 141

1. Introduction 141

2. Status 141

3. Progress During Report Period 144

a. Approach 144

b. Results 144

4. Plans for Upcoming Period 147

5. References 147

V-B INITIAL SAILPLANE PROJECT: THE RP-1 (F. P. Bundy, R. J. Diefendorf, H. Hagerup, H. Scarton) 149

1. Status 149

2. Progress During Report Period 150

Page

V-C SECOND SAILPLANE PROJECT: THE RP-2 (F. P. Bundy, R. J. Diefendorf, H. Hagerup, H. Scarton) 154

1. Status 154

2. Progress During Report Period 155

3. Plans for Upcoming Period 172

4. Current Publications or Presentations by Professor Scarton on this Subject 173

PART VI. TECHNICAL INTERCHANGE 175

PART VII. PERSONNEL, AUTHOR INDEX 189

PERSONNEL 191

AUTHOR INDEX 195

LIST OF TABLES

Number		Page
II-1	FIBER DIAMETER M ASUREMENT TECHNIQUES AND RESULTS	17
II-2	ROTATING TECHNIQUE FOR IRREGULAR AREA MEASUREMENT	17
III-D-	COMPARISON OF RESULTS OBTAINED USING S AND T FRACTURE CRITERIA	70
IV-A-1	COMPARISON OF PREDICTED AND EXPERIMENTAL RESULTS	111
IV-B-1	DECAY RATES (γ) FOR A 2-UNIT THICK ISOTROPIC PLATE	129
IV-B-2	DECAY RATES (γ) FOR A 2-UNIT THICK HOMOGENEOUS ANISOTROPIC PLATE	130
IV-B-3	FIRST FOUR DECAY RATES (γ) FOR VARIOUS BEAMS	134
IV-B-4	FIRST FOUR DECAY RATES (γ) FOR SKIN-STRINGER PANELS	134
V-A-1	CHEMICAL STRUCTURES OF THE MAJOR CONSTITUENTS OF MATRIX RESINS	145
V-A-2	CURING REACTIONS FOR HERCULES 3501-6 RESIN	146
VI-1	CALENDAR OF COMPOSITES-RELATED MEETINGS	178
VI-2	COMPOSITES-RELATED TECHNICAL MEETINGS ATTENDED OFF-CAMPUS	180
VI-3	COMPOSITES-RELATED MEETINGS/TALKS HELD AT RPI	182
VI-4	COMPOSITES-RELATED VISITS TO RELEVANT ORGANIZATIONS	183
VI-5	COMPOSITE MATERIALS AND STRUCTURES PROGRAM BROWN BAG LUNCH (BBL) SCHEDULE	188

LIST OF FIGURES

Number		Page
II-A-1	3-D Model of High Modulus Carbon Fiber	11
II-A-2	Onion Layered Model	14
II-A-3	Parallel Spring Fiber Model	15
II-A-4	Oxidative Thinning of Carbon Fibers	19
II-A-5	The Modulus Distribution of HMS, HTS and AS Carbon Fibers	20
II-A-6	The Modulus Distribution of T-300 Carbon Fiber with Radius	22
II-A-7	Measured Axial Contraction Versus Remaining Radius	24
II-A-8	Variation of Stress and Strain Through the Fiber	25
III-B-1	Normalized In-Phase Stiffness as a Function of Moisture Weight Gain of Postcured Composite Exposed to Boiling Water or Water Vapor	37
III-B-2	Normalized In-Phase Stiffness as a Function of Moisture Weight Gain of As-cured Composite Exposed to Boiling Water	38
III-B-3	Loss Factor Versus Moisture Content for Postcured Composite Exposed to Boiling Water or Water Vapor	39
III-B-4	Loss Factor Versus Moisture Content for As-cured Composite Exposed to Boiling Water	41
III-B-5	Normalized In-Phase Modulus as a Function of Moisture Weight Gain for Postcured Epoxy Exposed to Boiling Water or Water Vapor	42
III-B-6	Loss Factor Versus Moisture Content for Postcured Epoxy Exposed to Boiling Water or Water Vapor	43
III-B-7	Birefringence Pattern of As-cured Epoxy	45
III-B-8	Birefringence Pattern of Postcured Epoxy	45
III-B-9	Birefringence Pattern of Postcured Epoxy Exposed to Boiling Water for 6 Hours	46
III-B-10	Birefringence Pattern of As-cured Epoxy Exposed to Boiling Water for 6 Hours	46
III-B-11	Birefringence Pattern of Redried, Postcured Epoxy	48

Number		Page
III-C-1	Schematic of the Spherically Symmetrical Stress Field Produced by Swelling of Network Polymer of Outer Radius R_2 which contains an inhomogeneity of Characteristic Radius r	53
III-C-2	A Few Typical Positive Structural Fluctuation Fields Possible in Cured Epoxy Resin	53
III-C-3	Tangential Stress Distribution Associated With the Deformation Fields Shown in Figure III-C-2	54
III-C-4	Radial Stress Distribution Associated With the Deformation Field Shown in Figure III-C-2	54
III-C-5	Structural Fluctuation Fields of Nature Similar to Those in Figure III-C-2 but of Higher Magnitude	56
III-C-6	Stress Fields Associated With Fluctuation Fields Shown in Figure III-C-5	56
III-C-7	Schematic of a Rigid, Nonswelling Inclusion Surrounded by a Positive Gaussian Fluctuation Field	57
III-C-8	Stress Fields Associated With the Fluctuation Field Shown in Figure III-C-7	57
III-C-9	A Spherical Microvoid Surrounded by a Concentric Positive Gaussian Fluctuation Field	58
III-C-10	Stress Fields Associated With the Fluctuation Field Shown in Figure III-C-9	58
III-D-1	Fracture Loci for Slant Crack Problem Under Remote Tension	66
III-D-2	Fracture Load for Slant Crack Problem Under Remote Tension	67
III-D-3	Basic Geometry and Attributes for Slant Crack Problem	68
III-D-4	Finite Element Mesh for the Slant Crack Problem	69
III-D-5	Cracked Plate Example	74
III-D-6	Crack Plate Example With Additional Crack Propagation	75
III-F-1	Plate Geometry Breakdown for Analysis	88
IV-A-1	Lockheed L-1011 Engine Drag Strut (Schematic)	94
IV-A-2	Effect of Ductility on Net Tensile Joint Strength	99

Number		Page
IV-A-3	Stress Profile for an Unloaded Hole in an Isotropic Plate	101
IV-A-4	Stress Averaging Scheme Used by Agarwal	104
IV-A-5	Characteristic Curve for Point Stress Scheme of "BOLT"	105
IV-A-6	"Minimum-Gradient Fiber Strain" Averaging Scheme Proposed by Author	108
IV-B-1	Simple Prismatic Finite Element	125
IV-B-2	Beam Test Cases	131
IV-B-3	Skin-Stringer Test Cases	132
V-B-1	Two Types of Structural Joints Used in the RP-1 (lightly-loaded, low-cost composite structures)	151
V-B-2	Results of Tensile Tests to Failure of the Structural Joints Shown in Figure V-B-1	152
V-C-1	RP-2 Static Test Set-Up	156
V-C-2	RP-2 Test Set-Up	157
V-C-3	Flight Envelope - RP-2	159
V-C-4	Loading Plan for the RP-2 Torsion Test	161
V-C-5	Vertical Deflections Versus Span Position at Different Loadings: RP-2 Simple Wing Bending Test, June 21, 1983	163
V-C-6	Differences Between Before and After Test Vertical Readings at Zero Load	165
V-C-7	Pull-Out of the Aft Wing Pins from Their Fuselage Receptacles, Versus Loading: RP-2 Simple Wing Bending Test, June 21, 1983	166
V-C-8	Wing Twist Versus Span: RP-2 Torsion Loading Test	168

PART I
INTRODUCTION

INTRODUCTION

The promise of filamentary composite materials, whose development may be considered as entering its second generation, continues to generate intense interest and applications activity. Such interest and activity are well-founded, since they are based on the possibility of using relatively brittle materials with high modulus, high strength, but low density in composites with good durability and high tolerance to damage and which, when they do fail, do so in a non-catastrophic manner. Fiber reinforced composite materials of this kind offer substantially improved performance and potentially lower costs for aerospace hardware.

Much progress has been achieved since the initial developments in the mid 1960's. Rather limited applications to primary aircraft structure have been made, however, mainly in a material-substitution mode on military aircraft, except for a few experiments currently underway on large passenger airplanes in commercial operation and a few military developments which have not seen service use.

To fulfill the promise of composite materials completely requires a strong technology base. NASA and AFOSR recognize the present state of the art to be such that to fully exploit composites in sophisticated aerospace structures, the technology base must be improved. This, in turn, calls for expanding fundamental knowledge and the means by which it can be successfully applied in design and manufacture.

As the technology of composite materials and structures moves toward fuller adoption into aerospace structures, some of the problems of an earlier era are being solved, others which seemed important are being put into perspective as relatively minor, and still others unanticipated or put aside are emerging as of high priority. The purpose of the RPI program as funded by NASA and AFOSR has been to develop critical advanced technology in the areas of physical properties, structural concepts and analysis, manufacturing, reliability and life prediction.

Our approach to accomplishing these goals is through an interdisciplinary program, unusual in at least two important aspects for a university. First, the nature of the research is comprehensive - from fiber and matrix constituent properties research, through the integration of constituents into composite materials and their characterization, the behavior of composites as they are used in generic structural components, their non-destructive and proof testing and, where the state of the art will be advanced by doing so, extending the research effort into simulated service use so that the composite structure's long-term integrity under conditions pertinent to such use can be assessed. Inherent in the RPI program is the motivation which basic research into the structural aspects provides for research at the materials level, and vice versa.

Second, interactions among faculty contributing to program objectives - which is a group wider than that supported under the project - is on a day to day basis, regardless of organizational lines. Program management is largely at the working level, and administrative, scientific and technical decisions are made, for the most part, independent of considerations normally associated with academic departments. Involvement of this kind includes - depending on the flow of the research - faculty, staff and students from chemistry, civil engineering, materials engineering and the department of mechanical engineering, aeronautical engineering and mechanics.

Both of these characteristics of the NASA/AFOSR program of research in composite materials and structures foster the kinds of fundamental advances which are triggered by insights into aspects beyond the narrow confines of an individual discipline. This is a program characteristic often sought in many fields at a university, but seldom achieved.

Overall program emphasis is on basic, long-term research in the following categories: (a) constituent materials, (b) composite materials, (c) generic structural elements, (d) processing science technology and (e) maintaining long-term structural integrity. Emphasis has shifted, and can be expected to continue to shift from one time period to another, among these areas depending on the states of composite materials and structures. Progress in the program will be

reported in the following pages under these headings. Those computer methodology developments are also undertaken which both support Rensselaer projects in composite materials and structures research in the areas listed above and which also represent research with the potential of widely useful results in their own right.

In short, the NASA/AFOSR Composites Aircraft Program is a multi-faceted program planned and managed so that scientists and engineers in a number of pertinent disciplines will interact to achieve its goals. Research in the basic composition, characteristics and processing science of composite materials and their constituents is balanced against the mechanics, conceptual design, fabrication and testing of generic structural elements typical of aerospace vehicles so as to encourage the discovery of unusual solutions to present and future problems. In the following sections, more detailed descriptions of the progress achieved in the various component parts of this comprehensive program are presented.

PART II
CONSTITUENT MATERIALS

II-A MECHANICAL PROPERTIES OF HIGH PERFORMANCE CARBON FIBERS

II-A MECHANICAL PROPERTIES OF HIGH PERFORMANCE CARBON FIBERS

Senior Investigator: R. J. Diefendorf

1. Introduction

Transmission electron microscopy of carbon fibers reveals an undulating ribbon structure of graphitic basal planes with higher axial alignment of the ribbons near the surface and lower alignment toward the fiber's center because of higher amplitude ribbon undulations[1,2,3,4,5]*. Optical activity and preferred orientation determinations from electron diffraction also appear to confirm the changes in structure in carbon fibers with distance from the fiber center[5,6]. These changes in preferred orientation through fiber depth result in a modulus gradient, with the surface material having a higher modulus and the core a lower modulus[5,6,7].

The variation in axial preferred orientation also results in a gradient in the coefficient of thermal expansion in the radial direction across the fiber's diameter. This follows, since the basal plane direction of carbon filament is transverse to the fiber's longitudinal axis, and the coefficient of thermal expansion (CTE) transverse to the graphite basal plane is higher than it is in the basal plane.

*Numbers in brackets in this section refer to the references which are listed on page 27.

It would, therefore, be expected that the fiber's interior, having a higher amplitude/wavelength ribbon undulation (see Figure II-1), would have a higher CTE than near the fiber's surface.

As the fiber cools from its processing temperature, this variation of CTE places the restrained fiber core into tension and the fiber surface into compression. The surface compressive strength may account for the insensitivity of carbon fibers to surface flaws in tension[8,9,10,11], but it may also degrade the compressive strength by initiating microbuckling[12]. Qualitative evidence of the presence of residual stress was obtained when it was observed that a fiber curled when the surface layer on just one side was ion-milled away[12,13]. Preliminary quantitative data taken to evaluate the residual stress in high modulus carbon fibers (Hercules HMS) showed values of the order of several GPa axial compression at the surface[12]. The tensile strength of HMS fibers, however, is only 2 GPa (300 ksi). The effect of residual stresses on the performance of carbon fibers is the basis of this report.

2. Status

Carbon fibers can be considered, generally speaking, as brittle materials, and Hooke's law can be applied. The residual stress distribution within the fiber can be determined, in principle, by measuring the modulus gradient and

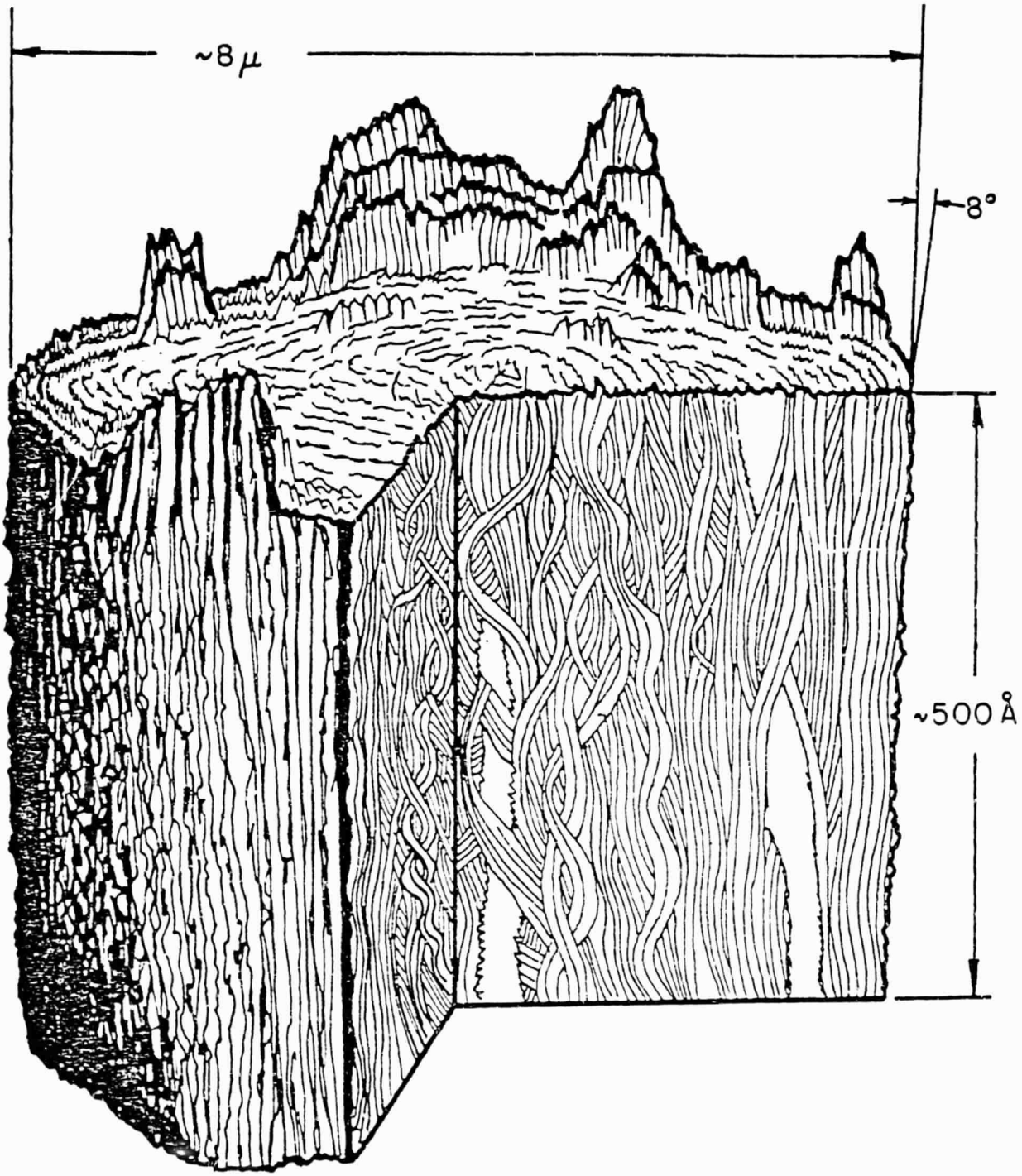

Figure II-A-1. 3-D Model of High Modulus Carbon Fiber. (after Tokarsky[34])

residual strain gradient. Accordingly, the course of the subject investigation was set as follows:

a) A theoretical prediction of the magnitude of radial, hoop and axial residual stress within the fiber caused by cooling down from high heat treatment temperature (HTT).

b) A precision method for diameter measurement.

c) A technique for uniform etching of the fibers.

d) A determination of Young's modulus gradient with depth, along a fiber diameter.

e) A determination of residual strain as a function of fiber diameter.

f) A study of the effect of HTT on the magnitude of residual stress.

3. Progress During Report Period

Equation (1) is a general equation for the radial stress (σ_r) developed during cooling from processing temperature levels, for a fiber with radial symmetry. It is expressed as follows:

$$r^2\frac{d^2\sigma_r}{dr^2} + Ar\frac{d\sigma_r}{dr} + B\sigma_r = C \qquad (1)$$

where

$$A = 3 + \frac{1}{1 - \nu_{\theta z}\nu_{z\theta}}\left(\nu_{r\theta} + \nu_{rz}\nu_{z\theta} - \frac{E_\theta}{E_r}\nu_{\theta r} - \frac{E_\theta}{E_r}\nu_{\theta r}\nu_{zr}\right)$$

$$+ \frac{rE_\theta}{1 - \nu_{\theta z}\nu_{z\theta}}\left[\frac{d}{dr}\left(\frac{1 - \nu_{\theta z}\nu_{z\theta}}{E_\theta}\right)\right]$$

$$B = 1 + \frac{\nu_{r\theta} + \nu_{rz}\nu_{z\theta}}{1 - \nu_{\theta z}\nu_{z\theta}} - \left(\frac{E_\theta}{E_r}\right)\left[\frac{\nu_{\theta r} + \nu_{\theta z}\nu_{zr} + 1 - \nu_{rz}\nu_{zr}}{1 - \nu_{\theta z}\nu_{z\theta}}\right]$$

$$+ \left(\frac{rE_\theta}{1 - \nu_{\theta z}\nu_{z\theta}}\right)\frac{d}{dr}\left[\left(\frac{\nu_{\theta r} + \nu_{\theta z}\nu_{zr}}{E_r}\right) - \left(\frac{1 - \nu_{\theta z}\nu_{z\theta}}{E_\theta}\right)\right]$$

$$C = \left(\frac{E_\theta}{1 - \nu_{\theta z}\nu_{z\theta}}\right)\left[\left(\varepsilon_r^T - \varepsilon_\theta^T\right) - \left(\nu_{rz} - \nu_{\theta z}\right)\left(\varepsilon_z^o - \varepsilon_z^T\right) - r\frac{d\varepsilon_\theta^T}{dr}\right]$$

$$+ r\frac{d}{dr}\left[\nu_{\theta z}\left(\varepsilon_z^o - \varepsilon_z^T\right)\right]$$

Solving Equation (1) requires knowledge of the variation of values of moduli (E_θ, E_r), coefficients of thermal expansion (α_r, α_θ, α_z) and Poisson's ratios (ν_{rz}, $\nu_{z\theta}$, ...) across the diameter of the fiber. We can reduce this to a managable level of complexity by using a simplified model; viz., a perfect onion skin model.

It is assumed that the material is homogeneous and has the configuration of a perfectly layered onion, as shown in Figure II-2. Properties such as modulus, Poisson's ratio etc., in the graphitic layer, are also assumed to be similar to those of pyrolytic graphite. It follows that the stresses in radial, hoop and longitudinal directions can be solved using Equation (1), yielding the following relations:

$$\sigma_r = 168[1 - (R/Ro)^{0.5}]^{ksi} \qquad (2)$$

$$\sigma_\theta = 168[1 - 1.5(R/Ro)^{0.5}] \quad (3)$$

and

$$\sigma_z = 82.4 - 103(R/Ro)^{0.5} \quad (4)$$

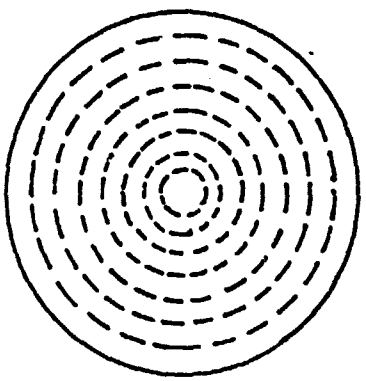

Figure II-A-2. Onion Layered Model

The high compressive hoop stress on the surface will cause a crenulated surface to form on the fiber. Both hoop and radial stresses contribute to the development of longitudinal stress in the fiber through Poisson's ratio effects, and so they will also be compressive on the surface and tensile inside of the fiber. The radial stress within the fiber will induce microcracks within it, and the stress relief due to cracking reduces hoop, radial and longitudinal stresses. Since the fiber is not homogeneous, however, another contribution from inhomogeneity must be added to these stresses.

Assume that the structure of the fiber is basically that of skin and core. Then, each of these constituents is treated as having different size, spring rate and coefficient of thermal expansion (CTE). The fiber model, therefore, appears as a pair of parallel springs, as shown in Figure II-A-3.

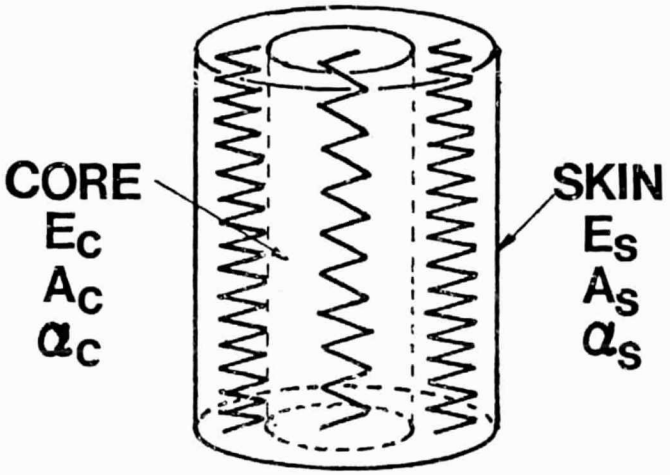

Figure II-A-3. Parallel Spring Fiber Model

The residual stress on the surface of the fiber, estimated from the parallel springs model, is compressive (.56 Pa or 73.4 ksi) and in the core is tension (0.027 Pa or 3.8 ksi), both as surmised from the earlier purely physical reasoning.

The magnitude of these stresses will be compared with those obtained in experiments.

The technique to determine the residual stress involves the measurement of fiber modulus and residual strain as a function of fiber diameter. The accuracy of values in the past has been limited by diameter errors. In the current work, however, the precision of fiber diameter measurements was improved by using a laser diffraction technique[14], rather than a purely optical or electro-optical method.

As shown in Table II-1, the laser diffraction technique provides better resolution than optical microscopy for circular fiber diameter measurements, and it is much faster. However, the cross sections of some of the carbon fibers are not round. For instance, T-300 fibers have cross sections mainly of kidney, ellipse and other slightly irregular shapes. To evaluate such fibers, a single filament is mounted vertically in a rotating stage. The diffraction pattern was measured repeatedly, after rotating the filament cross section by steps every ϕ degrees. The corresponding widths were determined, and the total area was calculated. The results are shown in Table II-2. In either kidney shaped or elliptical cross sections, the maximum errors (40~50%) arise from measuring one edge only ($p = 180°$), while the minimum error (~1%) occurs at 36° of rotation. Therefore, a rotating technique which used $\phi = 36°$ was selected as giving a very good representation of the true diameter.

TABLE II-1

FIBER DIAMETER MEASUREMENT TECHNIQUES AND RESULTS

	Mean Diameter (μm)	Standard Deviation (μm)	Number of Observations
A. Optical Microscopy			
1) Edge	7.0	.45	200
2) Vertical (bundle)	7.81	.31	53
3) Vertical (single)	8.25	.25	55
4) Oil immersion	8.37	.11	50
5) Image analysis	7.74	.52	53
B. Laser Diffraction			
1) Photodetector	8.03	.037	18
2) Visual	7.68	.08	30

TABLE II-2

ROTATING TECHNIQUE FOR IRREGULAR AREA MEASUREMENT

Rotating Angle	Percent Error (S. D.) Set 1.	Set 11.
180	37	50
90	-32(4.2)	-34(2.2)
60	-11(1.8)	-13(1.0)
45	-2.6(1.2)	-4.8(.8)
36	1.5(.5)	-.6(.3)
30	3.8(.3)	2.0(.5)
20	6.8(.1)	5.2(.6)
15	7.9(.2)	6.3(.3)
10	8.7	7.2
5	9.2	7.7

The modulus and residual strain in carbon fibers were measured by successively electrochemically milling away the fiber surface[14]. Electrochemical etching was found to remove the carbon fiber surface very uniformly in contrast with air and wet oxidation (see Figure II-A-4).

The modulus distributions of HMS, HTS and AS carbon fibers are shown in Figure II-A-5[15]; based on average values for each radius ratio. HMS, as received, fiber has an average modulus of 370 GPa (54 Msi), which drops to 260 GPa (38 Msi) as the radius of the fiber is etched away to 0.72 of the original radius. Further, the rate of range in modulus has a higher value near the surface and the rate of change is a more gradual decrease toward the center. This is consistent with the modeling of skin/core heterogeneity for Type I carbon fiber. As noted, the outside skin has more oriented graphitic layers parallel to the fiber surface, so that fibers which include this skin will have higher average modulus than those which do not. As the outside skin is etched away, the modulus of the remaining fiber decreases. HTS fibers with an average modulus of 267 GPa (39 Msi) change to 240 GPa (35 Msi) at the radius ratio of 0.61. The change of modulus across the fiber diameter is comparably smaller than that of HMS fiber. For AS fibers, the moduli changes from 212 GPa (31 Msi) to 185 GPa (27 Msi) at the radius ratio of 0.61. Again, the smaller change in moduli across the fiber diameter would be expected from the

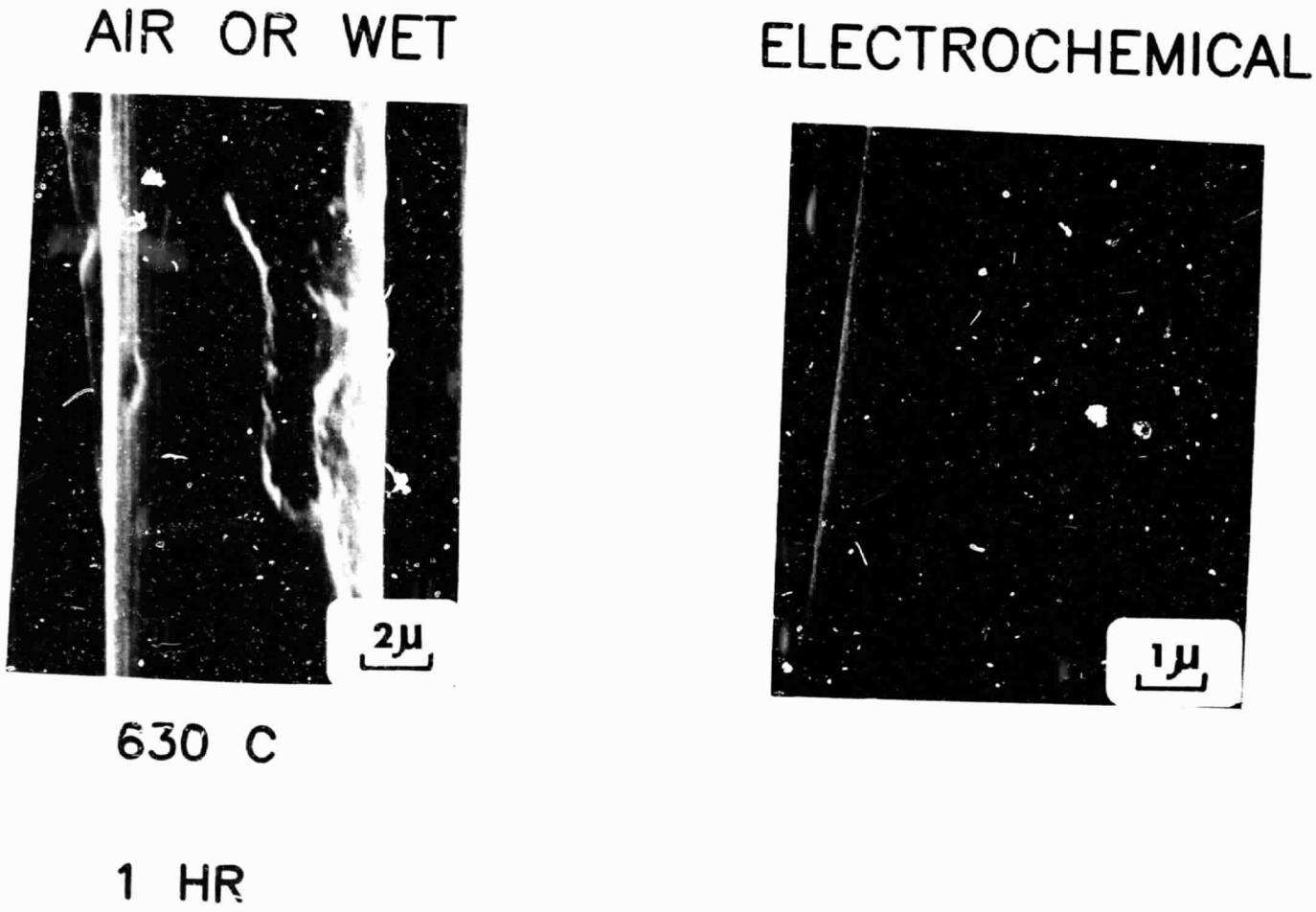

Figure II-A-4. Oxidative Thinning of Carbon Fibers

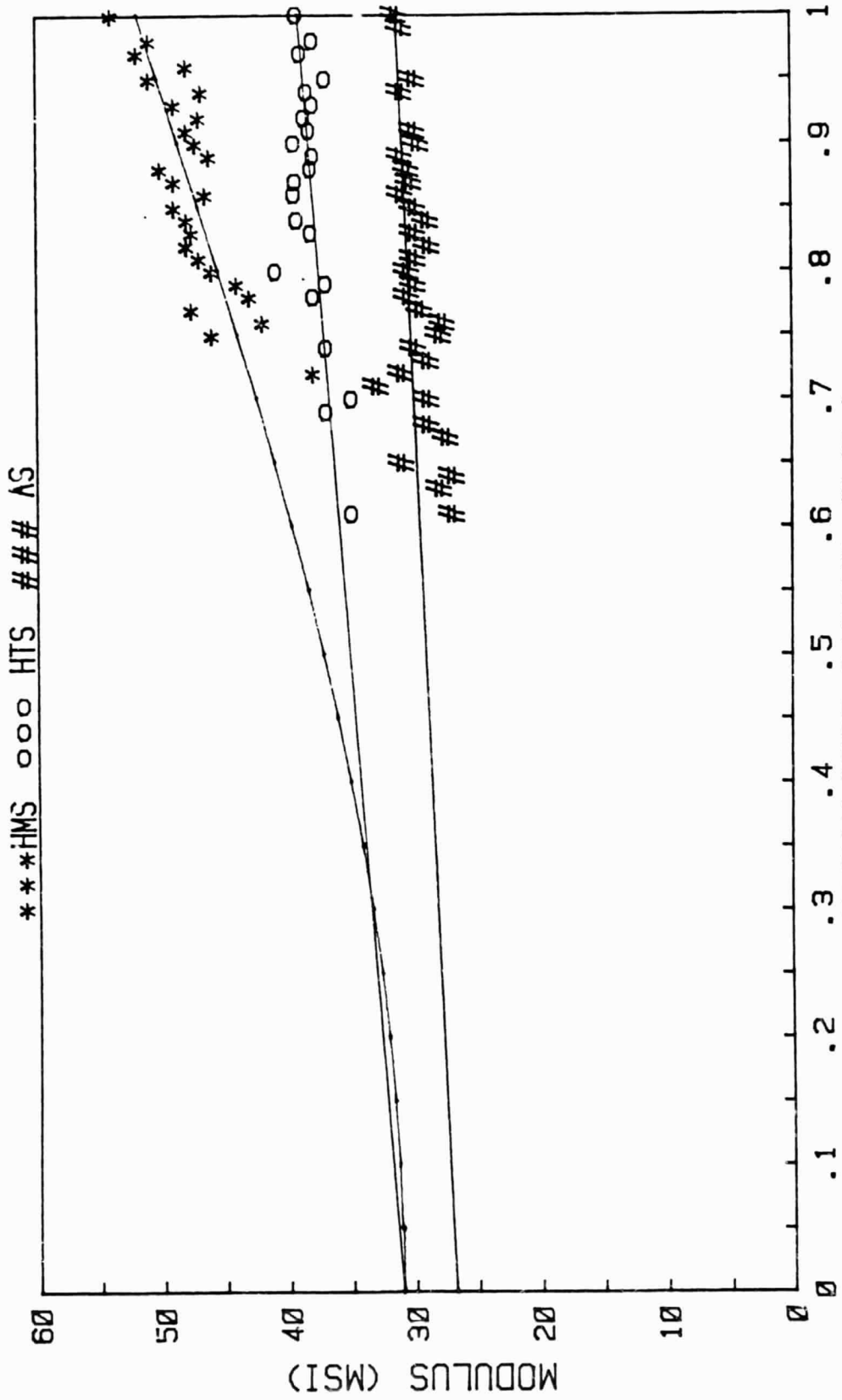

Figure II-A-5. The Modulus Distribution of HMS, HTS and AS Carbon Fibers

observation[16] that there is no skin/core heterogeneity in Type II and Type A fibers. However, Morita et al.[17] measured large radial gradients of Young's modulus from 280 GPa (41 Msi) to 171 GPs (25 Msi) for T-300 fibers (as shown in Figure II-A-4, curve 1). To verify these measurements, a bundle of T-300 fibers from Union Carbide was selected for modulus gradient measurement. The results for this case are also shown in Figure II-A-6 curve 2. The modulus changes from 205 GPa (30 Msi) to 178 GPa (26 Msi) at R/Ro = 0.58. By neglecting three low values in the small R/Ro region, we obtain curve 3, showing only a small change in modulus across the fiber. This is similar to AS fibers. It is noted that the cross section of T-300 fiber is not round, therefore, larger measuring errors can be expected if it is only measured with optical microscopy from the edge (see Table II-2). Another fiber, Hercules AS-4, was also examined. The modulus changed from 240 GPa (35 Msi) to 219 GPa (32 Msi) at R/Ro = 0.62. Again, the change of modulus is small across the fiber, but significant.

In conclusion, modulus gradients in carbon fibers show high values for HMS, low values for HTS, AS, T-300 and AS-4 fibers. These measurements are related to the observed microstructure. A skin/core structure will produce a sharp modulus gradient, otherwise, only a small gradient exists. Therefore, the following analysis of residual stress will focus on high modulus fiber only.

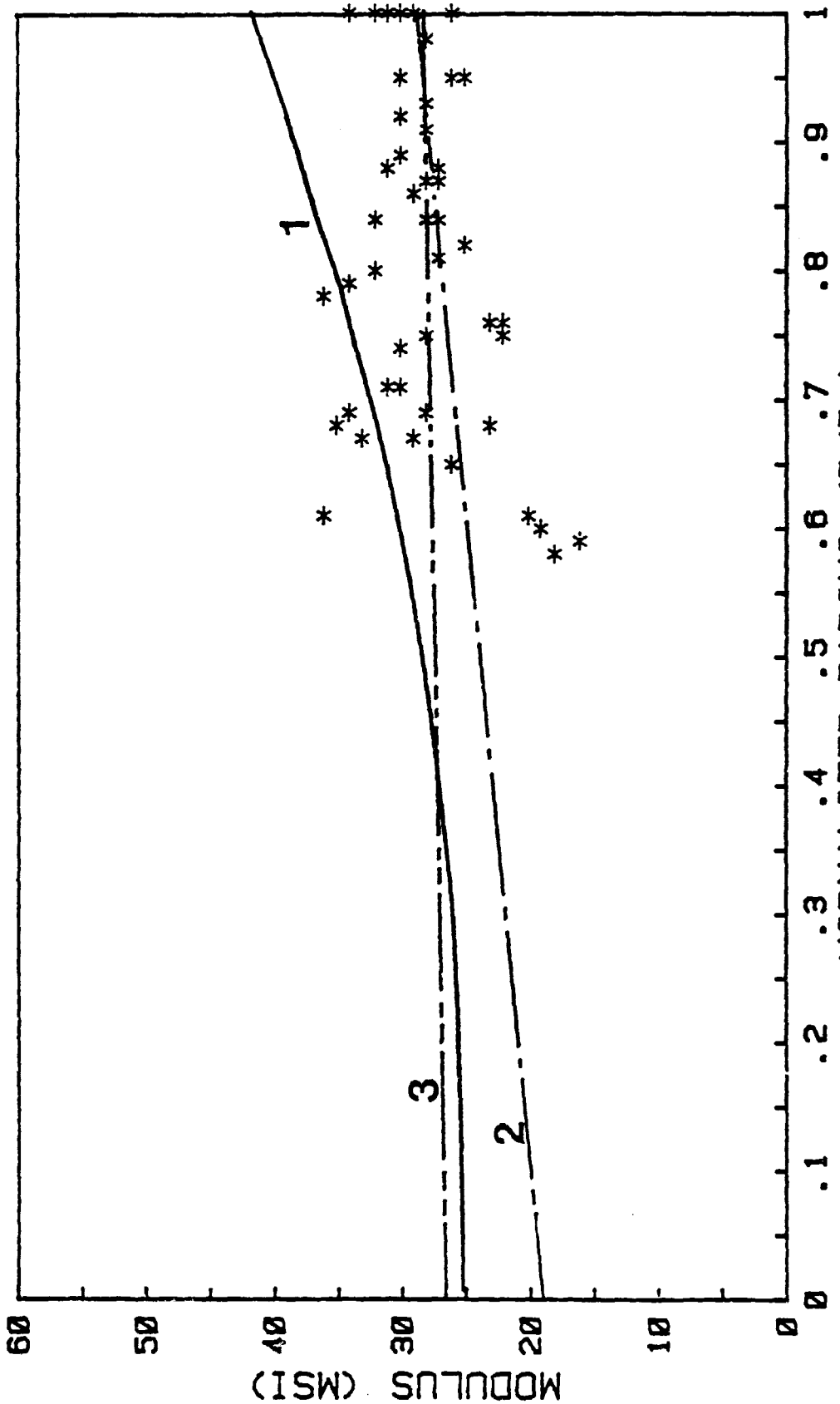

Figure II-A-6. The Modulus Distribution of T-300 Carbon Fiber with Radius: 1) after Morita et al.[44]; 2) this study and 3) by neglecting few small values from Curve 2.

Measured axial contractions[14] as a function of the radius of etched fiber for HMS fibers are shown in Figure II-A-7. There is a large contraction as the surface is etched away which implies the outside skin was under a compression stress state before that layer was removed. The sharp drop also is consistent with the skin/core fiber microstructure.

Knowing the measured fiber contraction function, e(r), the measured average modulus function, Y(r), and the local modulus, E(r), and assuming that the actual strain gradient, $\varepsilon(r)$, and its derivative are continuous, we then can determine $\varepsilon(r)$ using the following equation[14].

$$\varepsilon(r) = - e(r) - \frac{de(r)}{dr} \frac{\int_o^r rE(r)dr}{rE(r)} \qquad (5)$$

Here again, once the local modulus and local strain have been established, the residual stress within carbon fibers is observed to have a tensile axial residual stress in the center of the fiber and a compressive axial stress at the surface. The tensile residual stress in the middle of the fiber is not very sensitive to the form of the functions used for the modulus and strain gradients, provided the function produces an unique derivative at the center of the fiber. However, the calculated stress at the surface is dependent upon the kind of function used. The calculated residual compressive stress near the surface is about 0.55 GPa (80 ksi), but it rises rapidly to zero as depth below the surface is gained (see Figure II-A-8).

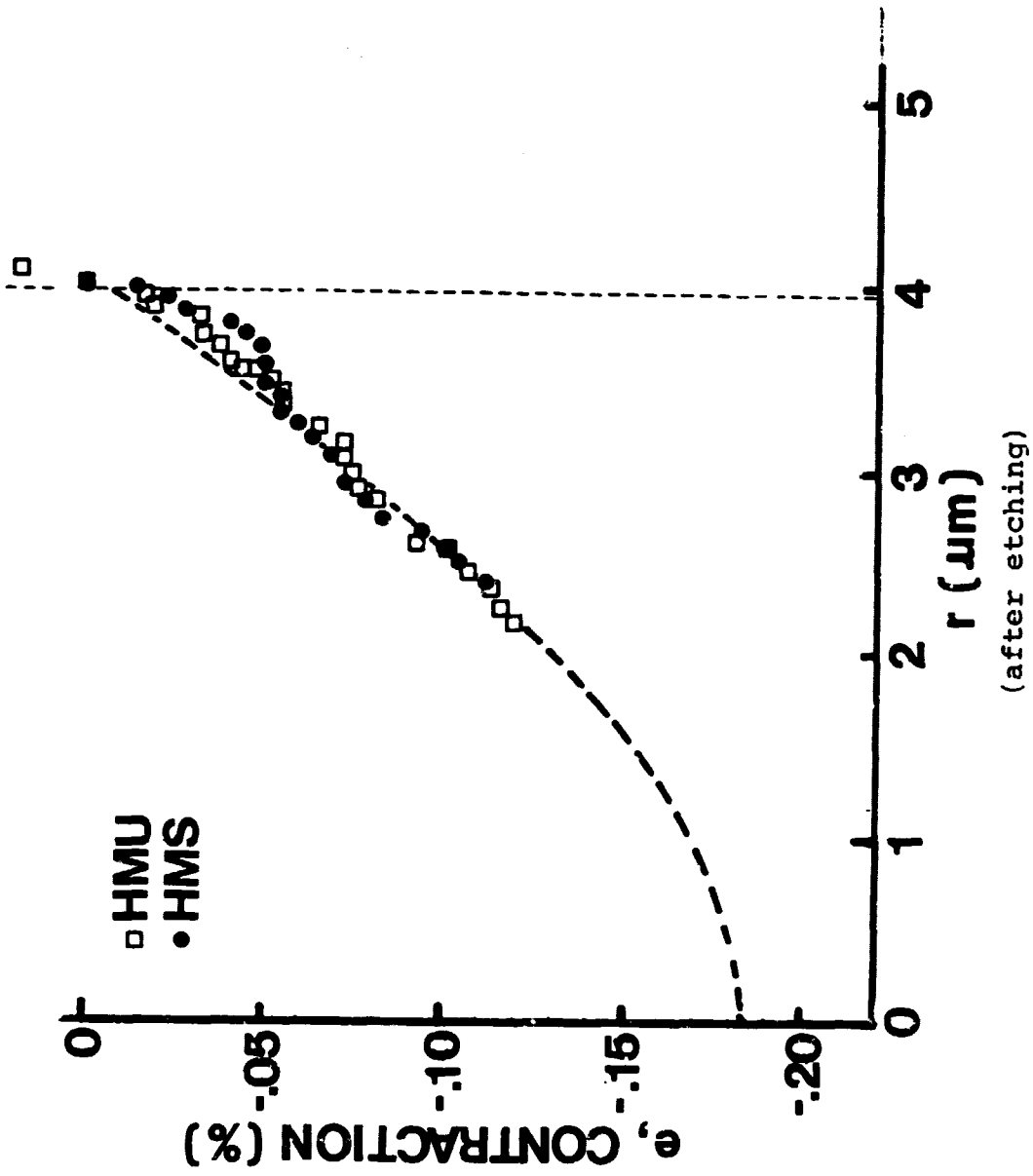

Figure II-A-7. Measured Axial Contraction Versus Remaining Radius

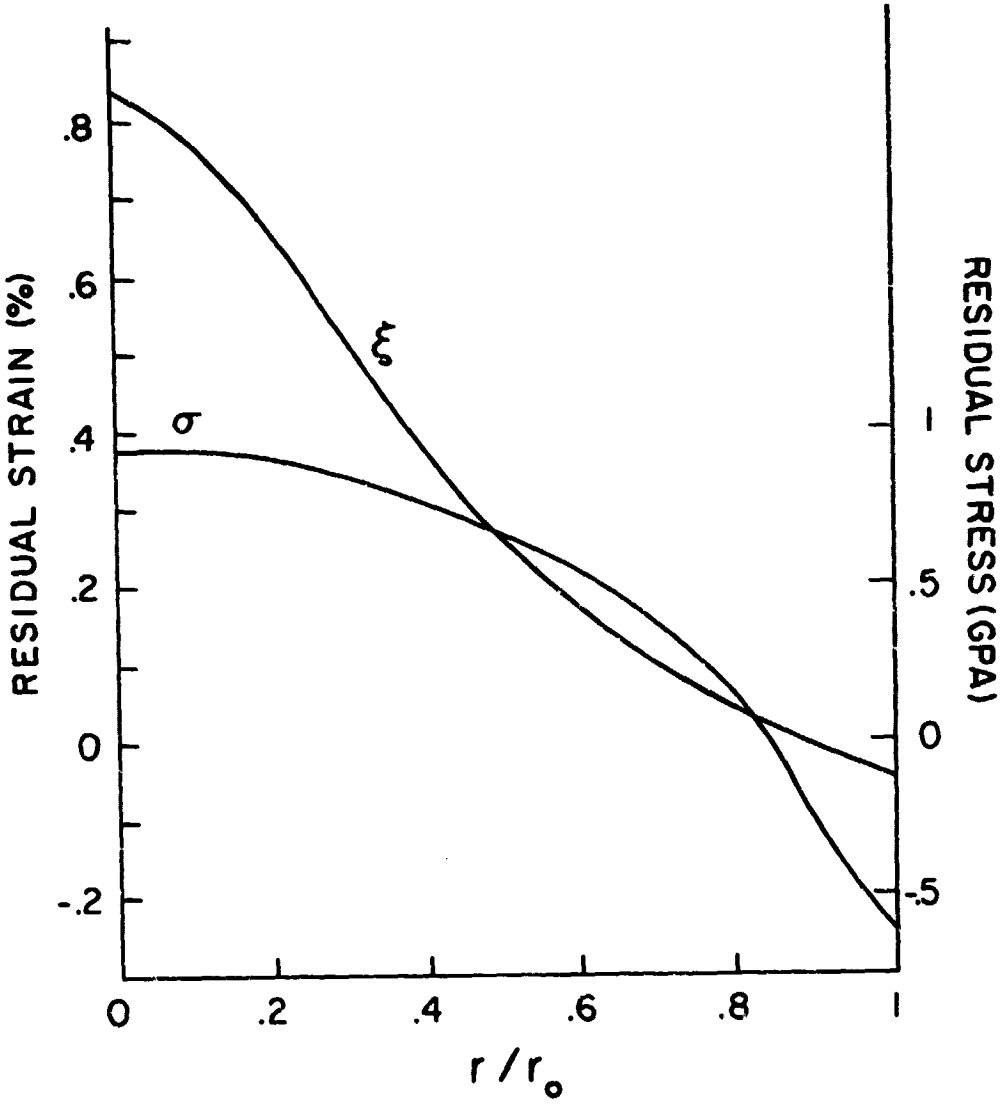

Figure II-A-8. Variation of Stress and Strain Through the Fiber

The residual stress predicted by the parallel springs model on the surface of the fiber is .5 GPa (73.4 ksi) [compression], which is very close to the experimental value, i.e., .55 GPa (80 ksi) [compression].

To summarize, high surface compression minimizes the effect of surface flaws[10], but high axial tensile stress in the interior may decrease strength by causing fracture to initiate at flaws in the interior rather than at the surface when the fiber is under tensile loads. Similarly, the high axial compressive stresses in the outer layers of a fiber may initiate buckling when the fiber is compressively loaded. Modifications of the residual stress pattern might allow increased tensile and/or compressive strengths to be obtained in high modulus carbon fibers. In addition, the modulus varies across a fiber diameter, with the modulus of the surface layers about twice the average fiber modulus and the interior modulus only one-half the average, for HMS fibers. This modulus gradient suggests that higher modulus carbon fibers could be produced if the modulus at their interior could be increased.

4. Plans for Upcoming Period

Much effort in the carbon fiber field has emphasized modulus gradient and residual stress, while little study has been done on the strength of the fibers. The high axial tensile stress in the interior may decrease strength by

causing fracture to initiate at flaws in the interior rather than at the surface. In order to verify this statement, the fracture surface of the fibers should be investigated. A technique has been developed to catch the fracture ends of tensilely failed fibers. Samples having different diameters, with residual stresses relieved by varying amounts of electrochemical etching, have been tested. The fracture ends were caught and will be investigated with SEM. Some SEM pictures show that for HMS, the fracture initiated from the interior of the fiber; other kinds of fibers fail from flaws at the surface. A group of samples are under investigation, and the results will be obtained within the next reporting period.

Another important property, Poisson's ratio, is under evaluation. If the longitudinal strain is 0.5% and the diamter of the fiber is about 8 μm, then the resolution needed to measure changes in diameter for a Poisson's ratio about 0.2 (to be evaluated) is about 0.8 μm. This is a very small dimension. Fortunately, with laser diffraction techniques such small dimensional changes appear to be within our measuring capabilities. We, therefore, will attempt to determine Poisson's ratio directly.

5. References

1. Johnson, D. and C. Tyson, "The Fine Structure of Graphatized Fibers", Brit. J. Phys. (J. Phys. D.), 2, 1969, pp. 787-795.

2. Fourdeux, A., C. Herinckx, R. Perret and W. Rutland, C. R. Acad. Sci., 269, 1969, p. 1597.

3. Hugo, J. A., V. A. Phillips and B. W. Roberts, "Intimate Structure of High Modulus Carbon Fibers", Nature, 226, 1970, p. 144.

4. Murphy, E. V. and B. F. Jones, "Surface Flaws on Carbon Fibers", Carbon, 9, 1971, p. 91.

5. Tokarsky, E. W., "The Relationships of Structure to Properties in Carbon Fibers", Ph.D. Thesis, Rensselaer Polytechnic Institute, Troy, New York, October 1973.

6. Butler, B. L. and R. J. Diefendorf, "Graphite Filament Structure", Proceedings of the 10th Carbon Composite Technology Symposium, Pub. by U. of New Mexico, 1970, pp. 107-124.

7. Jones, B. H. and R. G. Duncan, "The Effect of Fiber Diameter on the Mechanical Properties of Graphite Fibers Manufactured from Polyacrylonitrile and Rayon", J. Mat. Sci., 6, 1971, p. 289.

8. Johnson, W. and J. Thorne, "Effect of Internal Polymer Flaws on Strength of Carbon Fibers Prepared from an Acrylic Precursor", Carbon, 7, 1969, pp. 659-661.

9. Tyson, N., "Fracture Mechanism in PAN Fibers 1000-2800 C", J. Phy. D.: Appl. Physics, 8, 1975, pp. 749-758.

10. Riggs, D. M., I. W. Sorensen and R. J. Diefendorf, "The Relationship of Structure to Properties in Graphite Fibers", AFML-TR-72Y33, Part IV, November 1975.

11. Mehalso, R. M., "CVD of Boron on Carbon Monofilament", Ph.D. Thesis, Rensselaer Polytechnic Institute, Troy, New York, November 1973.

12. Stevens, W. C., J. H. Wang, and R. J. Diefendorf, "Residual Stress in High Modulus Carbon Fibers', Carbon '80, Deutchen Keramischen Gesellschaft, Bad Honnef, W. Germany, pp. 598-602.

13. Wang, J. H., "Residual Stress in High Modulus Carbon Fibers", M.S. Thesis, Rensselaer Polytechnic Institute, Troy, New York, 1981.

14. Chen K. J. and R. J. Diefendorf, "Residual Stress in High Modulus Carbon Fibers", Progress in Science and Engineering of Composites", T. Hayashi, K. Kawata and S. Umekawa, Eds., ICCM-IV, Tokyo, Japan, 1982.

15. Chen, K. J. and R. J. Diefendorf, "The Modulus Distribution in Carbon Fibers", 16th Biennial Conference on Carbon, Extended Abstracts and Program, U. of California, San Diego, CA, July 1983, pp. 490-491.

16. Bennett, S. C. and D. J. Johnson, "Electron-Microscope Studies of Structural Heterogeneity in PAN-Based Carbon Fibers", Carbon, 17, 1979, pp. 25-39.

17. Morita, K., H. Miyachi, K. Kobori and I. Matsubara, "Carbon Fibers with Large Breaking Strain", High Temperature-High Pressures, 9, 1977, pp. 193-198.

6. Current Publications or Presentations by Professor Diefendorf on this Subject

"The Physical Chemistry of Fiber/Matrix Interactions in Composite Materials"

Presented at the California Institute of Technology, May 10-11, 1983.

"The Effect of the Fiber/Matrix Interface on Composite Toughness"

Presented at NASA/Langley Meeting on Tough Composites, May 24-25, 1983.

"The Physical Chemistry of Pitch Mesophase Formation"

Presented Plenary Lecture at American Carbon Society Biennial Conference on Carbon, San Diego, CA, July 18-22, 1983.

"Mesophase Formation in Synthetic Pitches", with S. H. Chen, p. 11.
"Phase Behavior of Mesomorphic Binary Systems", p. 26.
"Mesophase Formation in Polynuclear Aromatic Compounds", with S. H. Chen, p. 28.
"Volatilized Compounds and Microstructural Development During Mesophase Growth in Pitch Fractions", with I. W. Sorenson, p. 34.
"The Effect of Shear on Mesophase Formation in A-240 Pitch", with I. W. Sorenson, p. 46.
"The Chemical Vapor Deposition of Carbon on Graphite Surfaces", with D. F. Cummings, p. 190.
"Molecular Weight Determination of Pitches", with S. H. Chen, p. 433.
"Mass Spectra of Species Evolved during Flash Pyrolysis of Mesophase Forming Pitches", with I. W. Sorenson, p. 435.
"The Intrinsic Viscosities of Pitches and Pitch Fractions", with S. H. Chen, p. 437.

"The Modulus Distribution in Carbon Fibers", with K. J. Chen, p. 490.
"Transverse Properties of Carbon and Kevlar Fiber Composites", with J. F. Helmer, p. 511.
"Solubility Theory of Polynuclear Aromatic Compounds", with S. H. Chen, p. 22.
"Solvent Extracted Pitch Precursors for Carbon Fibers", with D. M. Riggs, p. 24.

The preceeding 13 papers were presented at the Biennial Conference on Carbon, American Carbon Society, San Diego, CA, July 18-22, 1983.
Published in Proceedings of the 16th Biennial Conference on Carbon, Glen B. Engle and Robert Price, Eds., American Carbon Society, 1983.

"Mesophase Formation in Polynuclear Aromatic Compounds: A Route to Low Cost Carbon Fibers"
"Molecular Weight and Molecular Weight Distribution in Pitches", with S. H. Chen and W. C. Stevens.
"Pitch-Solvent Interactions and Their Effects on Mesophase Formation", with J. G. Venner.
"Solvent Extracted Pitch Precursors for Carbon Fibers", with D. M. Riggs.

The preceeding 4 papers were presented at the Polymers for Fiber Production Symposium, American Chemical Society, Washington, D.C., August 29-Sept. 1, 1983.
To be published in Polymers for Fibers and Elastomers, J. C. Arthur, R. J. Diefendorf et al., Eds., American Chemical Society, Washington, D.C., 1984.

PART III

COMPOSITE MATERIALS

III-A FATIGUE IN COMPOSITE MATERIALS

III-B EXPERIMENTAL STUDIES OF MOISTURE AND TEMPERATURE EFFECTS ON THE MECHANICAL PROPERTIES OF GRAPHITE/EPOXY LAMINATES

III-C THEORY OF INHOMOGENEOUS SWELLING IN EPOXY RESIN

III-D NUMERICAL INVESTIGATION OF THE MICROMECHANICS OF COMPOSITE FRACTURE

III-E FREE-EDGE FAILURES OF COMPOSITE LAMINATES

III-F ANALYSIS OF UNBALANCED LAMINATES

III-A FATIGUE IN COMPOSITE MATERIALS

Senior Investigator: E. Krempl

1. Introduction

The deformation and failure behavior of graphite/epoxy tubes under biaxial (axial and torsion) loading is being investigated. The aim of this research is to increase basic understanding of and provide design information for the biaxial response of graphite/epoxy composites.

2. Status

Manufacture of $[0, \pm 45]_s$ graphite/epoxy (Gr/E) tubes continued preparatory to undertaking a new series of tests, and a review of fatigue damage theories in composites was begun.

3. Progress During Report Period

Preparation of two technical papers giving the static elastic and strength properties and the biaxial fatigue performance, respectively, of $[\pm 45]_s$ Gr/E tubes continued.

Axial loading of $[\pm 45]_s$ Gr/E tubes produced significant time-dependent deformation (creep, relaxation and loading rate sensitivity). Those findings were considered unusual and probably due to insufficient curing and/or moisture pick-up.

Prolonged drying is being performed on two specimens. One will be subjected to a post-cure treatment. These

specially treated specimens will then be tested, in the next reporting period, to ascertain whether their time-dependent behavior has been altered by these treatments.

Two additional batches of six-layer $[0, \pm 45]_s$ Gr/E tubes were manufactured, and some tests have been completed.

A review of current fatigue theories for composites is underway in an effort to develop a life-prediction method for biaxial fatigue of composites.

4. Plans for Upcoming Period

The tasks outlined in Section 3 will be continued.

5. Current Publications or Presentations by Professor Krempl on this Subject

"Biaxial In-Phase and Out-of-Phase Fatigue Behavior of Graphite-Epoxy Tubes"

Presented at the ASTM meeting, (E-9) Committee on Fatigue, May 11, 1983 and was given the "1982 E-09 Best Presented Paper Award"

"Inelastic Work and Thermomechanical Coupling in Viscoplasticity"

Presented paper as a Topical Lecture at the Plasticity Today Meeting, Udine, Italy, June 1983.

III-B EXPERIMENTAL STUDIES OF MOISTURE AND TEMPERATURE EFFECTS ON THE MECHANICAL PROPERTIES OF GRAPHITE/EPOXY LAMINATES

Senior Investigator: S. S. Sternstein

1. Introduction

This project is concerned with those properties of high performance composites which are strongly dependent on the physical properties of matrix resin.

Moisture is known to adversely affect the properties of both neat epoxy resin and epoxy matrix composites. The inhomogeneous swelling makes a major contribution to the moisture degradation of mechanical properties, both in neat epoxy resin and composite laminates. It is postulated that the postcuring process can change structure-moisture interaction and alleviate its adverse effects. Such effects are being investigated.

2. Status

To date, specific investigations have included viscoelastic characterization of the glass transition region in both laminates and neat resins, delamination studies, moisture interactions and inhomogeneous swelling phenomena.

3. Progress During Report Period

During the present report period, our objective has been to further study the moisture interaction using

postcured samples. Graphite/epoxy composite laminates with 0/90 stacking sequence, were postcured at 180°C for twelve hours.

A set of these composite samples exposed to a boiling water environment for various periods of time were tested and the results of in-phase stiffness, M'(storage modulus), with moisture content are shown in Figure III-B-1. The values of M' are normalized both by the value of M' for the dry sample and by the cube of the thickness for the wet sample (as tested). It is clear that in-phase stiffness does not change with moisture uptake. These results are completely different from those for as-cured samples. In as-cured samples, there is a drastic change in slope around 2.5% moisture content. (For the reader's convenience, M' versus moisture content in as-cured samples is shown in Figure III-B-2.) Note that the maximum moisture uptake in postcured samples is about 2% by weight, which is less than that in as-cured samples (4.5%) for the same environmental conditions. This indicates that the postcuring process changes the network structure and alters dramatically the structure-moisture interaction, even though both the postcured and as-cured samples have the same chemistry to begin with. As expected, the in-phase stiffness retraces its path upon drying.

The loss factor, M"/M', for postcured composite samples is given in Figure III-B-3. The ordinate represents the

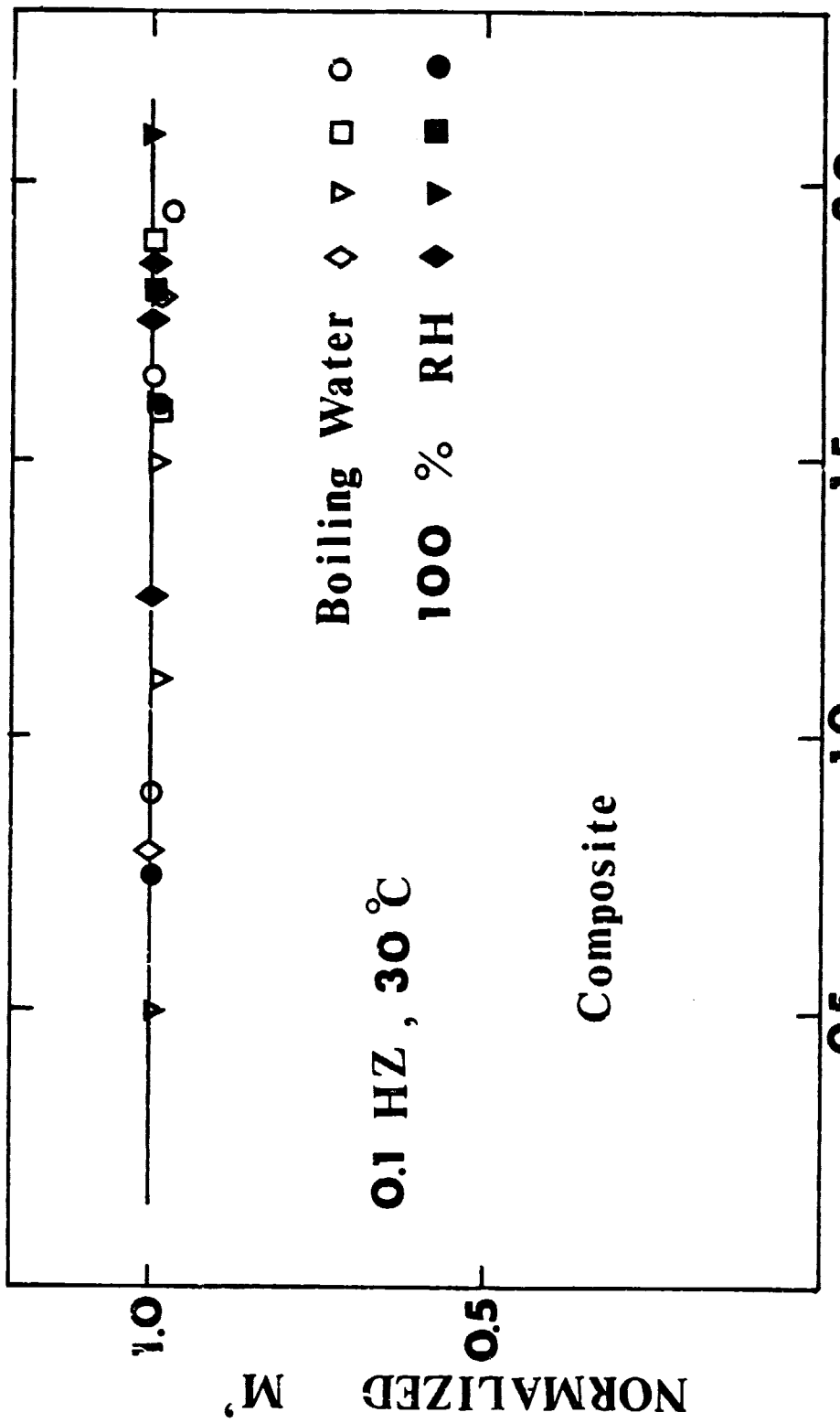

Figure III-B-1. Normalized In-Phase Stiffness as a Function of Moisture Weight Gain of Post-cured Composite Exposed to Boiling Water or Water Vapor

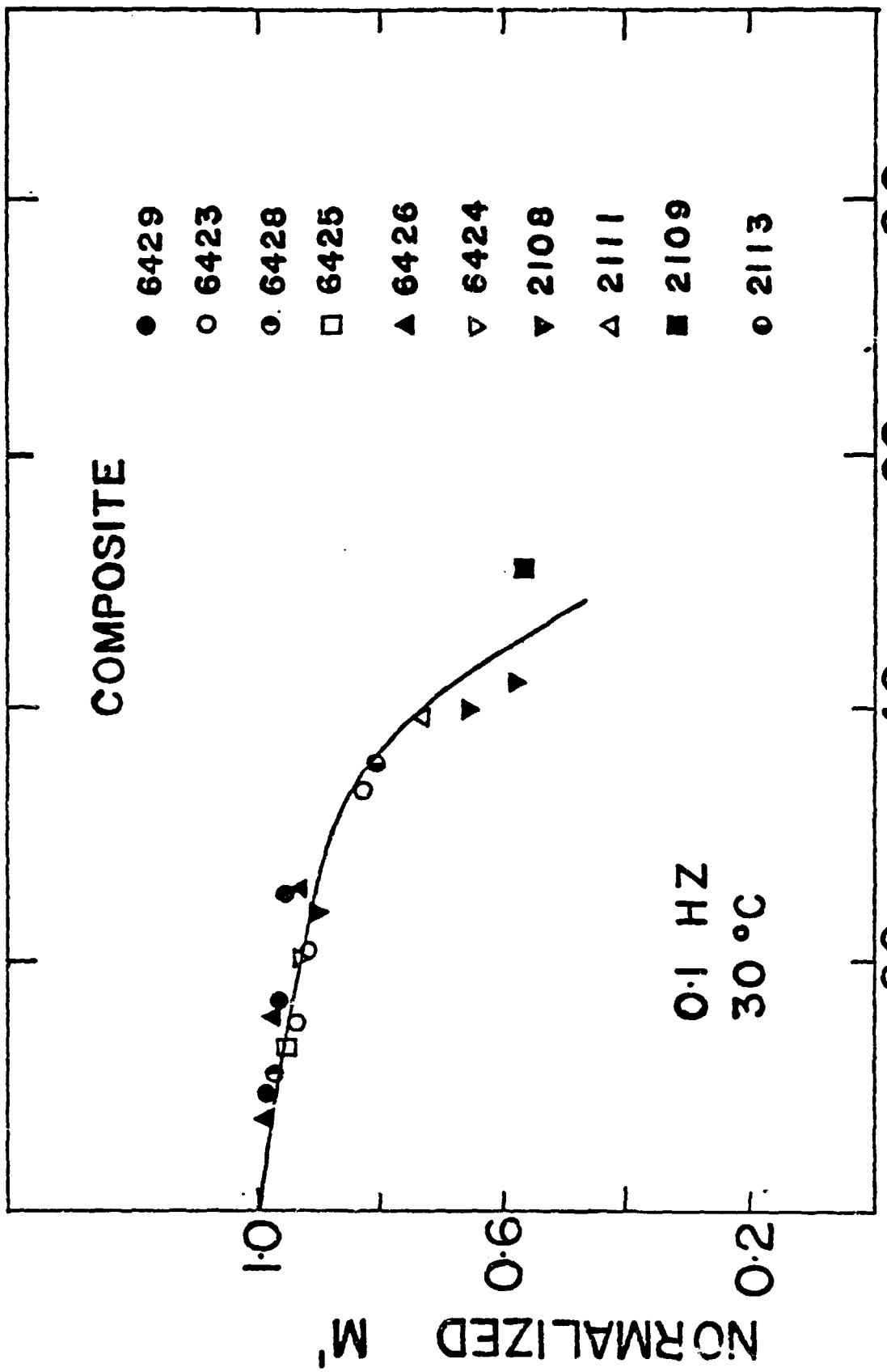

Figure III-B-2. Normalized In-Phase Stiffness as a Function of Moisture Weight Gain of As-cured Composite Exposed to Boiling Water

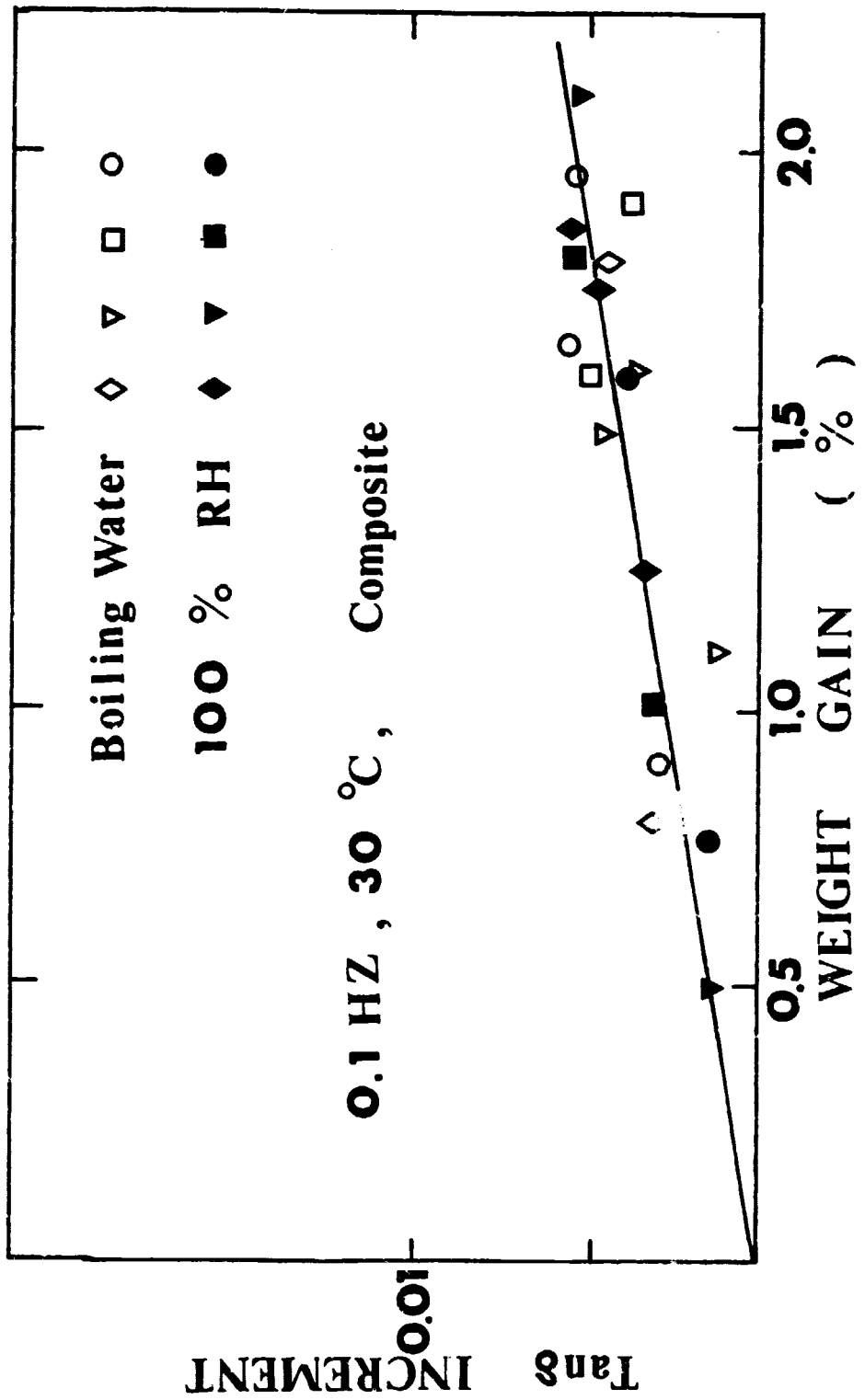

Figure III-B-3. Loss Factor Versus Moisture Content for Postcured Composite Exposed to Boiling Water or Water Vapor

increase (or increment) in loss factor in a wet sample relative to a dry sample. The loss factors increase linearly with increasing moisture uptake. If the sample is dried, the loss factors decrease accordingly, i.e., a dried sample would lie on the curve and not exhibit a large residual loss factor. This indicates that moisture has plasticized the epoxy matrix, and the mobility of the molecules has increased; conversely, drying would decrease the mobility. For comparison, Figure III-B-4 is a repeat of our previous result on loss factor hysteresis for as-cured samples. It suggests, once again, that structure-moisture interaction for as-cured and postcured composites are very different.

A similar set of experiments using postcured neat epoxy resins were performed. As shown in Figure III-B-5, M' decreases linearly with increasing moisture content. This indicates that the degree of softening is proportional to the extent of swelling. Note that the maximum moisture content is 4.5%, which is much less than that for as-cured samples (8%). In the as-cured samples, there is a drastic change in slope at 6.5% moisture content, which was discussed in a previous report. The loss factor for neat resin samples is shown in Figure III-B-6; it increases linearly with moisture content, and hysteresis effects do not occur. This result is very similar to that for as-cured neat resins.

The polarized light microscope was used to further illustrate the difference in moisture interaction between

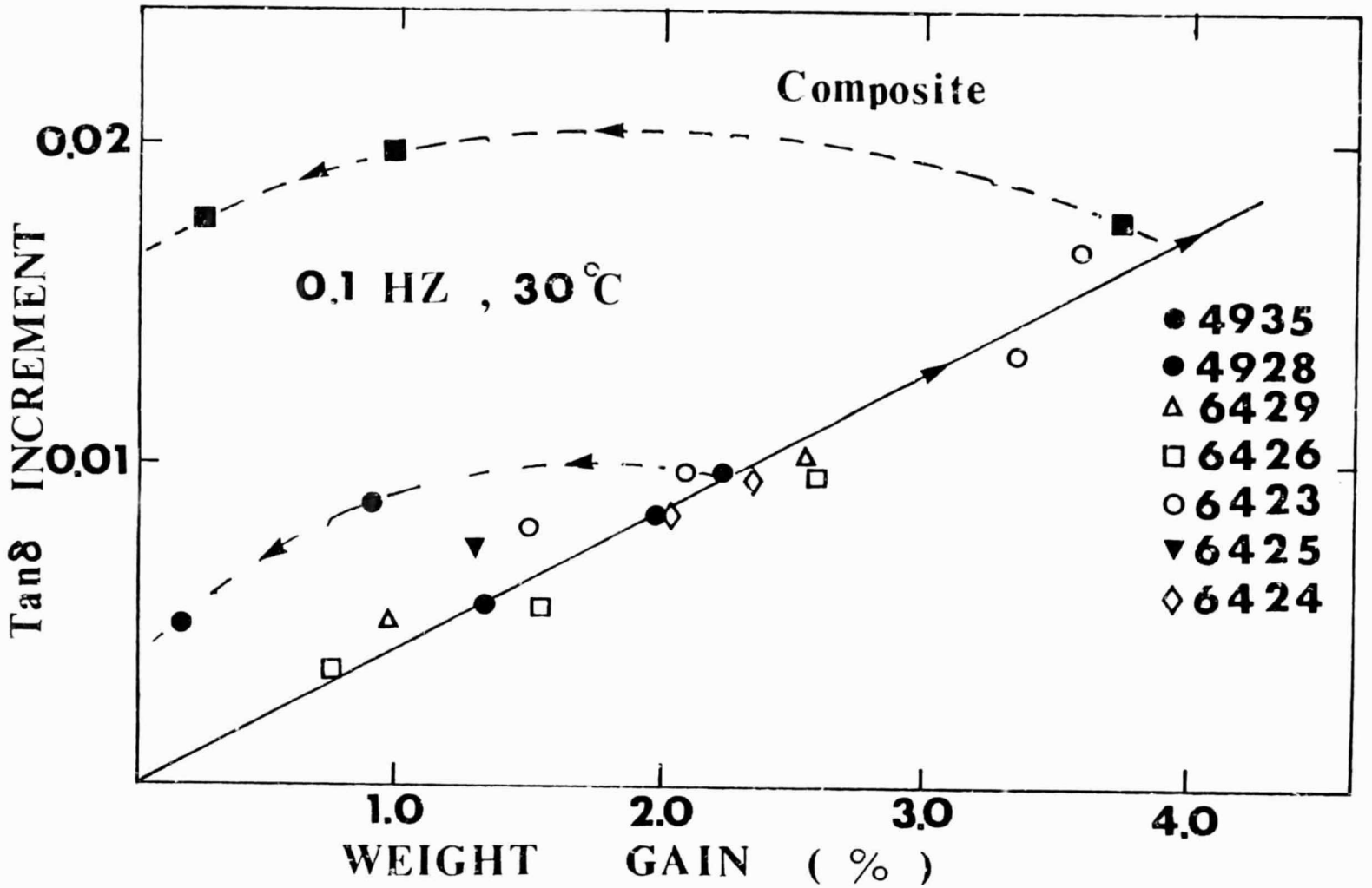

Figure III-B-4. Loss Factor Versus Moisture Content for As-cured Composite Exposed to Boiling Water

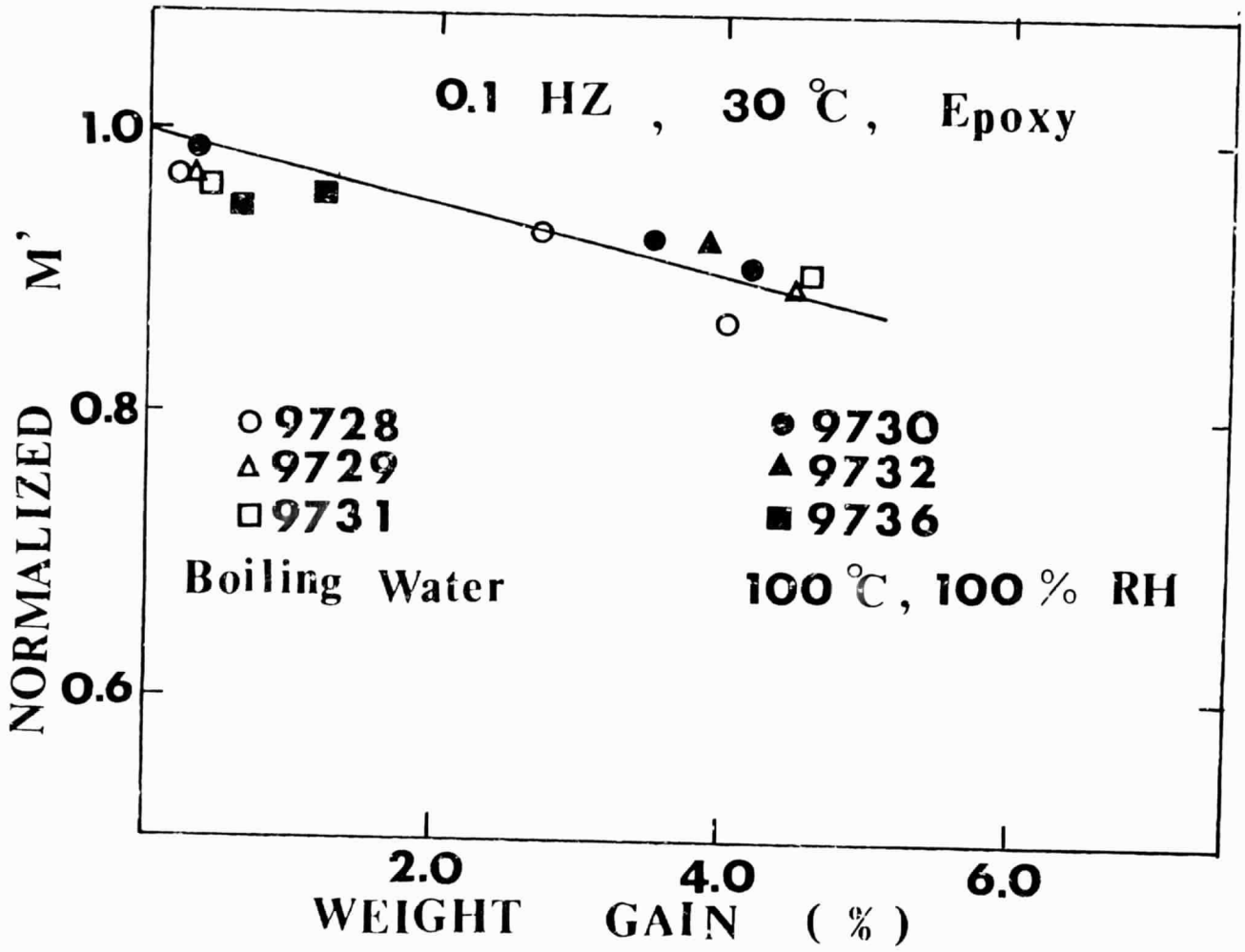

Figure III-B-5. Normalized In-Phase Modulus as a Function of Moisture Weight Gain for Postcured Epoxy Exposed to Boiling Water or Water Vapor

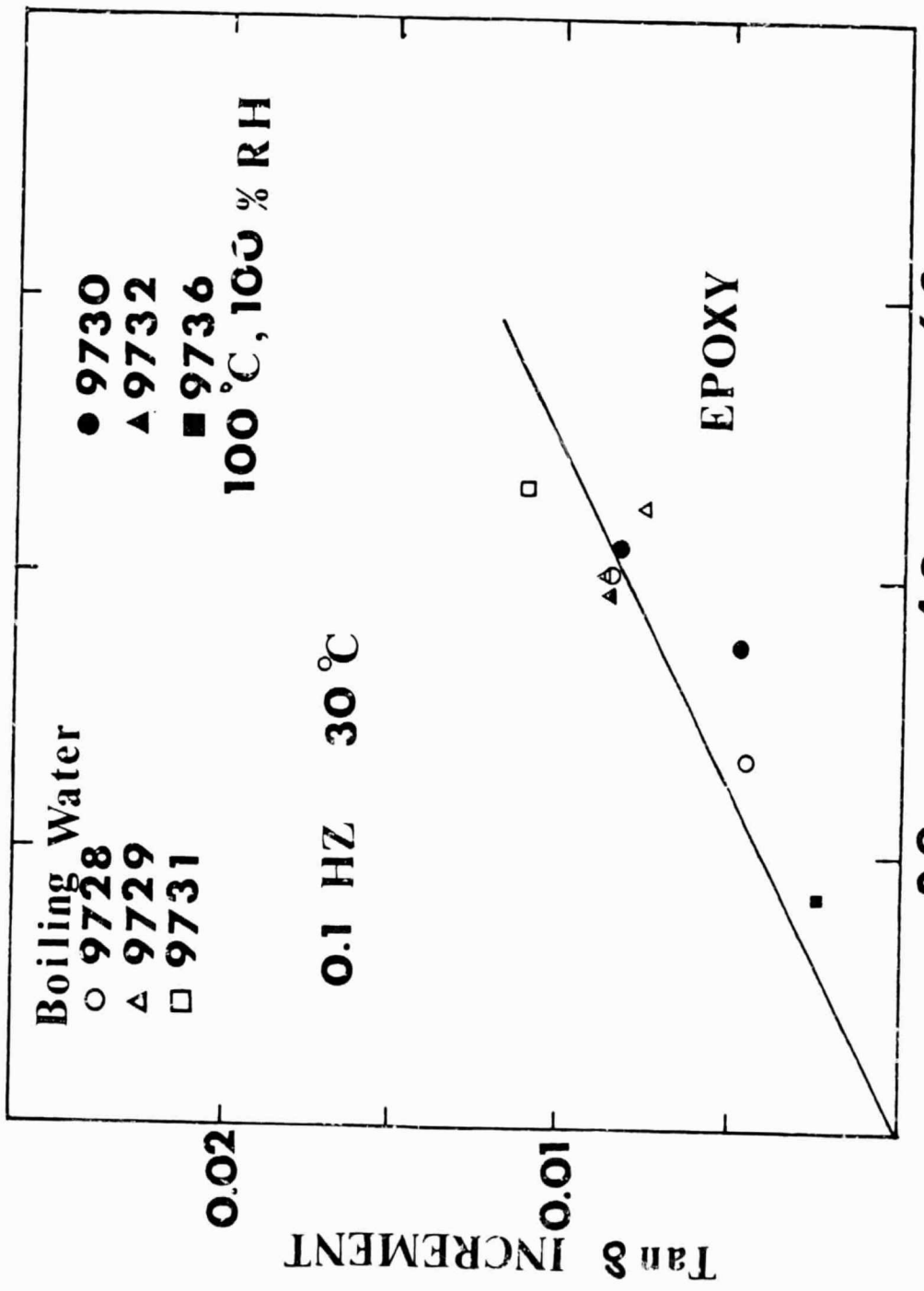

Figure III-B-6. Loss Factor Versus Moisture Content for Postcured Epoxy Exposed to Boiling Water or Water Vapor

postcured and as-cured samples. A micrograph of a dry, thin film (0.3mm) of as-cured epoxy is shown at 100 magnification in Figure III-B-7. The light intensity pattern suggests that epoxy resin is not a homogeneous material. The birefringence pattern produced after the postcuring process is shown in Figure III-B-8. The drastic difference between those two patterns indicates that the postcuring process induces a large variation in the network structure, and the light intensity pattern for postcured samples (see Figure III-B-8) bears no resemblance to the pattern for as-cured samples (shown in Figure III-B-7). It is believed that further crosslinking occurred during the postcuring process.

The birefringence pattern of a postcured epoxy resin sample exposed to a six-hour boiling water environment is shown in Figure III-B-9. The wet sample shows a pattern with a higher intensity, yet the pattern retains the same characteristics as that of the dry sample. This indicates that the swelling process in the postcured sample is different from that in the as-cured sample. In the as-cured case, the light intensity pattern of wet samples is characterized by a) the complete extinction along the polarizer and analyzer axis, b) approximate symmetry of the four quadrants, c) maximum interfacial retardation and d) decay of retardation with distance from the interface (between precipitate and surrounding matrix). All of this may be seen in Figure III-B-10.

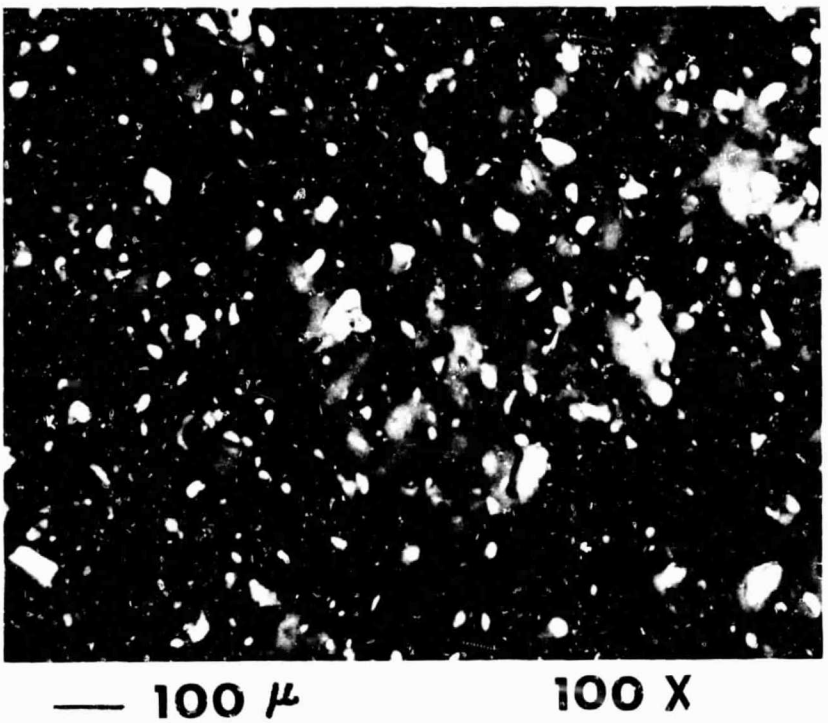

Figure III-B-7. Birefringence Pattern of As-cured Epoxy

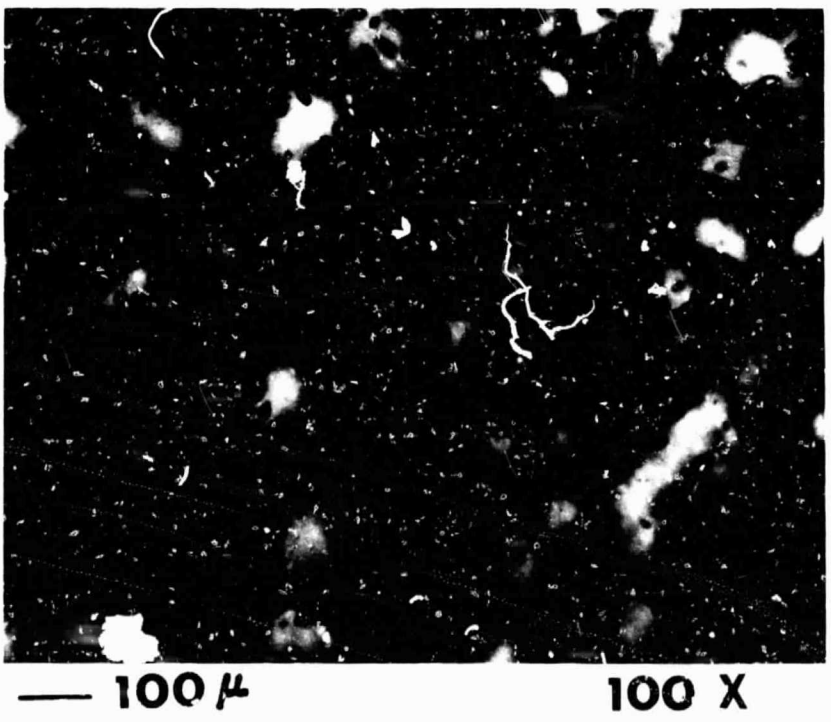

Figure III-B-8. Birefrengence Pattern of Postcured Epoxy

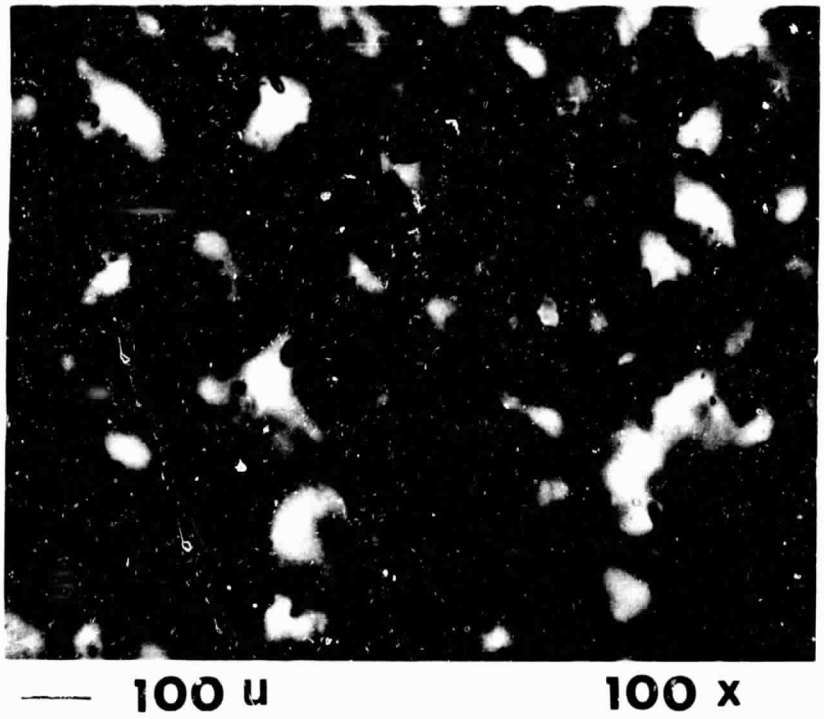

Figure III-B-9. Birefringence Pattern of Postcured Epoxy Exposed to Boiling Water for 6 Hours

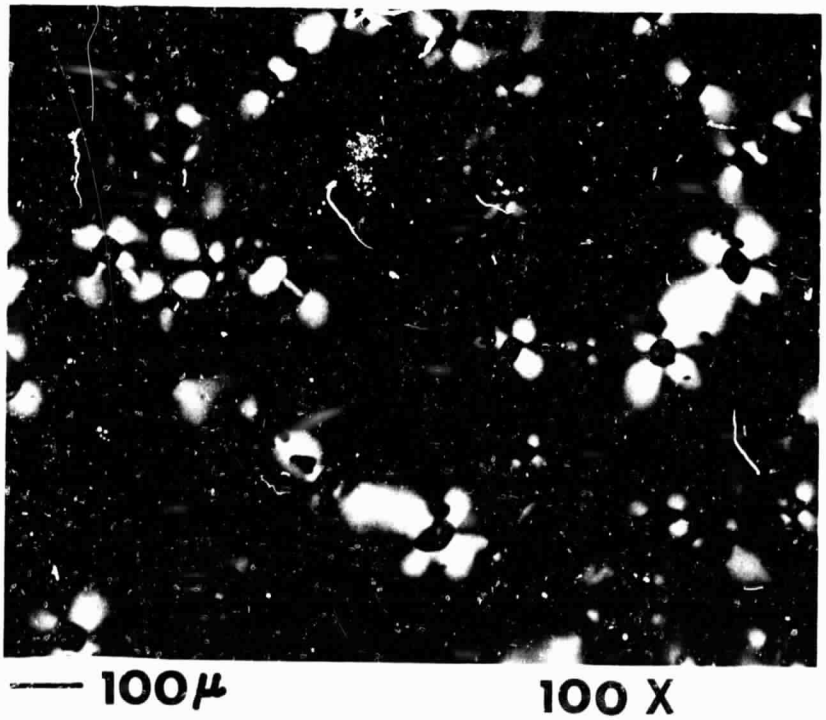

Figure III-B-10. Birefringence Pattern of As-cured Epoxy Exposed to Boiling Water for 6 Hours

The birefringence pattern of postcured samples, when the samples are redried, is shown in Figure III-B-11. The variation in birefringence is minimal. The reversibility and retention of light intensity pattern of postcured samples thus strongly support the results obtained in dynamic mechanical testing as presented earlier.

The dynamic mechanical data and birefringence patterns suggest that the effects of moisture and temperature on mechanical performance of postcured samples are minimal. The reversibility of moisture effects on mechanical properties of postcured samples suggests that plasticization and swelling are the major processes which occur upon exposure to moisture. All this suggests that the postcuring process is beneficial and necessary, in the sense that mechanical properties are retained under the same hostile environment which reduces the mechanical performance of as-cured samples.

In order to confirm the phenomena observed for postcured samples, a similar set of experiments was performed with postcured samples exposed for various periods of time to 100°C in an environment with 100% relative humidity (as opposed to a boiling water environment). The results are shown in Figures III-B-1,3,5 and 6. The dynamic mechanical data and polarized light micrographs indicate that the moisture effects on mechanical properties of postcured samples is the same regardless of the different states of moisture environment (boiling water versus water vapor at 100°C).

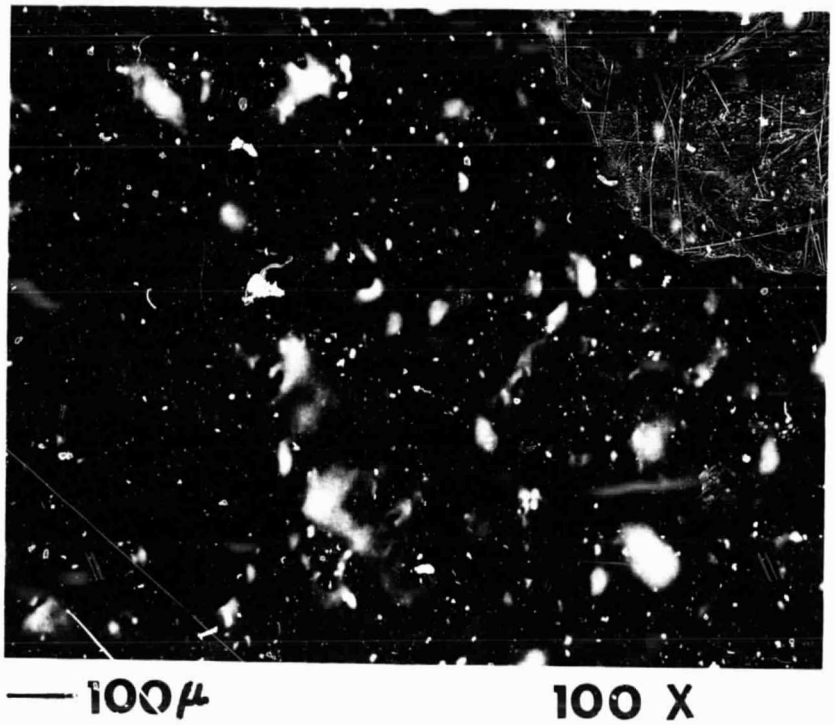

Figure III-B-11. Birefringence Pattern of Redried, Postcured Epoxy

4. Plans for Upcoming Period

It is clear that the structure-moisture interaction is a complicated phenomenon. To further quantify structure-moisture interactions, studies on the theoretical aspects of inhomogeneous swelling upon moisture absorption will be undertaken. The results to date suggest strongly that inhomogeneous swelling phenomena associated with the fiber-matrix interface, especially for the as-cured matrix, are the dominant effects governing moisture-induced damage in carbon-epoxy laminates.

5. Current Publications or Presentations by Professor Sternstein on this Subject

"Viscoelastic Characterization of Neat Resins and Composites"

Presented at Workshop on Toughening of Composites, NASA/Langley, May 24-26, 1983.

"Mechanical Characterization of Neat Resins and Composites"

Presented at Cleveland Symposium on Macromolecules, Case Western Reserve University, Cleveland, OH, June 13-15, 1983.

III-C THEORY OF INHOMOGENEOUS SWELLING IN EPOXY RESIN

Senior Investigator: S. S. Sternstein

1. Introduction

The objective of this research is to develop analytical procedures to predict the internal strain, stress and moisture fraction fields of inhomogeneous swelling produced by absorption of water in epoxy and epoxy based materials. The morphology of highly crosslinked, thermosetting network polymers like cured epoxy resin is not homogeneous, and it contains domains whose physical and/or chemical properties are different than those of the surrounding regions. These domains are mostly nodular regions of different crosslink density and are produced during curing processes due to factors such as improper mixing of reagents, excessive intranodular reaction, incipient formation of nodules before macrogelation and thermodynamically directed partial segregation. Also, the network polymers contain microvoids, air pockets, microcrystalline regions etc. When such a polymer absorbs a solvent, swelling of the network is no longer homogeneous and isotropic but rather inhomogeneous. This inhomogeneous swelling causes internal stress, strain and solvent fraction fields in the epoxy resin. This work is aimed at a quantitative evaluation of these effects.

2. Status

A detailed analysis of the nature of epoxy-water interaction has been conducted, and the intrinsically nonlinear

constitutive equation relating stress, strain and volume fraction of liquid in the swollen polymer at equilibrium with surrounding environment developed. Equations for inhomogeneous swelling in polymeric material with an isolated spherical inhomogeneity (see Figure III-C-1) were then derived for the case of zero external load, using conditions of local stress equilibrium. The inhomogeneity in this work is characterized by a single material gradient parameter, ρ, defined as a material property, of which the elastic and/or mixing behavior of inhomogeneity are functions. The numerical solution of the equations for Narmco 5208 epoxy resin (a resin more or less representative of the various structural epoxies in current use, in equilibrium with surrounding atmosphere of 100% relative humidity at 25°C) was obtained and results presented in the previous progress report for positive and negative Gaussian structural fluctuation fields and a positive Gaussian field dispersed in a negative fluctuation field.

3. Progress During Report Period

Additional studies have now been conducted to further investigate the effect of structural variation distributions on stress and water volume distributions. Figure III-C-2 shows some of these typical structural fluctuation fields, and Figures III-C-3 and 4 show the corresponding tangential and radial stress fields associated with those fluctuations. (Please refer to the previous report for definition of reduced radius and other details.)

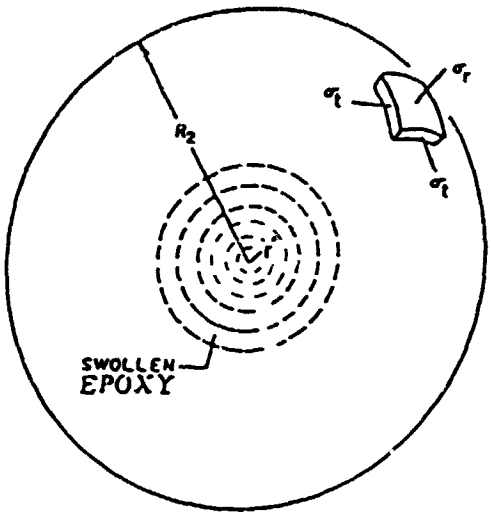

Figure III-C-1. Schematic of the Spherically Symmetrical Stress Field Produced by Swelling of Network Polymer of Outer Radius R_2 which Contains an Inhomogeneity of Characteristic Radius r

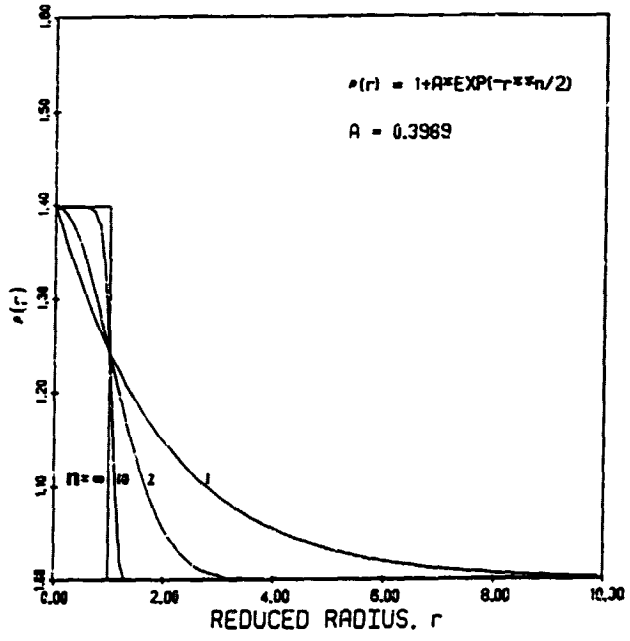

Figure III-C-2. A Few Typical Positive Structural Fluctuation Fields Possible in Cured Epoxy Resin

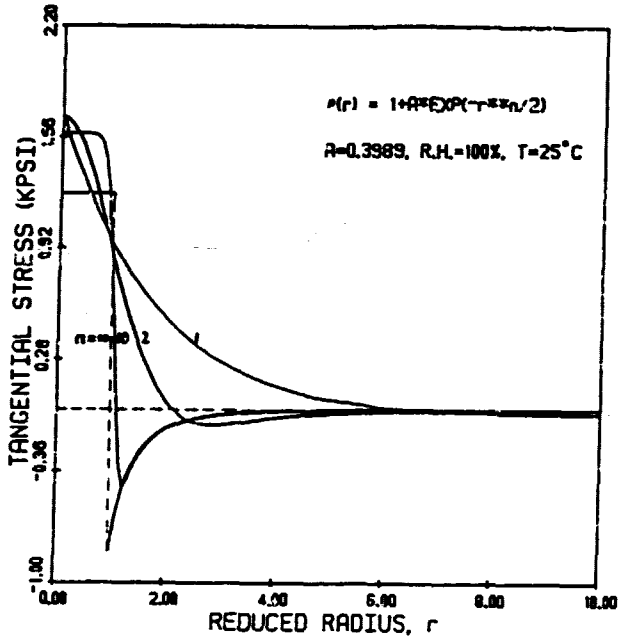

Figure III-C-3. Tangential Stress Distribution Associated With the Deformation Fields Shown in Figure III-C-2

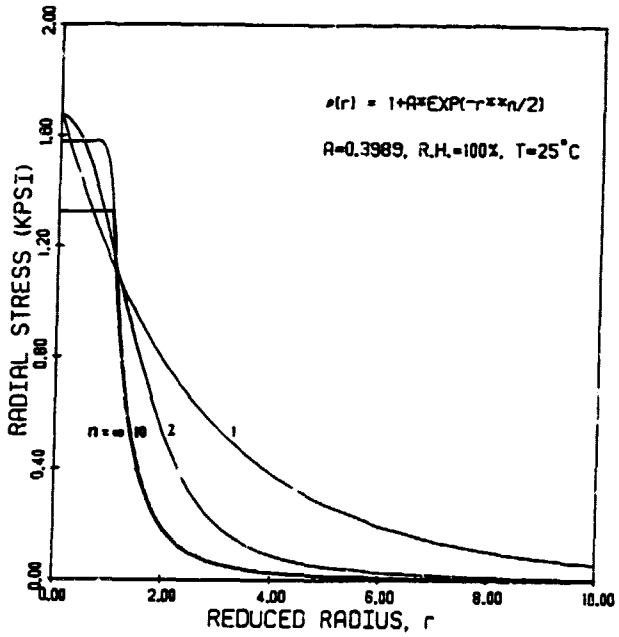

Figure III-C-4. Radial Stress Distribution Associated With the Deformation Field Shown in Figure III-C-2

Figure III-C-6 shows the stress fields produced due to the fluctuation field shown in Figure III-C-5. The stress fields produced clearly tell us that both a large positive mean normal stress causing cavitation, and octahedral shear stress favoring shear yielding (if possible), are caused by these fluctuation fields. These figures also show that the value of stress at any point not only depends on the value of a fluctuation parameter $\rho(r)$ at that point but also on the gradient of $\rho(r)$ in a small region surrounding that point.

Figures III-C-7 and 9 show two other kinds of inhomogeneities possible in epoxy or epoxy-based materials, and Figures III-C-8 and 10, respectively, show the stress field asscciated with these two kinds of inhomogeneities. It is important to note here that interaction between swelling fields of two inhomogeneities are not considered. As has been shown by Lumban-Tobing*, such considerations increase the magnitudes of stress produced. The magnitude and nature of these internal stresses are conducive to producing damage by themselves or in combination with stresses due to relatively small external loads (the two are not simple additive), and it is important to keep these facts in mind in designing any structural component with epoxy or epoxy-based materials.

---

*"Finite Element Analysis of Moisture Effects in Graphite-Epoxy Composites", F. E. R. Lumban-Tobing, M. Shephard and S. Sternstein. Symposium on Advances and Trends in Structural and Solid Mechanics, Wash., D.C., Oct. 4, 1982. (Also Computers and Structures, 16, Nos. 1-4, 1983, pp. 457-469)

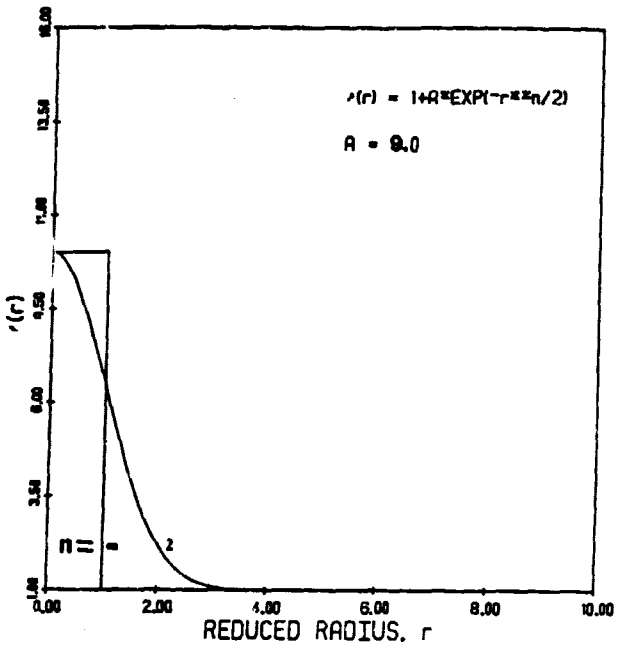

Figure III-C-5. Structural Fluctuation Fields of Nature Similar to Those in Figure III-C-2 but of Higher Magnitude

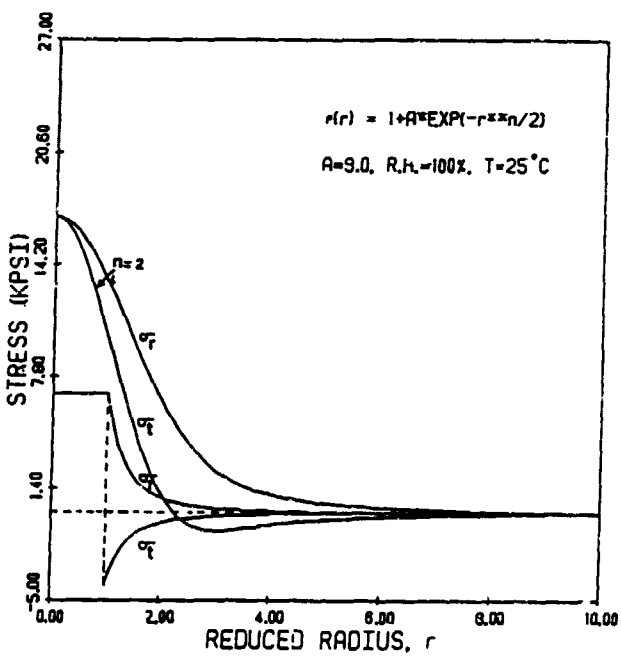

Figure III-C-6. Stress Fields Associated With Fluctuation Fields Shown in Figure III-C-5

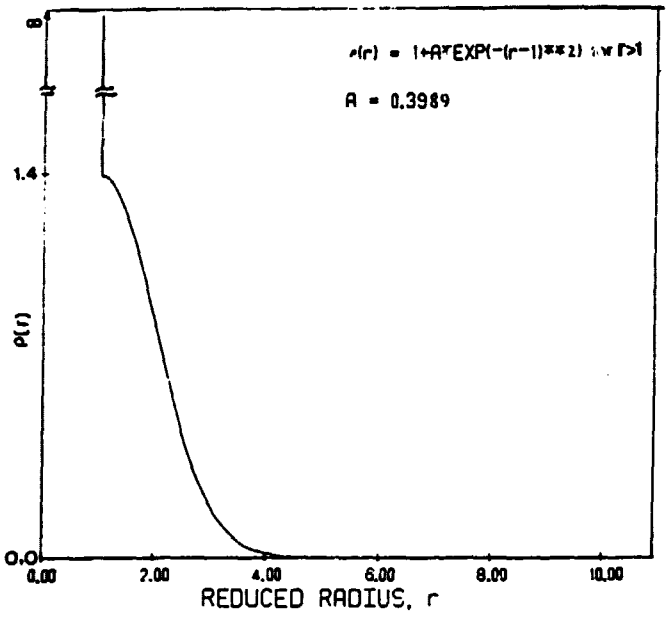

Figure III-C-7. Schematic of a Rigid, Nonswelling Inclusion Surrounded by a Positive Gaussian Fluctuation Field

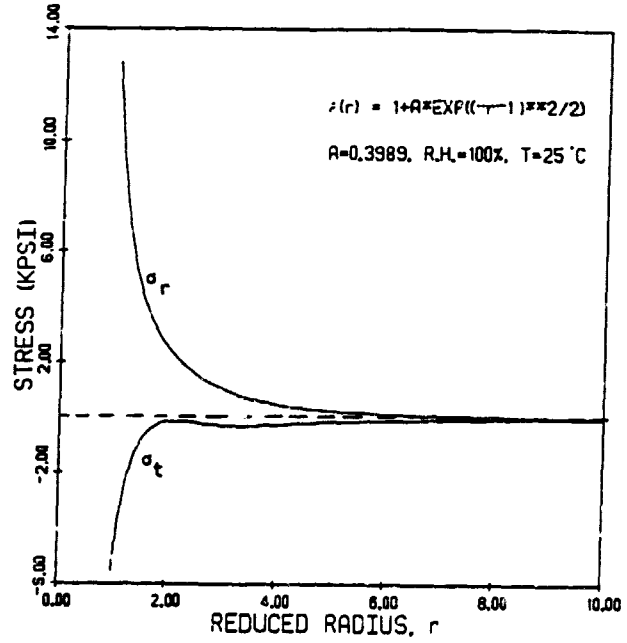

Figure III-C-8. Stress Fields Associated With the Fluctuation Field Shown in Figure III-C-7

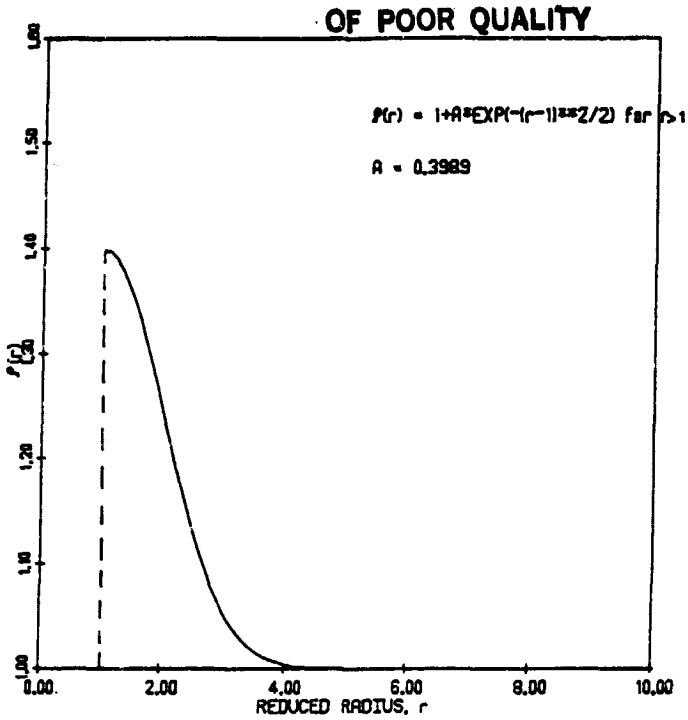

Figure III-C-9. A Spherical Microvoid Surrounded by a Concentric Positive Gaussian Fluctuation Field

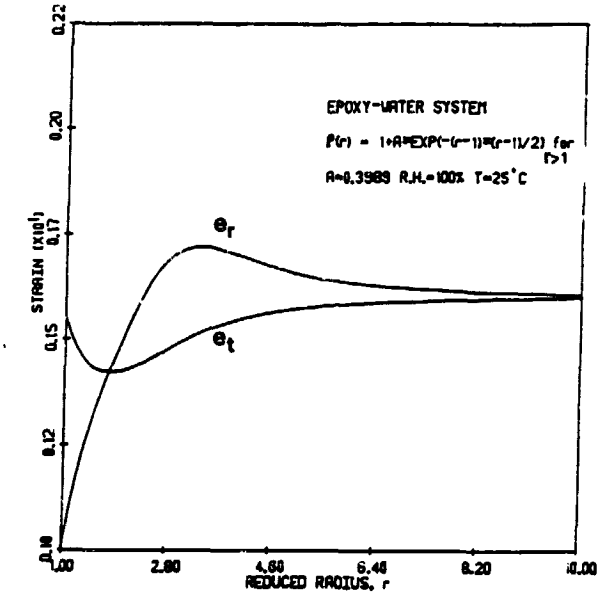

Figure III-C-10. Stress Fields Associated With the Fluctuation Field Shown in Figure III-C-9

4. Plans for Upcoming Period

Although the present study is the best approximation possible from the small amount of data available and within the capabilities of presently developed fundamental theories, this work leads to the conclusion that much remains to be done on both experimental and theoretical fronts in order to understand the mechanism of inhomogeneity formation and water absorption in cured epoxy. Dynamic mechanical and dielectric studies at low temperatures have a great potential for throwing light in that direction. Also, a detailed and carefully executed study to investigate the effects of temperature on the nature of equilibrium isotherms is crucial. Based on literature review and work in this laboratory, it is felt that a proper mixing of epoxy resin and curing agent and postcuring of the epoxy will help to minimize the problems due to absorption of water. We do not anticipate further work in this area, at this juncture, and upon publication of the conclusions summarized here, we plan to terminate this phase of our research.

5. Current Publications or Presentations by Professor Sternstein on this Subject

"Inhomogeneous Swelling Theory and Applications"

Presented at Gordon Conference on Thermosets, New Hampton, NH, August 22-26, 1983.

III-D NUMERICAL INVESTIGATION OF THE MICROMECHANICS OF COMPOSITE FRACTURE

Senior Investigator: M. S. Shephard

1. Introduction

To understand the mechanisms of failure in composites, it is necessary to develop insight into their micromechanical behavior, including interactions between matrix and fibers as the load is increased from zero to that corresponding to failure. Investigating these phenomena, either experimentally or numerically, is difficult. The purposes of this project, being carried out by graduate student Nabil Yehia, are to develop the nonlinear finite element analysis capability required for composites and to perform numerical investigations of significant examples of micromechanical failure in them.

2. Status

A generalized program for the two dimensional analysis of static crack growth problems is being developed. It is being used to conduct a detailed examination of fracture criteria and to develop new criteria needed to track cracks in composites at the micromechanical level. In addition, fully automatic finite element mesh generation techniques are being integrated directly into the analysis functions. This is an entirely new approach in program structure; it is being done to provide a means to automatically track discrete crack growth.

3. Progress During Report Period

During the last reporting period, our effort concentrated on the (a) development of a new crack propagation algorithm based on the T-criteria and (b) study of the application of fracture criteria to debonding. In addition, modifications, such as were required to allow the modified-quadtree mesh generator to automatically generate mesh geometries appropriate for cracked geometries, were developed and implemented.* Final testing of the automatic meshing algorithm, in the presence of a crack modification, is being carried out, and this software is being integrated with the analysis routines.

a. The Fracture Criteria for Crack Propagation

It was mentioned in the last progress report that the maximum strain energy density criterion was found to be a good alternative to the minimum strain energy density criterion for the crack propagation history. Further investigations during this period, however, led us to the conclusion that the T-criterion, neither as initially presented[1]† nor as restated[2,3], can be directly used for this purpose. These further investigations[4] led to the modified T-criterion for crack propagation tracking, which is outlined in the following paragraphs.

---

*This effort was carried out by graduate student Gary Burd under support external to the subject grant.

†Numbers in brackets in this section refer to the references which are listed on page 76.

The total strain energy density, T, can be decomposed to its two components as follows:

$$T = T_d + T_v \tag{1}$$

where:

T_d = the distorsional strain energy density, and

T_v = the dilatational strain energy density.

By employing relations representing the singular stress field at the crack tip, one can express both T_v and T_d for plane stress as follows:

$$T_d = \frac{S_d}{r} = \frac{1}{r}\frac{C_d}{2\pi}\left[f_x^2 + f_y^2 - f_x f_y + 3f_{xy}^2\right]$$

$$T_v = \frac{S_v}{r} = \frac{1}{r}\frac{C_v}{2\pi}\left[f_x + f_y\right]^2 \tag{2}$$

where:

$$C_d = \frac{(1+\nu)}{3E} \quad ; \quad C_v = \frac{1-2\nu}{6E}$$

E = Young's modulus; ν = Poisson's ratio

$$f_x \triangleq K_I\left(\cos\frac{\theta}{2} - \frac{1}{2}\sin\theta\sin\frac{3\theta}{2}\right) - K_{II}\left(2\sin\frac{\theta}{2} + \frac{1}{2}\sin\theta\cos\frac{3\theta}{2}\right)$$

$$f_y \triangleq K_I\left(\cos\frac{\theta}{2} + \frac{1}{2}\sin\theta\sin\frac{3\theta}{2}\right) + \frac{K_{II}}{2}\left(\sin\theta\cos\frac{3\theta}{2}\right) \tag{3}$$

$$f_{xy} \triangleq K_I\left(\frac{1}{2}\sin\theta\cos\frac{3\theta}{2}\right) + \frac{K_{II}}{2}\left(\cos\frac{\theta}{2} - \frac{1}{2}\sin\theta\sin\frac{3\theta}{2}\right)$$

$K_I, K_{II} \triangleq$ stress intensity factors of Mode I and Mode II failures, respectively.

The T-criterion states that the crack propagation occurs in the direction of maximum dilatational strain energy density, evaluated on the elastic-plastic boundary curve. In the present approach, the von Mises yielding criterion is

employed to obtain that boundary curve as follows:

$$r_b = \frac{C_d}{2\pi T_{do}} f_{::} + f_y - f_x f_y + 3f_{xy} \qquad (4)$$

The variation of the dilatational strain energy density along this elastic-plastic boundary is given by the following relation:

$$T_v\Big|_{r_b} = \frac{C_v T_{do}\left(f_x + f_y\right)^2}{C_d\left(f_x^2 + f_y^2 - f_x f_y + 3f_{xy}^2\right)} \qquad (5)$$

and the direction of crack propagation is defined by the following two conditions,

$$\frac{\partial T_v}{\partial \theta} = 0 \qquad \text{and} \qquad \frac{\partial^2 T_v}{\partial \theta^2} < 0$$

The T-criterion then states that the fracture will initiate from the crack tip where $t_{v_{max}}$ reaches the material critical value T_{vcr}. It has been found[4] that the latter condition is not a valid one for defining the fraction load, because $T_v\Big|_{r_b}$ in Equation (5) is not a load-dependent variable and, consequently, can not be used to determine the fracture load. To solve this problem, the modified T-criterion had been proposed for use in determining the fracture load as well as the crack propagation increment due to the current applied load. Instead of looking at T_v as the controlling parameter for fracture initiation, the modified T-criterion looks at the distance from the crack tip to the elastic-plastic

boundary in the direction of propagation, i.e., $r_b\big|_{\theta o}$ as the controlling parameter for fracture initiation and propagation. In other words, the second part of the T-criterion will be modified to state that the fracture will initiate from the crack tip when $r_b\big|_{\theta o}$ reaches the material critical value r_{bcr}. The modified T-criterion, denoted by R, is compared to the minimum strain energy density criterion, S, in Figure III-D-1, for predicting the fracture locus under tension, and in Figure III-D-2, for predicting the fracture load for a slant crack problem. It is interesting to note that such curves for the modified T-criterion can not be obtained from the original T-criterion statement[2,3]. It is also noted that the general trend of the R-curves is in agreement with those of the S-curves obtained by using the minimum strain energy criterion[5]. A complete comparison will be available shortly[6].

Another comparison of the S-criterion and the modified T-criterion has been carried out for a slant crack problem. The results appear in Figure III-D-3, where the angle β, between the crack and the applied load, is taken as 40 degrees. The associated finite element mesh is shown in Figures III-D-4a and 4b. Table III-D-1 summarizes the results obtained for both cases when the applied load is tension and compression. The following trends are noted from the data in this table for the finite element mesh considered.

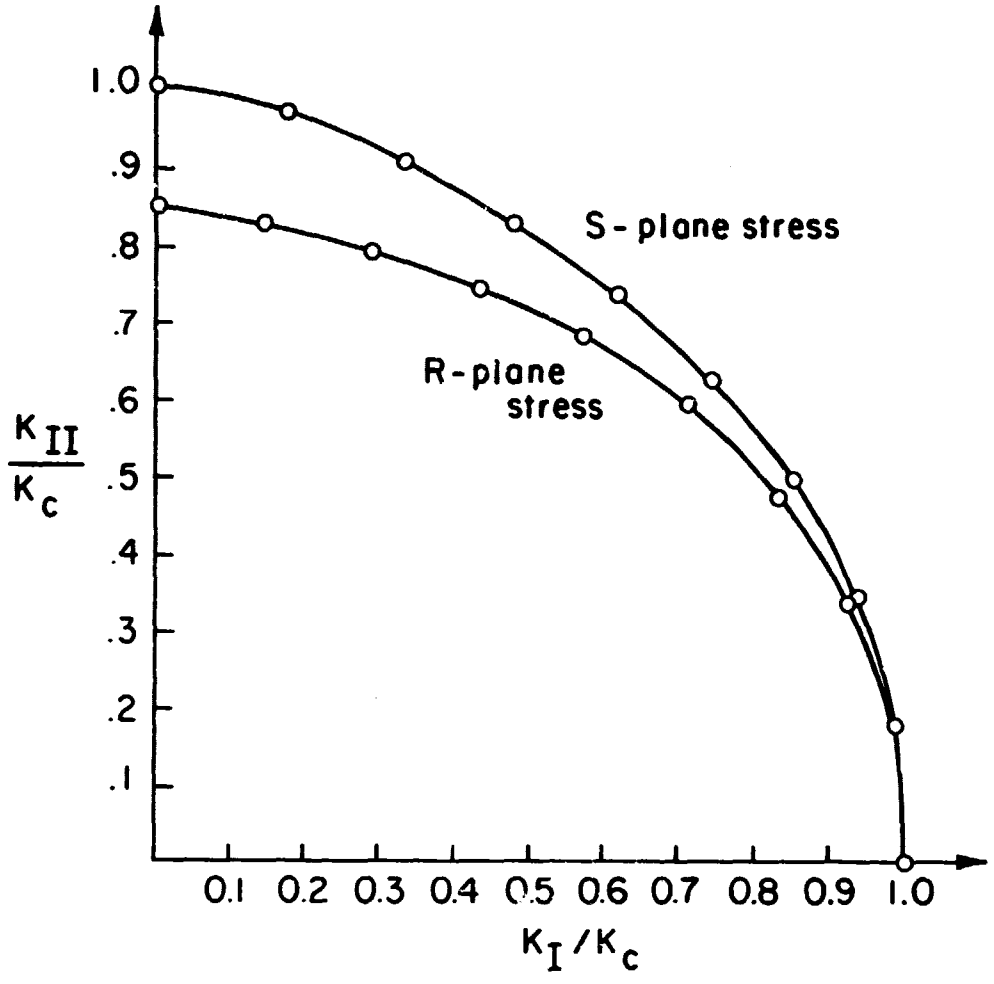

Figure III-D-1. Fracture Loci for Slant Crack Problem Under Remote Tension

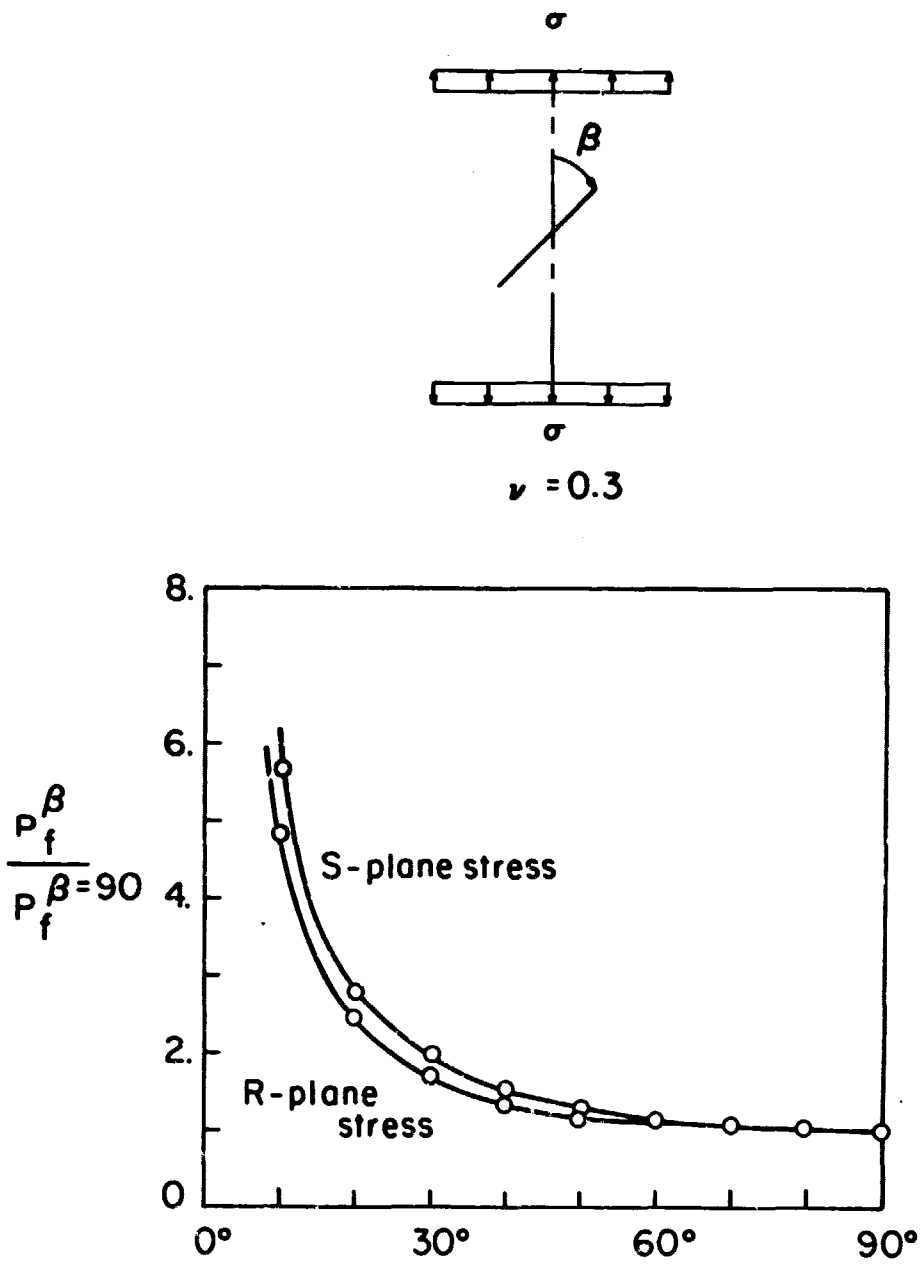

Figure III-D-2. Fracture Load for Slant Crack Problem Under Remote Tension

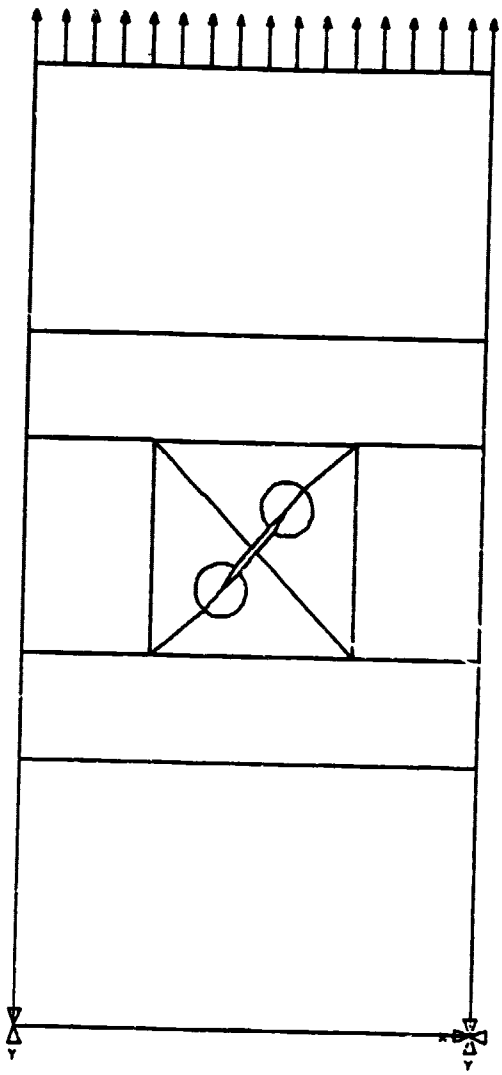

Figure III-D-3. Basic Geometry and Attributes for Slant Crack Problem

b) mesh around the crack tip

a) mesh away from the crack tip

Figure III-D-4. Finite Element Mesh for the Slant Crack Problem

TABLE III-D-1

COMPARISON OF RESULTS OBTAINED USING S AND T FRACTURE CRITERIA

Applied Load / Stress Intensity Factors	Tension			Compression		
	Disp. Corr.	Disp. Extr.	Exact*	Disp Corr.	Disp. Extr.	Exact*
$K_{I_{av}}$	4.099	3.901	3.922	-4.009	-3.901	-3.922
$K_{II_{av}}$	4.236	4.25	4.658	-4.236	-4.25	-4.658
Criterion Used						
S^{**}: $\theta_{o_{av}}$	-53.79°	-54.86°	-56.58°	+116.9°	+115.6°	+113.45°
S^{**}: P_{cr}	0.154	0.157	0.148	0.279	0.274	0.245
T: $\theta_{o_{av}}$	-60.47°	-61.81°	-63.98°	+138.2°	+136.8°	+134.65°
T: P_{cr}	0.153	0.155	0.146	0.153	0.155	0.194

*The 'exact" values presented for $\theta_{o_{av}}$ and P_{cr} are those obtained if the K_I and K_{II} values are used in the corresponding criteria.

**S-Criterion predictions depend on the assumed size of the core region.

1) As the error in evaluating K_I and K_{II} increases, so does the error in evaluating θo.

2) As the error in evaluating K_I and K_{II} increases, the error in evaluating the fracture load P_{cr} increases, in the case of compression and decreases, in the case of tension.

3) The error in evaluating the stress intensity factor, K_I, using displacement correlation technique[7] is greater than the error produced using the displacement extrapolation technique[8]. In both cases, the error associated with evaluating K_{II} is much bigger than the error associated with K_I.

b. Debonding at Bimaterial Interface

Debonding at a fiber-matrix interface may occur due to (a) failure in the matrix material adjacent to the interface, (b) failure in the fiber material adjacent to the interface, or (c) debonding of the interface between fiber and matrix. In some cases, this interface bonding material could have been formed during the fabrication and curing processes by adding a third, very thin homogeneous layer at the interface[9]. In these circumstances, since it is most likely that debonding will occur in this very thin layer, one can use the above mentioned modified T-criterion to determine the debonding distance at the interface, provided the following assumptions are acceptable:

1) The bonding material is too thin to be represented in the finite element mesh.

2) The stress intensity factors can be calculated from the two major materials at the interface.

3) The thin bonding material is isotropic and is only considered when studying the debonding process.

4) There is an analogy between debonding at the crack tip and the plastic zone in plastically deformable materials. This assumption has been successfully used in studying the damage zone of glass-resin composites on the macro scale[10].

5) The crack can only propagate along the interface and cannot change its axis to enter any of the materials at the interface sides.

The last assumption is a restriction necessitated because the exact stress field at a crack tip in the neighborhood of a bimaterial interface is not made use of in the fracture criterion. This was also the reason for adopting the third assumption.

If the above mentioned assumptions are acceptable, one can determine the crack propagation distance along the interface, i.e., the damage distance, using Equation (4) as:

$$r_d = \frac{C_d}{2\pi T_{do}}\left(f_x^2 + f_y^2 - f_x f_y + 3f_{xy}^2\right) \qquad (6)$$

where:

$$T_{do} = \frac{\sigma_t^2}{3} \qquad \text{or} \qquad T_{do} = \tau_{all}^2$$

σ_t: bonding material tensile strength

τ_{all}: bonding material shear strength

The critical damage zone distance r_{dcr} can be obtained by assuming the fracture is dominated by Mode I behavior at the interface (i.e., $\frac{K_{II}^2}{K_I^2} << \frac{1}{3}$). In this case:

$$r_{dcr} = \frac{C_d}{2\pi T_{do}} \cdot K_{IC}^2 \tag{7}$$

The crack along the interface will propagate if $r_d > r_{dcr}$. It should be noted that σ_t, τ_{all} and K_{IC} have been known for the bonding material a priori. This last approach is currently under investigation.

c. Automatic Meshing in the Presence of Crack Growth

As indicated in the previous report, several modifications are being made to the modified-quadtree mesh generator[11] for use in tracking crack growth. Complete details of the new meshing algorithms and the improved data structures are given in G. S. Burd's Masters Thesis[12]. Only an example demonstrating the resulting mesh is given here.

Figure III-D-5a shows a plate with a crack in it. Figure III-D-5b shows the mesh automatically generated for that plate. The mesh generated includes a ring of singular elements around the crack tip and has the mesh grading away from that point. Figure III-D-6 shows the same plate and resulting mesh after the crack has been propagated.

b) finite element mesh

a) crack geometry

Figure III-D-5. Cracked Plate Example

b) finite element mesh

a) crack geometry

Figure III-D-6. Crack Plate Example With Additional Crack Propagation

4. Plans for Upcoming Period

During the next reporting period, effort will concentrate on (a) finalizing the integration of the fully automatic meshing algorithms with the analysis procedures and (b) carrying out additional micromechanics analyses.

5. References

1. Theocaris, P. S and N. P. Andrianopoulos, "The Mises Elastic-Plastic Boundary as the Core Region in Fracture Criteria", Eng. Fract. Mech., 16, No. 3, 1982, pp. 425-432.

2. Theocaris, P. S. and N. P. Andrianopoulos, "The T-Criterion Applied to Ductile Fracture", Int. J. of Fract., 20, 1982, pp. R125-R130.

3. Theocaris, P. S., G. A. Kardomateas and N. P. Andrianopoulos, "Experimental Study of the T-Criterion in Ductile Fractures", Eng. Fract. Mech., 17, No. 5, 1982, pp. 439-447.

4. Yehia, N. A. B. and M. S. Shephard, "The T-Criterion for Predicting the Crack Propagation Growth Increment", in preparation.

5. Sih, G. C., "Strain-Energy Density Factor Applied to Mixed Mode Crack Problems", Int. J. Fracture, 20, No.3, September 1974, pp. 305-321.

6. Yehia, N. A. B., "In the Use of the T-Criterion on Ductile Fracture", in preparation.

7. Ingraffea, R. A. and C. Manu, "Stress-Intensity Factor Computation in Three Dimensions with Quarter-Point Element", Int. J. Num. Meth-Engr., 15, 1980, pp. 1426-1445.

8. Pu, S. L., M. A. Hussain and W. E. Lorenson, "The Collapsed Cubic Isoparametric Element as a Singular Element for Crack Problems", Int. J. Num. Meth. Engrg., 12, 1978, pp. 1727-1742.

9. Diefendorf, R. J., personal communications.

10. Gaggars, S. and L. J. Broutman, "The Development of a Damage Zone at the Tip of a Crack in a Glass Fiber Reinforced Polyester Resin", Int. J. Fracture, 10, 1974, pp. 606-608.

11. Yerry, M. A. and M. S. Shephard, "A Modified Quadtree Approach to Finite Element Mesh Generation", IEEE Computer Graphics and Application, 3, No. 1, 1983, pp. 39-46.

12. Burd, G. S., Masters Thesis, Department of Mechanical Engineering, RPI, in preparation.

6. Current Publications or Presentations by Professor Shephard on this Subject

"Computer Graphics in the Development of an Automatic Three-Dimensional Mesh Generator"

Published in Recent Advances in Engineering Mechanics and Their Impact on Civil Engineering Practice, Vol. 1, ASCE, New York, May 1983, pp. 110-113.

Presented at 4th Engng. Mech. Div. Special Conf., Purdue University, May 24, 1983.

"Finite Element Mesh Generation for Use with Solid Modeling and Adaptive Analysis", with M. A. Yerry.

To appear in Proceedings of G. M. Research Labs. Conf. Solid Modeling by Computers: From Theory to Applications, 1983.

Presented at G. M. Research Labs. Int. Sym. on Solid Modeling by Computers, G. M. Research Labs., Detroit, Sept. 26, 1983.

"Automatic Three-Dimensional Mesh Generation by the Modified-Octree Technique", with M. A. Yerry.

To appear in Int. J. Num. Meth. Engng.

"Linear Multipoint Constraints Applied via Transformation as Part of a Direct Stiffness Assembly Process"

To appear in Int. J. Num. Meth. Engng.

III-E FREE-EDGE FAILURES OF COMPOSITE LAMINATES

Senior Investigator: T. L. Sham

1. Introduction

The failure of structural composite laminates is a very complex phenomenon, because different mechanisms control the failure events at different size scales. As one example, failure can occur at the structural level as a result of the catastrophic loss of global stiffness of the structure at a certain critical load. However, the same structural composite component may fail at the local level by delamination at the ply interface, translaminar cracking and fiber splitting etc. For structures under service conditions, these failure mechanisms do not usually occur in isolation, but rather, they are coupled in a very complicated way. For example, interply delamination could lead to intralaminar cracking or vice versa, or these failure mechanisms could take place in a convoluted manner. The complexity and the interlocking nature of the failure mechanisms in composite laminates prohibit a comprehensive study of the detailed evolution of all of these failure events. It can still be fruitful, however, to treat each individual mechanism separately and to understand the mechanics involved, be it at the macroscopic or microscopic level, for each failure mode.

The specific failure mechanism under study in this newly initiated research is that of the free-edge delamination of

graphite/epoxy composite laminates. Due to the presence of steep stress gradients (especially in the thickness direction of the laminate), in localized regions where lamina interfaces meet the traction free surface of the laminate, together with the relatively low ductility of the matrix material (resin), delamination from the free edge is one of the more important modes of failure in composite laminates. It is worth noting that free edges are present in almost every composite structure; for example, a free edge is formed whenever a hole is drilled. The immediate objective of this research is to obtain global parameters that characterize the initiation of the free-edge delamination process.

2. Status

This is a new project and was started on May 1, 1983.

Recent theoretical stress analyses[1-3]* of perfectly bonded unidirectional laminae with different fiber orientations reveal that the stresses are singular at the point where the interface intersects the free edge. Depending on the fiber orientations and the stacking sequence of the laminae, the stress singularities are of the power type (exceedingly weak) and/or the logarithmic type. However, it does not seem plausible that a single-parameter characterization of the stress field near the free edge, in the same spirit as the stress intensity factor of Linear Elastic Fracture Mechanics (LEFM), could be judiciously chosen from

*Numbers in brackets in this section refer to the references which are listed on page 82.

the singular stress field. Further, the use of the amplitude factors from the singular stress field to characterize the initiation of free edge delamination is further clouded by the small region of dominance of the singular terms in the field, which is of the order of the fiber thickness or less.

Another school of thought, as represented by Wang, Crossman and co-workers[4-7], takes the view that microflaws are inherently present in composite laminates. A proper continuum idealization of a composite laminate would then involve not only the smearing-off of the discrete identities of individual fibers and matrix material within the ply, but also a representation of microflaws in the continuum idealization. Hence, an empirically defined "effective" crack size is introduced, and the energy release rate concept of LEFM is applied to the hypothetical crack to obtain critical conditions for the onset of free-edge delamination. The prediction of critical loads at the onset of free-edge delamination is reported to correlate well with the experiment. However, the choice of the "effective" size for the hypothetical crack appears to be rather arbitrary.

3. Progress During Report Period

A different viewpoint is taken by this investigator in examining the initiation of free-edge delamination. The approach adopted is that of continuum mechanics, with each lamina idealized as homogeneous and anisotropic. The ply

interface is treated as a surface of discontinuity where the components of the elasticity tensor, with respect to the stressing direction, undergo a "jump". Continuity of the displacement vector and traction vector across the interface is enforced. A generalized plane strain, elastic boundary value problem has been set up on this basis, corresponding to a composite laminate with symmetric lay-ups under in-plane loading conditions. Energy variation with load and/or geometry of such a body is being considered.

4. Plans for Upcoming Period

The analysis of the energy variation for the problem formulated above will be continued during the next reporting period.

5. References

1. Wang, S. S. and I. Choi, "Boundary-Layer Effects in Composite Laminates: Part 1 - Free-Edge Stress Singularities", Journal of Applied Mechanics, 49, 1982, p. 541.

2. Wang, S. S. and I. Choi, "Boundary-Layer Effects in Composite Laminates: Part 2 - Free-Edge Stress Solutions and Basic Characteristics", Journal of Applied Mechanics, 49, 1982, p. 549.

3. Zwiers, R. I., T. C. T. Ting and R. L. Spilker, "On the Logarithmic Singularity of Free-Edge Stress in Laminated Composites Under Uniform Extension", Journal of Applied Mechanics, 49, 1982, p. 561.

4. Wang, A. S. D., F. W. Crossman and G. E. Law, "Interlaminar Failure in Epoxy-Based Composite Laminates", Proceedings of the 29th MFPG Symposium on Advanced Composites-Design and Applications, NBS, 1979, p. 255.

5. Wang, A. S. D. and G. E. Law, "An Energy Method for Multiple Transverse Cracks in Graphite-Epoxy Laminates", Modern Development in Composite Materials and Structures, J. R. Vinson, Ed., ASME, 1979, p. 17.

6. Wang, A. S. D. and F. W. Crossman, "Initiation and Growth of Transverse Cracks and Edge Delamination in Composite Laminates: Part 1. An Energy Method", Journal of Composite Materials, Supplement Volume, 1980, p. 71.

7. Crossman, F. W., W. T. Warren, A. S. D. Wang and G. E. Law, "Initiation and Growth of Transverse Cracks and Edge Delamination in Composite Laminates: Part 2. Experimental Correlation", Journal of Composite Materials, Supplement Volume, 1980, p. 88.

III-F ANALYSIS OF UNBALANCED LAMINATES

Senior Investigator: E. G. Brunelle*

1. Introduction

Unbalanced laminates are those whose properties are such that loads of one kind result in deflections of another. Examples include those for which bending moments result in torsion deflections, or where axial loads cause torsional deflections. There are many potentially useful applications in aerospace vehicle structures. Stabilizing a swept-forward wing against bending-torsion divergence, might use coupling of the first kind noted above, passive RPM control of turbo-fan blades or helicopter rotors might make use of the second.

2. Status

Bending-torsion coupling is the subject of considerable work aimed at the development of the forward swept wing. This aspect in the analysis of unbalanced laminates will be the subject of future work but is not discussed in this report. Instead, the coupling between axial loads and torsion has been chosen for analysis.

After examining several mathematical approaches, the following sequential scheme was adopted:

a) Whitney's solution for the deflection of anti-symmetric angle-ply laminates with S3 boundary conditions would be extended to find the Green's functions for in-plane "spike" loadings (Dirac Delta functions).

* On academic leave at the Air Force Institute of Technology

b) Classical methods would then be used to construct the response to axial loadings using the Green's functions.

c) The plate idealization for the structure of interest is then embedded in the larger S3 plate, and by imposing distributed generalized loadings about the blade periphery, the subject plate is forced to assume the desired CL-F-F-F boundary conditions typical of wing/turbine blade/helicopter blade applications.

This research is being carried out as part of the doctoral degree requirements of graduate student I-Horng Yang.

3. Progress During Report Period

The equations of motion for antisymmetric angle-ply composite plates with S3 boundary conditions have been solved for the associated Green's function $G_{ij}(x,y;\xi,\eta)$. Note that the first subscript, i, denotes the deflection direction, for example, $u_i(x,y)$, and that the second subscript, j, denotes the "spike" load direction, for example, $f_j(\xi,\eta)$, so that nine Green's functions are generated.

The plate response to axial load has been formulated, and some simple numerical checks are being performed. The formulation for the boundary integral technique has been completed and has been checked twice.

The paper by C. W. Pryor, Jr. and R. M. Barker entitled "Finite Element Analysis of Bending-Extensional Coupling in Laminated Composites" (J. Com. Materials, 4, October 1970)

predicts maximum deflection as a function of antisymmetric angle-ply orientation for a graphite/epoxy square plate with all edges clamped (Cl B.C.) under uniform transverse loads. The subject problem (which considers both in-plane loads and transverse loads), then has been specialized so as to compare directly with the Pryor/Barker results. That is, considering a simply-supported laminated plate, which has embedded in it the Cl B.C. plate of Pryor/Barker (as described above), the Pryor/Barker case has been solved using the method under development. If we define (see Figure III-F-1)

NML = number of boundary mesh lengths,

NIP = number of internal load points,

M,N = number of Fourier terms and

W = maximum deflection,

then, the results obtained to date from the subject computational program using the 35° ply-orientation laminate in the Pryor/Barker paper and evaluating various modelling aspects can be presented as follows:

a) Influence of Number of Fourier Terms

NML	NIP	M,N	W		Diff.
4	25	20	2.1685	>	0.7625
4	25	40	2.9310	>	0.3383
4	25	60	3.2693	>	0.2039
4	25	80	3.4732	>	0.0453
4	25	85	3.5185		

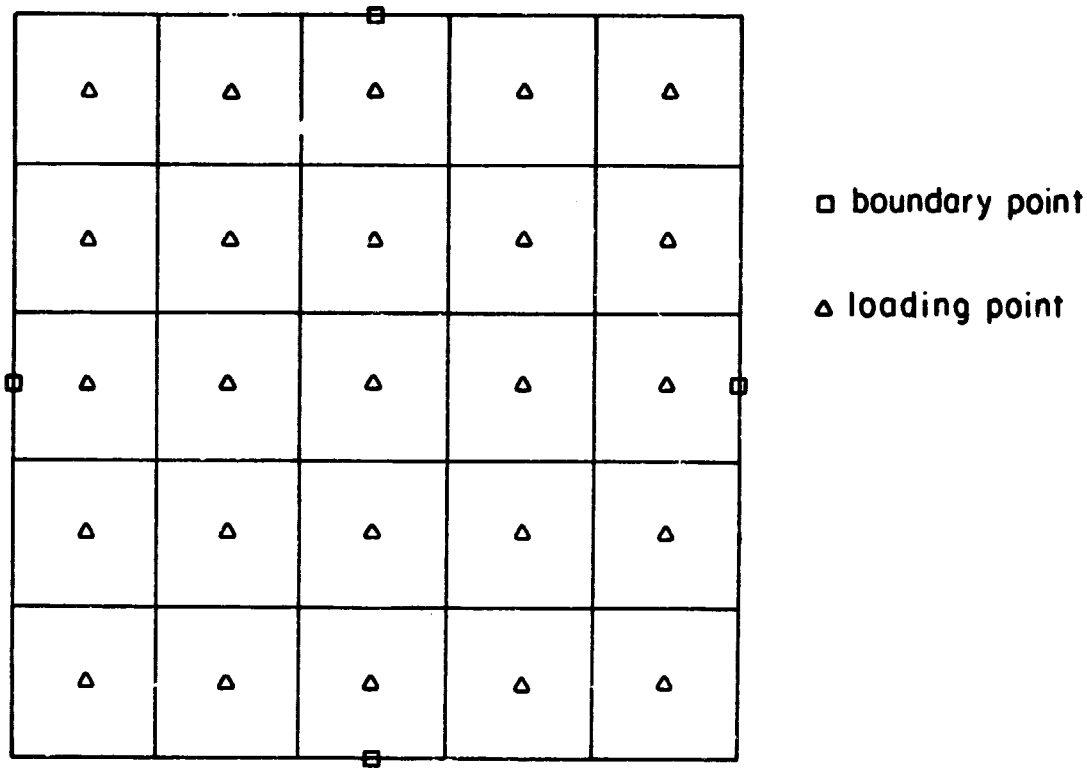

Figure III-F-1. Plate Geometry Breakdown for Analysis

b) Influence of Number of Mesh Elements

NML	NIP	M,N	W		Diff.
8	64	60	4.689	>	1.9128
16	64	60	2.7762	>	0.0909
20	64	60	2.6853	>	0.0503
32	64	60	2.635		

c) Influence of Number of Internal Load Points

NML	NIP	M,N	W		Diff.
8	25	60	4.7145	>	0.0255
8	64	60	4.689		
32	64	60	2.635	>	0.0015
32	100	60	2.6365		

d) Influence of Combination of Mesh Elements and Internal Load Points

NML	NIP	M,N	W		Diff.
8	64	60	4.689	>	1.9128
16	64	60	2.7762	>	0.1412
32	64	60	2.635	>	0.0015
32	100	60	2.6365	>	0.02
40	100	60	2.6165		

The maximum deflection in the Pryor/Barker paper is 2.76. It appears that the maximum displacement, W, converges little by little to the value of 2.62, and that NML = 40, NIP = 100 provides the most accurate answer. For other ply orientations, similar results were obtained.

4. Plans for Upcoming Period

Preliminary results for the complete problem should be available at the end of the next period. Additionally, the

current affine transformations used in the governing equations are being compared with some other possible stretching schemes.

PART IV

GENERIC STRUCTURAL ELEMENTS

IV-A COMPACT LUG DESIGN

IV-B QUANTIFICATION OF SAINT-VENANT'S PRINCIPLE FOR A GENERAL PRISMATIC MEMBER

IV-A COMPACT LUG DESIGN

Senior Investigator: D. B. Goetschel

1. Introduction

A critical aspect of many aerospace structural elements is the load transfer that takes place between the connecting lugs at the ends of the structure and the portions of the structure wherein the loads are well-distributed if not uniform. Such lugs are often highly loaded and have very complex stress states. Further, since they must mate with connecting parts, these lugs are usually designed within rather stringent dimensional envelope constraints. As compared to lugs which are made from high-strength steel, for example, meeting the geometric constraints, even with a composite structural design making maximum use of unidirectional graphite-epoxy, has proven to be a difficult task. This research is intended to solve the load-volume problem in favor of composites rather than either reverting to designs using 200 ksi steel lugs attached to a composite strut or forcing the dimensional constraints to be relaxed with a redesign of the mating parts.

The drag strut of the Lockheed L-1011 is a specific primary structure which has been taken as an example to investigate heavily loaded pinned connections. While it is readily assumed that the column aspect of the structure (see Figure IV-A-1) could be redesigned of graphite/epoxy, it is

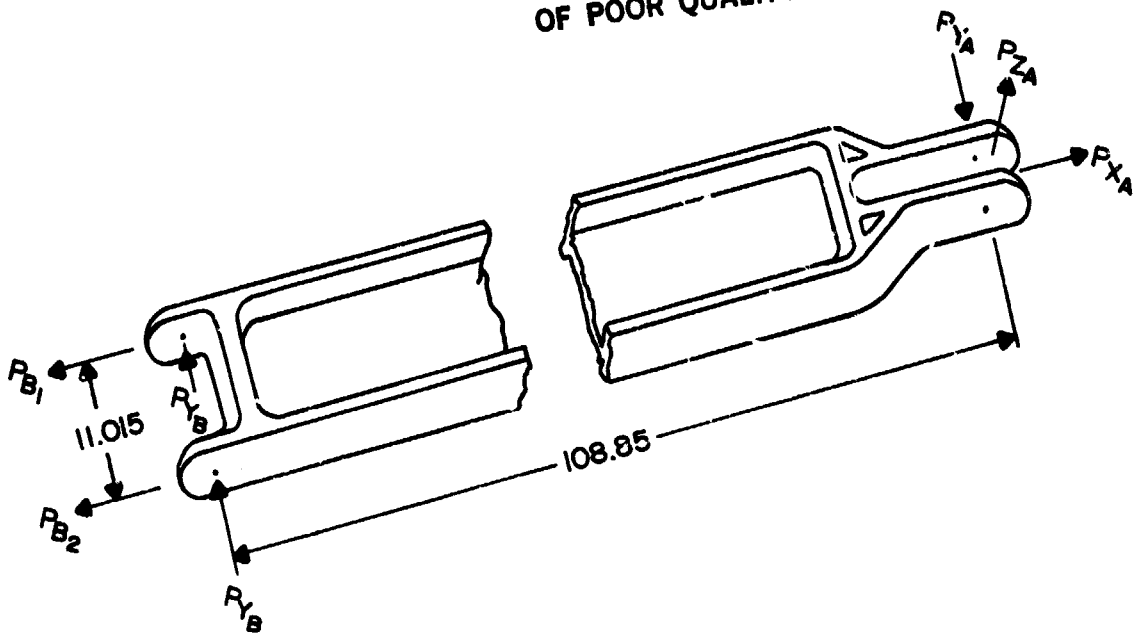

Figure IV-A-1. Lockheed L-1011 Engine Drag Strut (Schematic)

not so clear as to whether a graphite/epoxy pinned lug connection can be designed to withstand the design loads, given the original geometric constraints.

2. Status

Testing of various lug configurations has been completed. Specimens with stress relief cuts were made in a configuration that forced net tensile failure. These specimens showed a 21% increase in strength due to the slots. Further tests were performed on capstrip configurations. Problems encountered in fabricating capstrip configurations were solved with

the use of a specially designed jig. No significant increase in strength was found; various changes in the failure modes resulted, however, indicating that capstrips would probably be useful in some lug configurations. These studies were the work of graduate student Matt Cackett.

3. Progress During Report Period

Preliminary investigations were carried out to evaluate a new failure criterion for handling stress concentrations in composite parts with general, complicated geometries and loadings and to complete a very extensive literature review. All the available papers which were pertinent to this work were identified and evaluated. Where contradictions exist, conclusions were drawn as to what procedure appears to be best. This review is available[56]. Some of the conclusions from this review follow.

a. Literature Survey

As a result of the literature survey, a large number of parameters that influence strength in terms of average stress for the general case of mechanically fastened connections were identified. Of particular interest is the fact that absolute hole diameter and absolute thickness emerged, since these are unimportant parameters in the case of conventional aerospace joints. It is concluded that a generalized

---

*Numbers in brackets in this section refer to the references which are listed on page 112.

empirical description of composite joint strength cannot readily be obtained.

The stress analysis of a loaded hole in an orthotropic plate is most often performed using the finite element method. Several levels of sophistication in finite element modeling of the problem are presented in the literature. The most rigorous model of the physical case would include effects due to friction, the contact angle, pin bending, clearance and interlaminar stresses. Although no model containing all of these effects was found, a representation by Wilkinson, et al.[18] is considered to be the most sophisticated.

b. Failure Theory

A finite element program has been prepared to analyze the stress around a loaded hole in an orthotropic member. These results will now be applied using an appropriate failure theory to predict the ultimate strength of the joint. The application of joint strength analysis has typically followed the procedure:

1) Determination of basic lamina strength,
2) Determination of joint stress distribution and
3) Prediction of strength and failure modes.

A quick review of each of these steps emphasizes the difficulty involved in accurately predicting joint strength.

The basic laminar material strengths are necessary parameters in any failure analysis. In particular, the tensile and compressive strength in the direction of and transverse to the fibers and the ply shear strength are all required,

in general. Given variations in the materials themselves, in cure cycles, environmental factors, scaling effects and testing methods, determining strength indeces with accuracy is an ambitious task in itself. The fact that different researchers use different physical failure criteria (e.g., maximum load, first peak in the load/extension plot, load at which cracks become visible etc.) complicates matters further and results in inconsistent published data[42]. Untouched laminate strengths are found using these basic laminar material properties in conjunction with some failure criterion for the laminate.

The prediction of strength, in both notched and unnotched laminates is still an unsettled area of research. No particular failure criterion has been found to be accurate over a wide range of load cases and material systems[43]. Among the traditional criteria that have been used in conjunction with mechanical joint strength analysis are "maximum stress"[37], "maximum strain"[32,33], "distortion energy"[28] and the "tensor polynomial failure criterion"[36]. These criteria tend to be extremely conservative when applied to peak stress near a loaded hole.

The work of Whitney and Nuismer[20], in 1974, involving the technique of stress averaging over local regions of high stress concentration, led to the development of the two-parameter strength models presently in use. A two-parameter model predicts failure by using the unnotched laminate strength

and some form of a characteristic distance. The latter is found to be reasonably constant for a given material system regardless of stress distribution.

The motivation for using a two-parameter criterion instead of simply using unnotched laminate strengths and peak stresses is provided by three facts. First, the finite element and theory of elasticity solutions for the stress distributions around a joint assume ideal, linear elastic material behavior to failure. Even with this assumption, the peak stresses calculated from the finite element model are also dependent on mesh refinement and may become singular near a discontinuity[33].

Second, the actual stress distribution near a hole is both non-linear and non-singular. This is due to plastic deformation which is found to occur in regions of high stress concentration in the typically brittle composites of interest. Plastic deformation typically occurs in the form of fiber breakage and shear transfer through the matrix. This localized yielding has the effect of redistributing stresses near the hole and blunting the peak stress concentration. This effect has long been recognized in ductile materials but was identified with brittle fiber/matrix systems only in the past ten years. A plot of strength reduction against W/D for materials of various ductilities is reproduced in Figure IV-A-2.

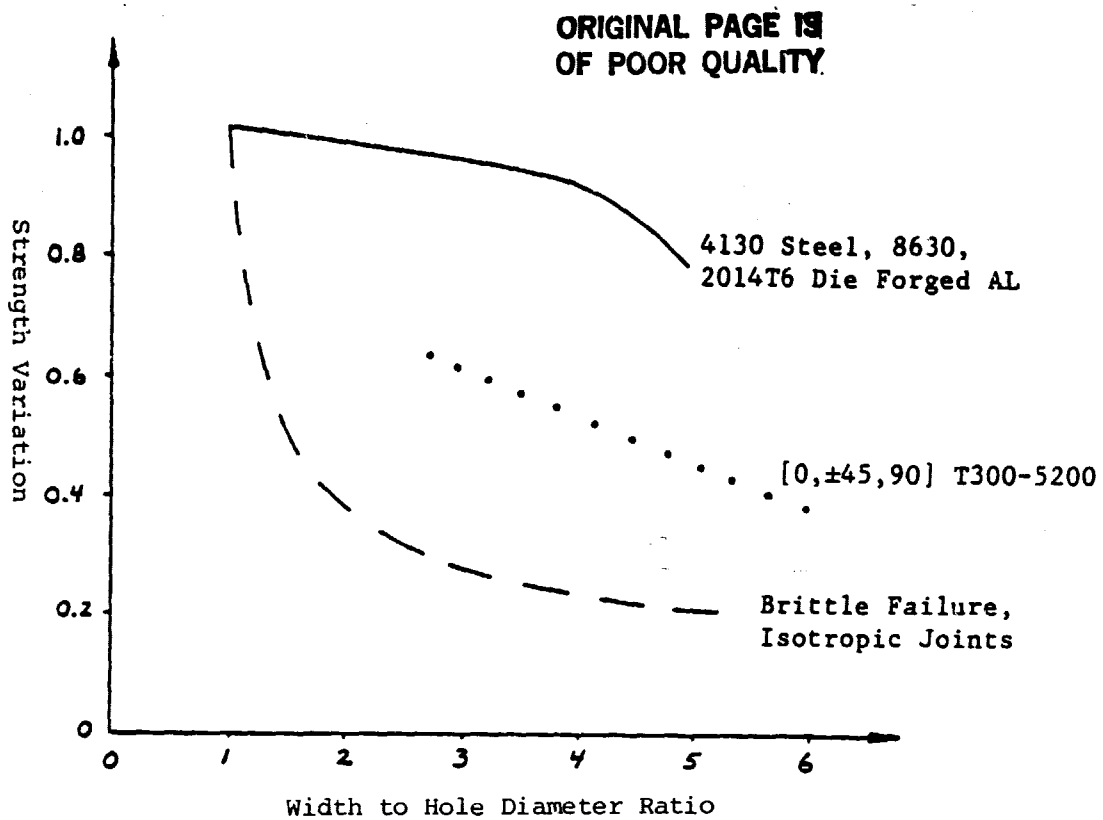

Figure IV-A-2. Effect of Ductility on Net Tensile Joint Strength[5]

The third point, and the physical conceptualization of the criterion, is derived from Griffith's critical flaw theory, "in particular, brittle failure of a body under a given stress field is generally attributed to the existence of inherent flaws of various dimensions distributed throughout the body"[44]. The implication of this is that, if a high level of stress is maintained over a longer distance from the loaded hole, then failure is more probable. This is similar to the well-known composite hole size effect[8,45]

wherein unloaded holes of different sizes will have equal peak stresses, but since the larger hole will have a higher stress over a larger area, as its stress profile decays more slowly, it is more likely to fail. This may be applied to volumetric considerations also, as a greater volume under equivalent average stress will tend to fail sooner.

This critical flaw phenomenon is thought of as occurring only within a material-dependent characteristic dimension. This dimension may take the form of an averaging distance, a point stress distance, a point stress curve or an assumed crack length. The particular choice among these two-parameter models is not as important as using some appropriate dimension in lieu of a one-parameter criterion[46].

In this study, a variation on the Whitney-Nuismer stress averaging criteria was used. The original form was developed by them[20] to explain the aforementioned hole-size effect. In that case, the line of failure (net tension) was known beforehand. The failure-inducing stress component, σ_y, was also known, and its profile described by a classical isotropic elasticity solution. This case is shown in Figure IV-A-3, where:

R $\triangleq$ hole radius,

y $\triangleq$ distance from the center of the hole, measured in the direction of the load,

NOTE: by these definitions, the abscissa (y-R) is the distance a point is, in the load direction, from the edge of the hole.

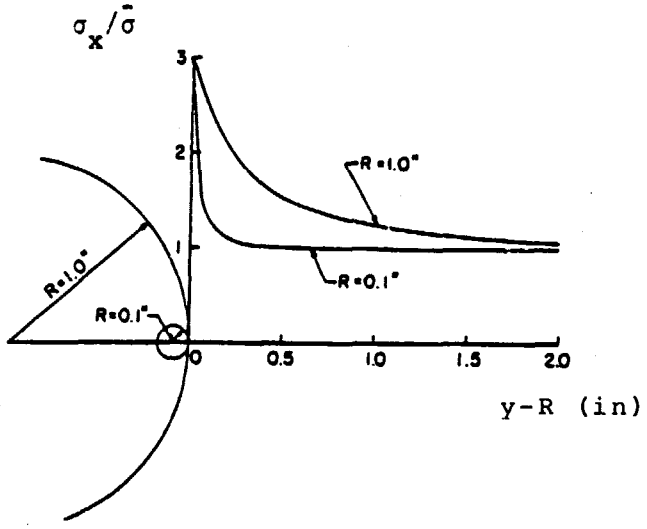

Figure IV-A-3. Stress Profile for an Unloaded Hole in an Isotropic Plate[20]

$\sigma_x \triangleq$ stress normal to the direction of load and

$\bar{\sigma} \triangleq$ average of stress σ_x on the cross section.

The average stress criterion is implemented using the following formulation:

$$\bar{\sigma}_x = \frac{1}{a_o} \int_{R_o}^{R_o + a_o} \sigma_x(y,0)\,dy$$

where:

$a_o \triangleq$ the characteristic dimension.

Failure is said to occur when the average net tensile stress,

$\bar{\sigma}_x$, reaches the unnotched laminate strength. Note that the peak tensile stress at the hole edge is (by definition) no longer a critical quantity in the failure calculation. Similarly, the exact stress profile is not critical so long as the numerically determined profile is reasonably close. The averaging tends to reduce distribution errors, while a point stress formulation would be sensitive to small deviations in the stress profile[45].

General application of the Whitney-Nuismer concept has not been rigorously tested. Several obstacles to its wider use seem clear. Complex states of stress are not readily dealt with. Cases where the line of failure is not well-defined also defy straightforward application of the averaging technique. Nuismer has stated that rather than generalize the criteria and sacrifice its simplicity it may be necessary to develop "...a failure theory that takes into account the role of damage and stress redistribution in failure in a load path-dependent, incremental way"[45]. In the case of a slanted crack, he chose to find an equivalent straight crack definition rather than apply the averaging technique to the general stress field.

Validity of the averaging technique, however, has been shown in predicting strength at discontinuities under compressive loading[47]. It was found that laminates are less sensitive to compressive stress concentrations than to tensile stress concentrations. As a result, the characteristic dimension

(defined a_{o_b} for bearing) is larger than that for tensile loading (a_{o_t}). For the AS/3501-5 system, the values a_{o_b} = 0.244 inches and a_{o_t} = 0.09 inches were found to correlate well with experimental data. However, it must again be noted that the load was uniaxial and the line of failure known in advance, allowing simple application of the stress averaging technique.

Application of this technique to the case of a mechanical connection was apparently first published by Agarwal[32], in 1980. His approach was to extend the technique so as to average certain stress components along the characteristic distance in a radial direction from the hole edge. This averaging scheme is shown in Figure IV-A-4. The method is as follows, "for tension failure the stresses normal to the radial direction are averaged over a distance, a_{o_t}, along several radial lines. Failure is predicted along the line where the average stress reaches the laminate tensile strength in the direction tangent to the point on the circumference under consideration (lines AB)"[32]. A similar procedure is used for bearing and shear failure except the stresses in line with the averaging line are averaged rather than those normal to the radial line.

Although Agarwal shows reasonable correlation with experimental data, some predictions are conservative by as much as fifty percent for angle-ply and cross-ply laminates in graphite/epoxy. The nonlinear response of these

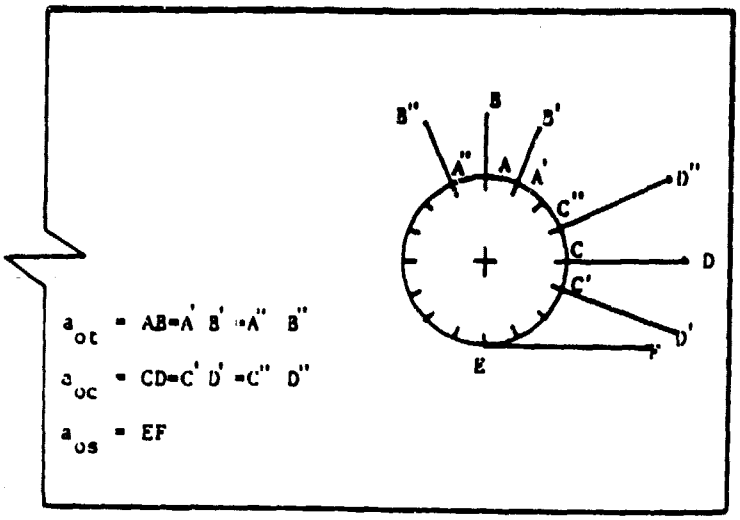

Figure IV-A-4. Stress Averaging Scheme Used by Agarwal[32]

particular laminates may have contributed to the discrepancy. This author believes, however, that there are at least four inadequacies to this approach. The first three were postulated by Goetschel[48] and developed under U. S. Army funding[57]. These points are related to the direction and nature of the averaged stresses. First, the averaging of stresses normal to a given radial line is considered arbitrary. Second, the stress tensor, in each ply, would seem to require full evaluation, not merely a given average component. Third, interaction of stress components should also be accounted for in a failure theory of general applicability. The fourth point is that the averaging scheme should be more general rather than restricting failures to propagate along radial lines only.

An improved two-parameter model developed at the University of Michigan[31] remains to be reviewed before the criteria developed in this study are presented.

Chang et al.[31] have developed a general finite element analysis package, "BOLT", which includes a failure analysis postprocessor. In it, the point stress criterion, also proposed by Whitney[20], has been generalized to account for a continuous variation in potential failure mode from net tension to shear-out to bearing. The point stress characteristic curve and its analytical form are shown in Figure IV-A-5. This has been obtained using the Yamada strength theory to

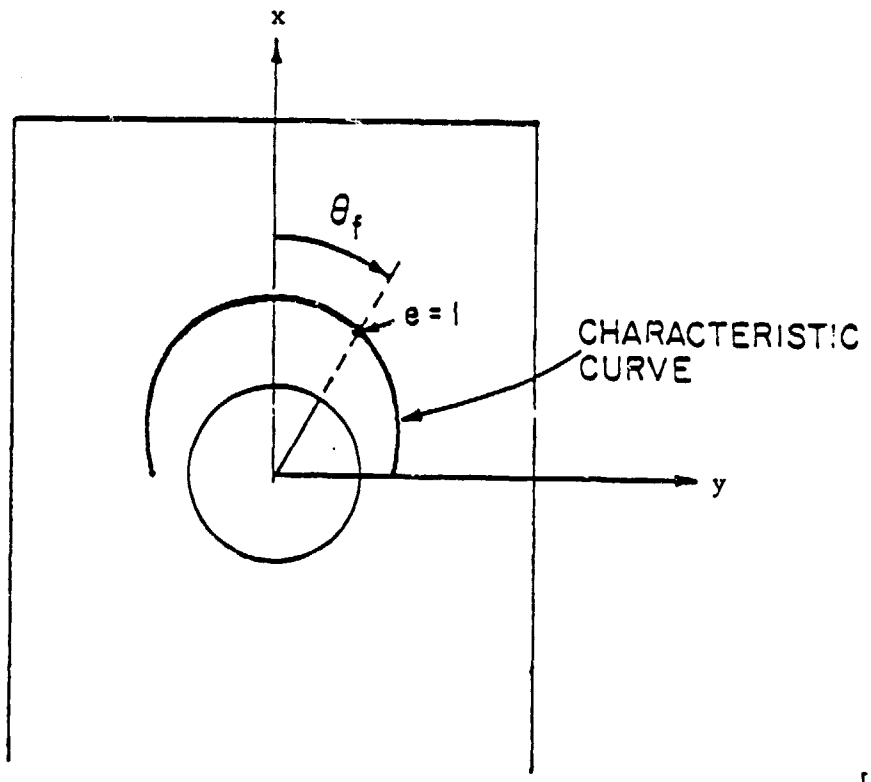

Figure IV-A-5. Characteristic Curve for Point Stress Scheme of "BOLT"[31]

determine the unnotched strength of each ply. That is:

$$\left(\frac{\sigma_x}{X}\right)^2 + \left(\frac{\sigma_{xy}}{S_c}\right)^2 = e^2 \qquad \begin{array}{ll} e \leq 1 & \text{No failure.} \\ e \geq 1 & \text{Failure.} \end{array}$$

where:

X = ply strength in x direction and

S_c = ply shear strength.

When the Yamada criteria is reached (e = 1) at any point along the characteristic curve for any ply, the joint is said to have failed along a radial line to that point. The mode of failure is then associated with the relative location of the failure point. This has an added advantage over Agarwal's scheme in that ply stresses (which may be of significantly different distribution) are evaluated instead of simply using the average laminate stresses.

This method still seems inadequate since it also assumes, by virtue of its characteristic curve, a radial line of maximum average stress. This would preclude, for example, identifying a high average line of shear stress along the shear plane for a typical characteristic shear dimension, a_{o_j} (as defined by Agarwal). While the Yamada failure theory includes shear stress effects, which is more rigorous than Agarwal's use of the maximum strain criterion, a fiber strain failure criterion would seem to have greater physical significance and would also account for effects on a ply by ply level.

i) The minimum-gradient fiber strain criterion. A discussion of the application of the fiber strain criterion should be introduced by some consideration of its range of validity. The fiber strain failure criterion states that the laminate will fail when any fiber is strained beyond its maximum strain limit. Failures of the matrix are neglected assuming that they will not influence the ultimate strength of the laminate. Thus, this failure theory is only valid for application to those laminates where incipient matrix failures will not cause catastrophic failures of the laminate. The fiber strain criterion should, it is emphasized, be applied to laminates having at least three widely spaced ply orientations, i.e., $[0/\pm45]_s$. Despite such limitations, the fiber strain criterion is seen as useful for many composite structures and, for such cases, does define good design practice[49].

The fiber strain failure criterion is easily applied to an interactive finite element postprocessor, such as "FELOOK" of the "POFES" system developed at RPI. Contours of fiber strain are mapped out for any component ply orientation. A new variation of this averaging technique is now being used. Instead of averaging fiber strain over various radial lines, it is averaged over the line of minimum-gradient fiber strain from the point of highest peak fiber strain (see Figure IV-A-6). This allows failure lines extending in any direction from the hole to be identified. As in Agarwal's scheme, the

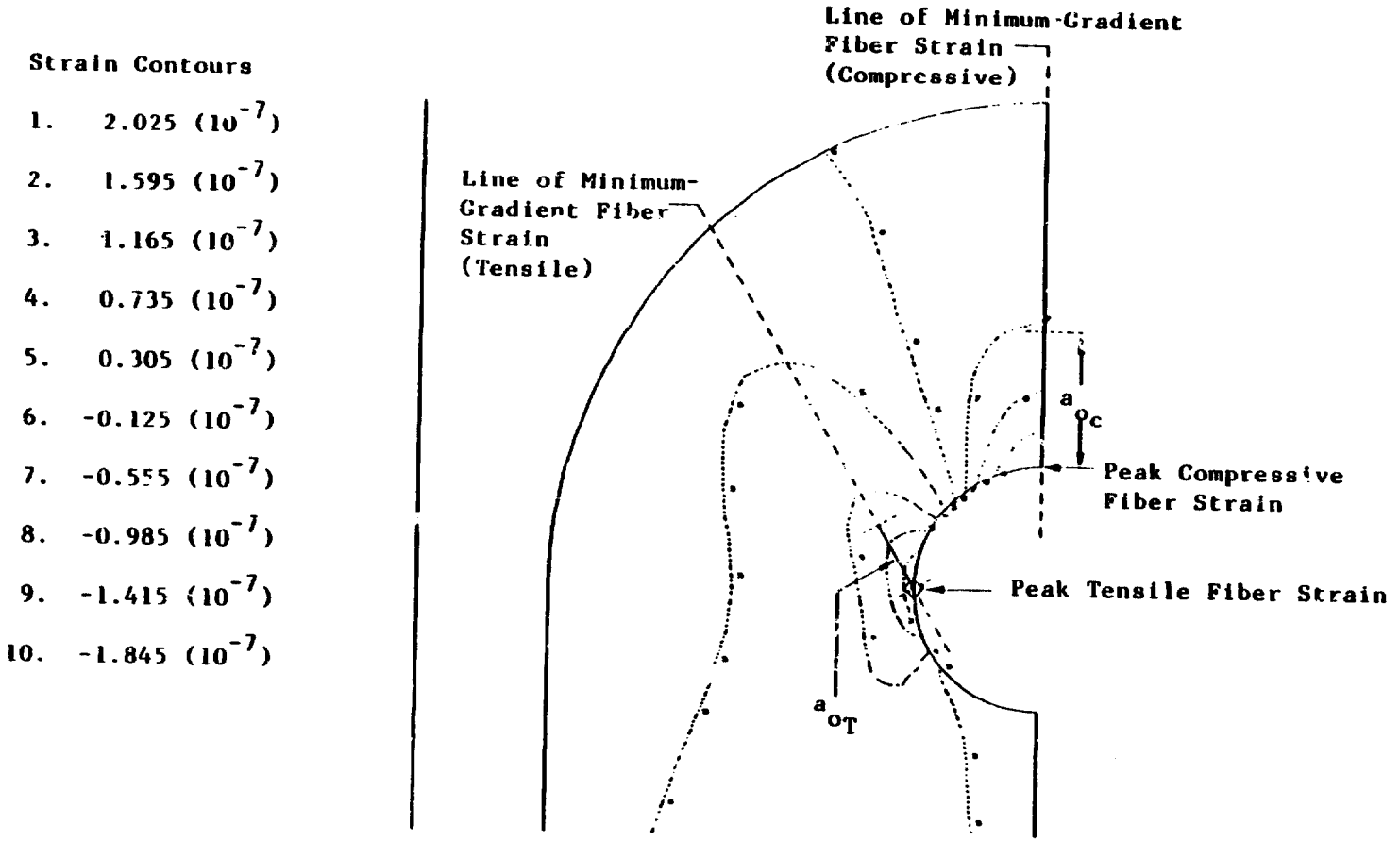

Figure IV-A-6. "Minimum-Gradient Fiber Strain" Averaging Scheme Proposed by the Author

failure mode is inferred from the location of the maximum average line.

The characteristic dimensions a_{o_t}, a_{o_b} and a_{o_s} are exchanged in favor of a_{o_T} and a_{o_C}. The latter pair corresponds to characteristic dimensions for fiber strain tension and compression, respectively. They will have to be experimentally determined for a given material system. It is assumed, at this point, that they are constant for any geometry using a given material system. They will probably vary with material systems, but it is hoped that they will be shown to be independent of lay-up and geometry.

At present, the location of the line of minimum-gradient fiber strain is being identified visually, and contour values are read along that line and recorded. The data is then fitted with a curve of polynomial form using a reduced-order, curve fit algorithm. The empirically determined strain profile is then integrated exactly over the appropriate characteristic distance. Although this method can be used without great difficulty, an automated postprocessing routine would greatly enhance its accessibility and eliminate error due to eye-balling the contours ($\leq$5%).

The modified postprocessor FELOOK can also plot contours of ply stress should it be found more accurate to use a failure criterion based on lamina stress. Similarly, contours of strength ratio could be plotted with another modification.

Complete verification of this failure theory was considered beyond the scope of the research reported here. The method is appealing, however, because of the physical basis of its interpretation and its ability to predict nonradial failure lines. Correlation with experimental data can be readily accomplished by using a series of finite element models corresponding to published data[50] for T300/SP286 graphite/epoxy. Preliminary verification using limited experimental data was performed and the results are presented in Table IV-A-1. As can be seen, the error is about 10% as compared with 33% to 40% for predictions based on peak strain.

c. Conclusions

For purposes of strength prediction, a work-equivalent cosine normal load distribution was used in conjunction with a new variation of the Whitney-Nuismer stress averaging failure criterion as the most useful approach for evaluating compact lug designs. The new criterion, minimum-gradient fiber strain, shows good correlation with limited experimental results.

A parametric study for the drag strut lug led to a redesign for the full scale part. It was shown that scaling effects were very significant in the range of the redesign. Several other quarter-scale design concepts, including stress relief cuts, unidirectional capstrips and steel bushings, were tested. These designs were found to be slightly

TABLE IV-A-1

COMPARISON OF PREDICTED AND EXPERIMENTAL RESULTS

Design	Failure Mode	Experimental Strength*	Predicted Strength Minimum Fiber Strain Gradient	% Error	Predicted Strength Maximum Strain	% Error
Control $[0/\pm45]_{12S}$	Bearing	------	82.058**	---	56,045	---
	Net Tension	------	93.131	---	41,411	---
	Shear	70.144 (65°)$^{\Delta}$	63.560 (20°)	-9.4	42,346	-39.6
Stress Relief Cut $[0/\pm45]_{12S}$	Bearing	------	90.000**	---	70,354	---
	Net Tension	------	96.015	---	50,850	---
	Shear	71.933 (40°)	81.800 (20°)	13.7	48,080	-33.2

*Strength measured in terms of average bearing stress (psi)

**Bearing strength averaged over a_{o_C} = .15 (very conservative)

$^{\Delta}$Angle of shear failure plane

stronger than the [0/±45] laminate designs, but the improvements were not considered substantial enough for this particular lug geometry to justify the manufacturing complications involved.

In summary, it is clear that a heavily loaded mechanical joint, in an orthotropic composite laminate, can be designed with a strength to weight ratio greater than that of steel, if geometric constraints do not interfere. When constraints force a compact lug design, the practicality of composites appears to be a matter to be decided on a case by case basis.

4. Plans for Upcoming Period

This work is being concluded with this report, although a paper is planned for submission to an appropriate journal.

5. References

1. Goetschel, D. B., "Lockheed L-1011 Engine Drag Strut (CAPCOMP)", Composite Structural Program, Composite Structural Materials 41st Semi-Annual Progress Report, Rensselaer Polytechnic Institute, December 1981, pp. 105-114.

2. Chen, S., "Local Buckling of Anisotropic Cylindrical Thin Walled Shells", M.Sc. Thesis, Department of Mechanical Engineering, Aeronautical Engineering and Mechanics, Rensselaer Polytechnic Institute, August 1982.

3. "Advanced Composites Design Guide, 1, 3rd Edition, Contract No. F33615-74-C-5075, Flight Dynamics Laboratories, U. S. Air Force, 1976.

4. Slawson, G. St. J. and D. R. Andrews, "Composites - A Joining Problem?", Welding and Metal Fabrication, November 1973.

5. Oplinger, D. W., "On the Structural Behavior of Mechanically Fastened Joints in Composite Structures", 4th Conf. Fibrous Composites in Design, E. Lenog, D. Oplinger and J. Burke, Eds., Army Materials and Mechanics Research Center, Watertown, MA, Plenum Press, Nov. 14-17, 1978, pp. 575-602.

6. Quinn, W. J. and F. L. Matthews, "The Effect of Stacking Sequence on the Pin-Bearing Strength in Glass-Fiber Reinforced Plastic", J. Composite Materials, 11, April 1977, pp. 138-143.

7. Matthews, F. L., C. M. Wong and S. Chryssafitis, "Stress Distribution Around a Single Bolt In-Fiber-Reinforced Plastic", Composites, July 1982, pp. 316-322.

8. Hart-Smith, L. J., "Mechanically Fastened Joints for Advanced Composites - Phenomenological Considerations and Simple Analysis", 4th Conf. Fibrous Composites in Design, E. Lelong, D. Oplinger, J. Burke, Eds., Army Materials and Mechanics Research Center, Watertown, MA, Plenum Press, Nov. 14-17, 1978, pp. 543-574.

9. Matthews, F. L., A. A. Roshan and L. N. Phillips, "The Bolt Bearing Strength of Glass/Carbon Hybrid Composites", Composites, July 1982, pp. 225-227.

10. "A Guide to Cutting and Machining Kevlar Aramid", DuPont Bulletin.

11. Kim, W., "Stress Analysis Methods for Clearance-Fit Mechanical Joints in Laminated Composites", Ph.D. Thesis, Department of Mechanical Engineering, Aeronautical Engineering and Mechanics, Rensselaer Polytechnic Institute, Troy, NY, August 1982.

12. Cole, R. T., E. J. Bateh and J. Potter, "Fasteners for Composite Structures", Composites, July 1982, pp. 233-240.

13. Cluley, A. P. and R. P. Scoular, "Jointing of Components Molded in Carbon Fiber-Reinforced Thermoplastics", Composites, January 1983, pp. 19-26.

14. Hoff, N., Y. Hirano and K. Kenmochi, "CAPCOMP - (Composite Aircraft Program Component)", Composite Structural Materials, 36th Semi-Annual Progress Report - Composite Structural Program, Rensselaer Polytechnic Institute, July 1979, pp. 27-42.

15. Collings, T. A., "On the Bearing Strengths of CFRP Laminates", Composites, July 1982, pp. 241-252.

16. Collings, T. A., "The Strength of Bolted Joints in Multi-Directional CFRP Laminates", Composites, 8, No. 1, January 1977, p. 43.

17. Advanced Composites Design Guide, II, 3rd Ed., Contract No. F33615-74-C-5057, Flight Dynamics Laboratory, U. S. Air Force, 1976.

18. Rowlands, R. E., M. V. Rahman, T. L. Wilkinson and Y. I. Chiang, "Single and Multiple Bolted Joints in Orthotropic Materials", Composites, July 1982, pp. 273-278.

19. Sendeckyj, G. P. and M. D. Richardson, "Fatigue Behavior of a Graphite-Epoxy Laminate Loaded Through an Interference-Fit Pin", Proc. of 2nd Air Force Conference on Fibrous Composites in Flight Vehicle Design (AFFDL-TR-74-103) September 1974, pp. 469-520.

20. Whitney, J. M. and R. J. Nuismer, "Stress Fracture Criteria for Laminated Composites Containing Stress Concentrations", J. Composite Materials, 8, 1974, pp. 258-265.

21. Crews, J. H., Jr., C. S. Hing and I. S. Raju, "Stress Concentration Factors for Finite Orthotropic Laminates With a Pin-Loaded Hole", NASA Technical Paper 1862, National Aeronautics and Space Administration, 1981.

22. Godwin, E. W. and F. L. Matthews, "A Review of the Strength of Joints in Fiber-Reinforced Plastics. Part 1, Mechanically Fastened Joints", Composites, July 1980, pp. 155-160.

23. Wilkins, D. J., "Environmental Sensitivity Tests of Graphite-Epoxy Bolt Bearing Properties", Composite Materials: Testing and Design (Fourth Conference), ASTM STP 617, American Society for Testing and Materials, 1977, pp. 149-152.

24. Kim, R. Y. and J. M. Whitney, "Effect of Temperature and Moisture on Pin Bearing Strength of Composite Laminates", Journal of Composite Materials, 10, 1976, pp. 149-152.

25. Walthers, R. E., "A Finite Element Analysis of a Graphite/Epoxy Aircraft Engine Drag Strut Lug", Unpublished class project, May 1982,

26. DeJong, T., "Stresses Around Pin-Loaded Holes in Elastically Orthotropic or Isotropic Plates", Journal of Composite Materials, 11, July 1977, pp. 313-331.

27. Shephard, M. S., "RPIFEP An Interactive Finite Element Package - Introduction Manual", Preliminary Draft, Department of Civil Engineering, Rensselaer Polytechnic Institute, Troy, NY, 1980.

28. Waszczak, J. P. and T. A. Cruse, "Failure Mode and Strength Predictions of Anisotropic Bolt Bearing Specimens", Journal of Composite Materials, 5, July 1971, pp. 421-425.

29. Bickley, W., "The Distribution of Stress Round a Circular Hole in a Plate", Phil. Trans. Roy. Soc., A (London), 227, 1928, p. 383.

30. Wong, C. M. S. and F. L. Matthews, "Single and Two-Hole Bolted Joints in Fiber Reinforced Plastic", Journal of Composite Materials, 5, September 1981, pp. 481-490.

31. Chang, F. K., R. A. Scott and G. S. Springer, "Strength of Mechanically Fastened Composite Joints", Journal of Composite Materials, 16, November 1982, pp. 470-494.

32. Agarwal, B. L., "Static Strength Prediction of Bolted Joints in Composite Materials", AIAA Journal, 18, No. 11, November 1980, pp. 1371-1375.

33. Ramkumar, R. L., "Bolted Joint Design", Test Methods and Design Allowables for Fibrous Composites, ASTM STP 749, 1981, pp. 376-385.

34. Wilkinson, T. L. and R. E. Rowlands, "Analysis of Mechanical Joints in Wood", Experimental Mechanics, 21, No. 11, November 1981, pp. 408-414.

35. Oplinger, D. W. and K. R. Gandhi, "Stresses in Mechanically Fastened Orthotropic Laminates", Proceedings of the 2nd Conference on Fibrous Composites in Flight Vehicle Design, May 1974, pp. 813-834.

36. Soni, S. R., "Failure Analysis of Composite Laminates With a Fastener", Joining of Composite Materials, ASTM STP 749, 1981, pp. 145-164.

37. Wilson, D. W., J. W. Gillespie, J. L. York and R. B. Pipes, "Failure Analysis of Composite Bolted Joints", Center for Composite Materials, U. of Delaware, Newark, Delaware, Sponsored by NASA Grant No. 1409, 1980.

38. Wilkinson, T. L., R. E. Rowlands and R. D. Cook, "An Incremental Finite-Element Determination of Stresses Around Loaded Holes in Wood Plates", Computers and Structures, 14, Nos. 1 - 2, 1981, pp. 123-126.

39. Cook, R. D., "Concepts and Applications of Finite Element Analysis, John Wiley & Sons, New York, 1981, pp. 84-85.

40. Gallagher, R. H., "Finite Element Analysis Fundamentals", Prentice-Hall, Inc., Englewood Cliffs, New Jersey, 1975, pp. 141-143.

41. Segerling, L. J., "Applied Finite Element Analysis", John Wiley & Sons, New York, 1976.

42. Johnson, M. and F. L. Matthews, "Determination of Safety Factors for Use When Designing Bolted Joints in GRP", Composites, April 1979, pp. 73-76.

43. Jones, R. M., "Mechanics of Composite Materials", McGraw-Hill Book Company, New York, 1975, pp. 188-193.

44. Griffith, A. A., "The Phenomenon of Rupture and Flow in Solids", Phil. Trans. of the Roy. Soc., A (London), 221, 1920, p. 163.

45. Nuismer, R. J. and J. D. Labor, "Applications of the Average Stress Failure Criterion: Part I - Tension", Journal of Composite Materials, 12, July 1978, pp. 238-249.

46. Eisenmann, J. R., Private communication, 1983.

47. Nuismer, R. J. and J. D. Labor, "Applications of the Average Stress Failure Criterion: Part II - Compression", Journal of Composite Materials, 13, January 1979, pp. 49-60.

48. Goetschel, D. B., Private commumication, 1983.

49. Greenwood, J. H., "German Work on GRP Design", Composites, 8, No. 3, July 1977, p. 175.

50. Van Siclen, R. C., "Evaluation of Bolted Joints in Graphite/Epoxy", Proceedings of the Army Symposium on Solid Mechanics: Role of Mechanics in the Design of Structural Joints, September 1978, pp. 120-138.

51. Burk, R. C., "Standard Failure Criteria Needed for Advanced Composites", Astronautics and Aeronautics, 21, No. 6, June 1983, pp. 58-62.

52. Choi, I. and C. O. Horgan, "St. Venant's Principle and End Effects in Anisotropic Elasticity", Journal of Applied Mechanics, 44, No. 3, September 1977.

53. Ogunlari, O., "Static Strength Prediction of Uniaxially Loaded Composite Laminates With Unloaded Notches", M.Sc. Thesis, Department of Mechanical Engineering, Aeronautical Engineering and Mechanics, Rensselaer Polytechnic Institute, Troy, NY, December 1982.

54. Tsai, S. W. and H. T. Hahn, "Introduction to Composite Materials, Technomic Publishing Company, Westport, CT, 1980, pp. 277-325.

55. Furness, K., "Bolted Connections in Composite Shafts", Department of Mechanical Engineering, Aeronautical Engineering and Mechanics, Rensselaer Polytechnic Institute, Troy, NY, August 1983.

56. Cackett, M. T., "Design Considerations and Failure Analysis of a Pin-Loaded Hole in an Orthotropic Composite Laminate", M.Sc. Thesis, Department of Mechanical Engineering, Aeronautical Engineering and Mechanics, Rensselaer Polytechnic Institute, Troy, NY, August 1983.

57. "Center of Excellence in Rotorcraft Technology", Contract DAAG29-82-K-0093, U. S. Army Research Office with Rensselaer Polytechnic Institute, July 8, 1982.

IV-B QUANTIFICATION OF SAINT-VENANT'S PRINCIPLE FOR A GENERAL PRISMATIC MEMBER

Senior Investigator: D. B. Goetschel

1. Introduction

Saint-Venant's principle states that all statically equivalent systems of load on a body will produce nearly identical stress fields in regions that are remote from the loaded area. An alternative statement is that the stress fields resulting from self-equilibrated systems of load decay to zero in regions remote from the loaded area. These are equivalent statements for a linear elastic material, because any load system can be considered to be made up of a statically equivalent loading plus an appropriate set of self-equilibrated loads. This allows the solution for a simple loading to be used in place of the solution for a complex loading except in the immediate vicinity of the loaded area, if only a small fraction of the surface is acted on by tractions or a small fraction of the volume is subjected to body forces. The importance of Saint-Venant's principle is that it is the basis for justifying many widely useful technical theories, e.g., the Bernoulli-Euler beam theory.

Until recently, Saint-Venant's principle was only a qualitative statement. It's quantification existed only in very approximate rules of thumb that were based on past experience. The increasing use of anisotropic materials and

inhomogeneous construction has dramatized the need for a more reliable theoretical quantification of Saint-Venant's principle for prismatic members loaded only on the ends. A semianalytic finite element method will be described that will be capable of handling any arbitrary cross-sectional geometries and material properties. The material properties can be both inhomogeneous and anisotropic.

Toupin[1]*, in 1965, and Knowles[2], in 1966, independently presented theorems for upper bond estimates of the strain energy in a part of a body as a function of the distance away from the region of applied tractions. The main result of their theorems is a strain energy decay inequality in the form

$$V(x) \leq V(0) * \exp(-2\gamma x) \qquad (1)$$

where:

γ is the characteristic decay rate,

$V(0)$ is the total strain energy and

$V(x)$ is the strain energy in that part of the body beyond x.

Because of the quadratic nature of strain energy in terms of the mechanical variables, an immediate consequence is the capability for pointwise estimates of displacement, strain and stress, in the forms

*Numbers in brackets in this section refer to the references which are listed on page 136.

$$u_i(x) \leq u_i(0) * \exp(-\gamma x)$$

$$\xi_{ij}(x) \leq \xi_{ij}(0) * \exp(-\gamma x) \qquad (2)$$

$$\tau_{ij}(x) \leq \tau_{ij}(0) * \exp(-\gamma x)$$

Horgan[3,4] extended Knowles' analysis to plane problems with anisotropic materials. Choi and Horgan[5,6] went farther to obtain exact solutions for the decay rates for two general cases of plates in plane strain, i.e., a homogeneous anisotropic plate and a sandwich plate. These solutions employ the Airy stress function, ϕ, which - in accordance with compatibility - leads to a generalized biharmonic governing equation. For the rectangular region, the solution form is taken as a product function of an exponential decay away from the loaded region and an undetermined function in the transverse direction.

$$\phi(x,y) = F(y) * \exp(-\gamma x) \qquad (3)$$

This solution form enables the eigenvalue problem to be reduced to a fourth order ordinary differential equation in $F(y)$. The eigenvalue, γ, with the smallest real part, characterizes the dominant (slowest) exponential decay rate.

Dong and Goetschel[7] developed a method for finding the decay rates of edge effects in a plate composed of an arbitrary number of anisotropic layers. For handling any type of laminate construction, a semianalytic finite element approach was employed. Instead of the Airy stress function, the

in-plane displacements were adopted as the primary dependent variables. One-dimensional finite element polynomial interpolation functions were used to model the behavior through the thickness of the plate. The behavior away from the loaded edge was assumed to be an exponential decay. A second order eigenvalue problem emerged, whose roots are the characteristic decay rates. The corresponding eigenvectors are the displacement distributions through the thickness of the plate.

For the isotropic cylinder an upper bound inequality for the exponential decay was established by Knowles and Horgan[8]. The exact solution to the end problem for isotropic circular cylinders has been dealt with by numerous investigators, e.g., [9,10,11]. The case of transversely isotropic circular cylinders, limited to torsionless axisymmetric loading, is considered in [12,13,14]. Solutions for more general cases of prismatic members are not available.

Numerous investigators[15,16,17] have used finite element and finite difference techniques to examine edge and end effects for composite structural elements, but these have all been a standard static analysis for particular loadings or boundary conditions. The type of analysis discussed above and proposed here finds the general solutions to the end effect problem for any loading. Suitable restrictions on the finite element degrees of freedom allow the program to solve the plate edge effect problem, including displacements

parallel to the edge. This is an expansion on the capabilities of the work reported by Dong and Goetschel [7]

Saint-Venant's principle underlies nearly all structural analysis, yet this principle has never been quantified for the case of the general prismatic member. The research reported here was undertaken to rectify this potentially troublesome situation. End effects are becoming even more important with the increasing use of laminated composite materials which are so sensitive to interlaminar stresses.

2. Status

Previous to this reporting period, the method described had been conceptually developed, the governing equations formulated and the implementing computer program written but only partially debugged.

The governing equations can be formulated using a variational method [7], however, a different but equivalent method is reviewed here. This alternate approach was chosen because it is mathematically simpler and provides greater physical insight into the problem. The semianalytic finite element formulation assumes a displacement field of the form

$$u(x,y,z) = P(y,z) * \exp(-\gamma x) \qquad (4)$$

where:

$P(y,z)$ is the polynomial interpolation across the cross section,

$\exp(-\gamma x)$ is the exponential decay along the length of the member and

γ is, in this formulation, the unknown decay rate,

As a visual aid, consider the simple prismatic finite element in Figure IV-B-1. The small arrows, marked 1 through 12, are finite element degrees of freedom. The activation of any one of these degrees of freedom will define a displacement field throughout the element. This displacement field can be differentiated to provide the stress field throughout the element. Evaluation of this stress field on the end and side surfaces of this element will provide the surface traction distributions that would have to exist to maintain this displacement field. The stress field can also be differentiated throughout the volume of the element to obtain the body force field that would have to exist to satisfy equilibrium throughout the volume of the element for this displacement field to exist

$$T_{ij,j} + f_i = 0 \qquad (5)$$

If these surface traction distributions and volume body force fields are integrated using the displacement field corresponding to any displacement degree of freedom, the finite element force field corresponding to that degree of freedom is obtained. If this is done using the displacement field for each displacement degree of freedom as a weighting function, one column of the finite element stiffness matrix is obtained. If this procedure is followed for the stress

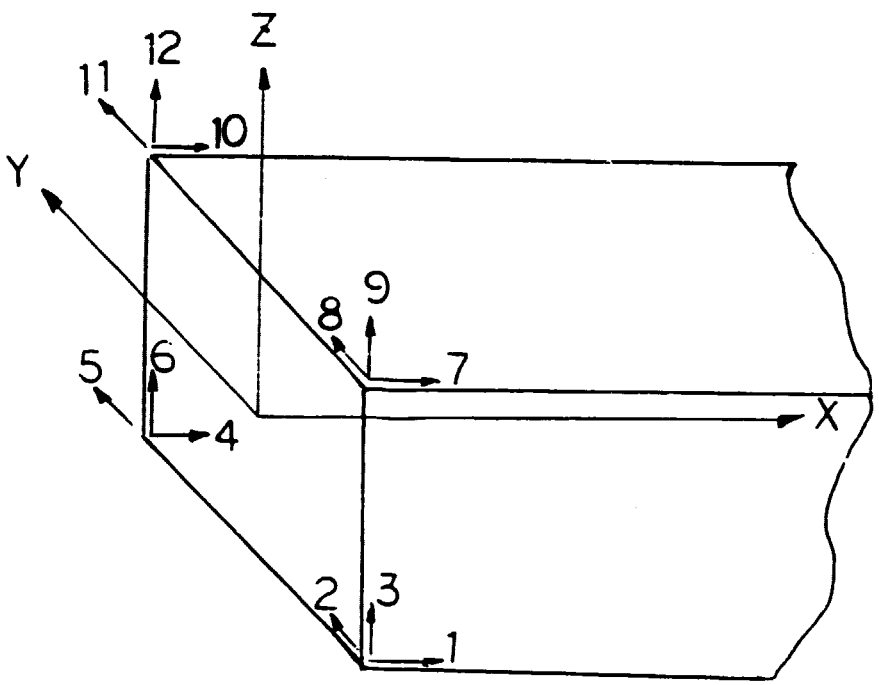

Figure IV-B-1. Simple Prismatic Finite Element

fields corresponding to each displacement degree of freedom, then the entire stiffness matrix is obtained

$$[k]\{u\} = \{f\} \tag{6}$$

where:

[k] is the stiffness matrix,

{u} is a vector of the displacement degrees of freedom and

{f} is a vector of the corresponding force degrees of freedom.

Now this stiffness matrix can actually be viewed as being composed of three parts resulting from (i) the integration of surface tractions over the end of the element, (ii) integrating the tractions over the four sides of the element and (iii) integrating the body forces over the volume of the element

$$[k] = [k_e] + [k_s] + [k_v] \tag{7}$$

where the subscripts e, s and v denote end, side and volume, respectively.

The problem under consideration requires that there not be any tractions on the sides or body forces within the interior of the element. The mathematical equivalent of this statement, using the finite element discretization, is

$$[(k_s) + (k_v)]\{u\} = \{0\} \tag{8}$$

The partial stiffness matrix contained within the parenthesis in Equation (8) is actually made up of three different

matrices with different powers of γ

$$([k_s] + [k_v]) = (\gamma[k_2] + [k_1] + \frac{1}{\gamma}[k_0]) \tag{9}$$

These factors of γ result from the differentiation with respect to x of Equation (4). Inserting Equation (9) into Equation (8) and multiplying through by γ gives

$$(\gamma^2[k_2] + \gamma[k_1] + [k_0])\{u\} = \{0\} \tag{10}$$

This is now a second order eigenproblem whose solution is the desired one. Equation (10) is for a single element, but multiple elements can be assembled together in the conventional way. Using capital letters to denote an assemblage of elements, the equivalent of Equation (10) would be

$$(\gamma^2[K_2] + \gamma[K_1] + [K_0])\{U\} = \{0\} \tag{11}$$

The matrices $[K_2]$ and $[K_0]$ are symmetric and $[K_1]$ is antisymmetric. The eigenvalue and eigenvector solutions to this equation are, in general, complex quantities.

This problem is mathematically similar to the problem of damped free-vibration structural dynamics. Note that the tractions on the end of the member do not enter the solutions for decay rate; they correspond to the initial displacements and velocities. The x dimension corresponds to time, and γ corresponds to the natural frequency for the structural dynamics problem. Similarly, $[K_2]$, $[K_1]$ and $[K_0]$ correspond to the mass, damping and stiffness matrices in the dynamics problem.

The decay rate γ can also be viewed as the inverse of the decay length. To be precise, it is only the real part of γ that should be interpreted as the decay rate or inverse of the decay rate. The inverse of the real part of γ is the distance in which irregular stresses will decay by a factor of 2.7 - the base of the natural logarithm.

3. Progress During Report Period

For verification of the numerical method and computer code, an isotropic plate and a homogeneous graphite-epoxy composite plate were analyzed since exact solutions exist for these cases.

Choi and Horgan[5] show the characteristic equation for the decay rate, γ, for an isotropic plate with unit half-thickness, to be

$$\sin 2\gamma \pm 2\gamma = 0 \tag{12}$$

where + and - refer to symmetric and antisymmetric modes, respectively. Table IV-B-1 contains the analytic and numerical results. Numerical results using several different mesh refinements are given. As can be seen, the agreement is excellent, and the method converges rapidly.

Units of length are not given for geometry dimensions or decay rates because the numbers would not change for any consistent units. The units for the decay rates are the inverse of the units for geometry dimensions.

TABLE IV-B-1

DECAY RATES (γ) FOR A 2-UNIT THICK ISOTROPIC PLATE

Mode	Analytic Solution	Computed From 2 Elements with 2 x 3 Nodes	Computed From 8 Elements with 2 x 2 Nodes	Computed From 8 Elements with 2 x 3 Nodes
1st Symm.	2.1062 ±1.1254i	2.0771 ±1.2218i	2.1180 ±1.1389i	2.1067 ±1.1256i
1st Anti-symm.	3.7489 ±1.3844i	3.9694 ±1.3637i	3.8807 ±2.3915i	3.7545 ±1.3843i
2nd Symm.	5.3563 ±1.5516i	----- -----	----- -----	5.3665 ±1.5444i
2nd Anti-symm.	6.9500 ±1.6761i	----- -----	----- -----	7.0535 ±1.6428i

To test the sensitivity of the method to material orthotropy, a homogeneous, unidirectional graphite/epoxy plate was analyzed. Again, a unit half-thickness was used, and material properties were taken as in References [5] and [7]; i.e.,

$$E_L = 137.92 \times 10^9 \text{ Pa} \qquad E_T = 6.896 \times 10^9 \text{ Pa}$$

$$G_{LT} = G_{TT} = 4.138 \times 10^9 \text{ Pa} \qquad \nu_{LT} = \nu_{TT} = 0.25$$

Results from the above references and from the current work are given in Table IV-B-2. The excellent agreement shows that the method has little trouble with highly orthotropic material properties.

TABLE IV-B-2

DECAY RATES (γ) FOR A 2-UNIT THICK HOMOGENEOUS ANISOTROPIC PLATE

Mode	Analytic Solution	Computed From Reference [7]	Computed From 8 Elements with 2 x 3 Nodes
1st Symm.	0.564288 ±0.0i	0.564288 ±0.0i	0.56445 ±0.0i
1st Anti-symm.	0.796485 ±0.0i	0.796485 ±0.0i	0.79710 ±0.0i
2nd Symm.	1.13448 ±0.0i	1.134479 ±0.0i	1.13890 ±0.0i
2nd Anti-symm.	1.369816 ±0.0i	1.369817 ±0.0i	1.38120 ±0.0i

Cross section geometry and material anisotropy are the two factors that determine a structure's natural decay rates. To investigate these effects, results are given for various cross-sectional geometries for homogeneous isotropic material properties and various nonhomogeneous, anisotropic composite lay-ups. Figure IV-B-2 shows the three-beam cross sections considered. The area moments of inertia about a horizontal neutral axis are the same for each cross section. The various material properties are also indicated. Figure IV-B-3 shows two composite skin-stringer constructions which have been considered. These same skin-stringer geometries

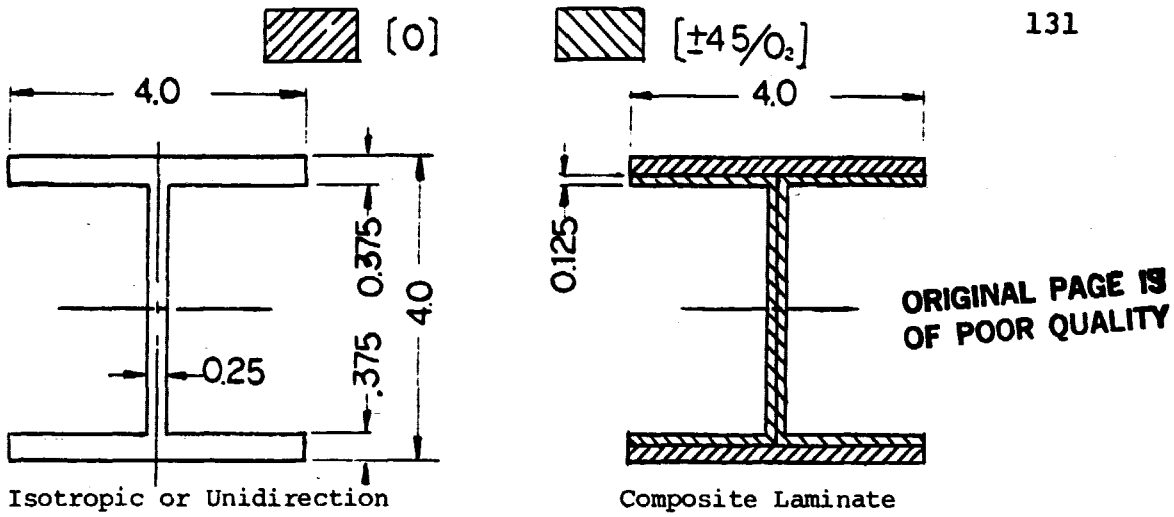

I-Beam (proportional to M 4 x 13)

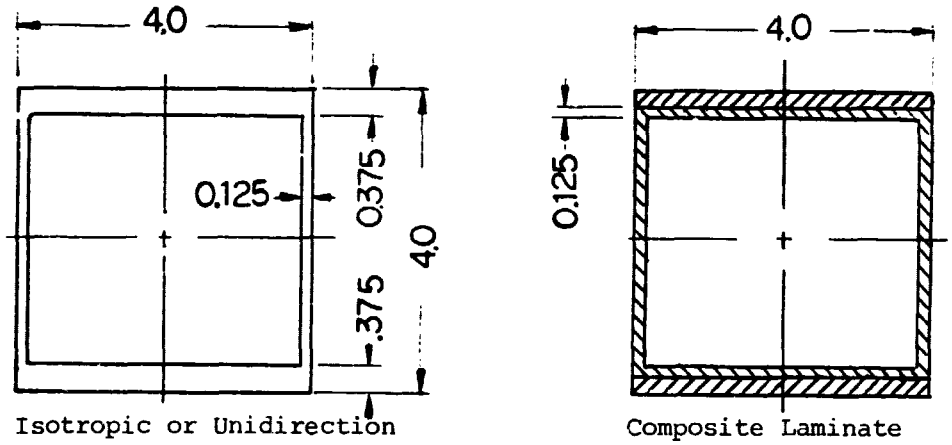

Box-Beam

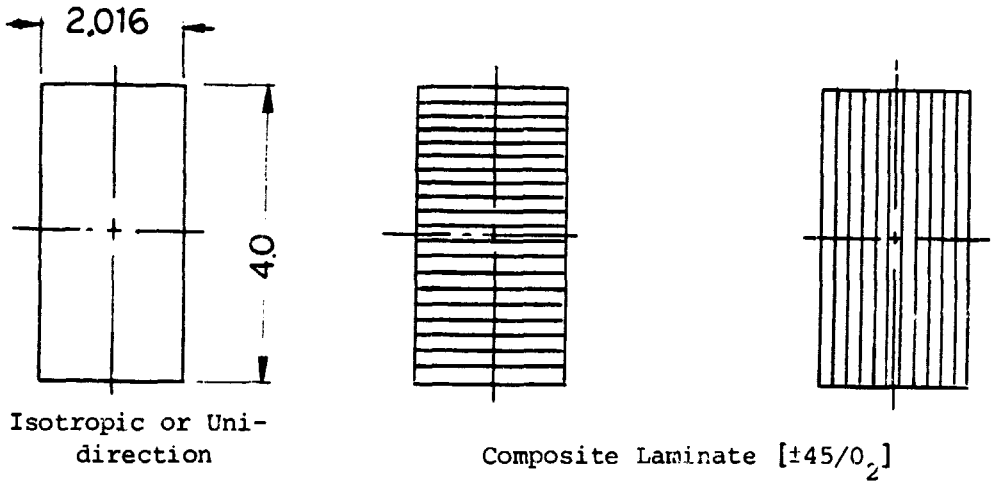

Rectangular-Beam (line directions indicate ply orientation)

Figure IV-B-2. Beam Test Cases

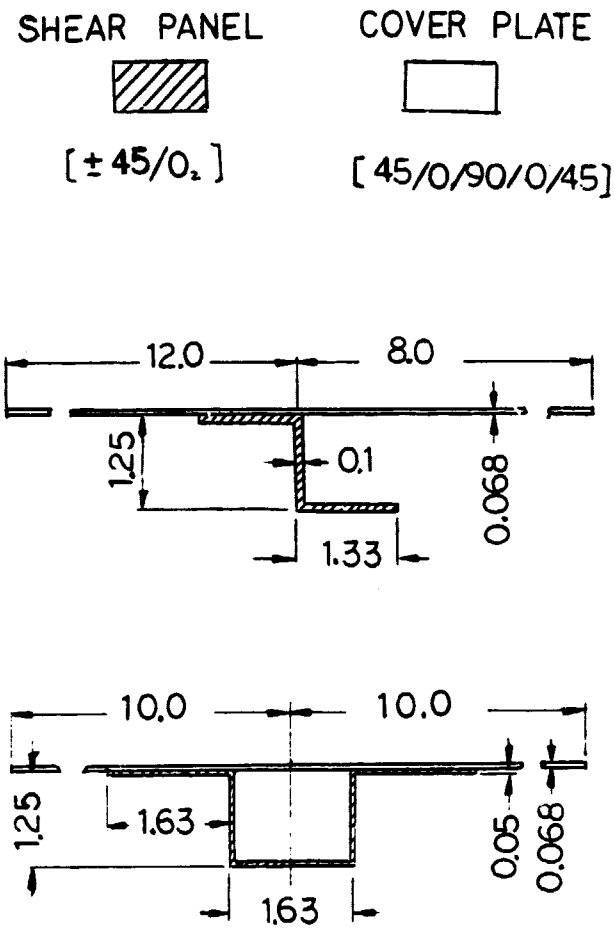

Figure IV-B-3. Skin-Stringer Test Cases

were also analyzed for a purely homogeneous isotropic material. The various composite lay-ups use the graphite/epoxy properties listed above.

Tables IV-B-3 and 4 contain the calculated results for these various cases. Several general observations can be made. Any of the thin-walled cross sections show a much lower decay rate than the solid rectangular section. The most dramatically slow decay rates are associated with the open sections, particularly the I-beam. The slowest decay rates for the isotropic I-beam and rectangular beam are, respectively, .0703 and .9286, so an isotropic I-beam can have a decay rate thirteen times slower than that of a solid rectangular beam. It can also be seen that the higher modes for the I-beam decay only twice as slowly as for the rectangular beam, so for careful selection of boundary conditions, the unfavorable ratio for the I-beam could be reduced to a factor of about two.

Anisotropy has an important effect on decay rate. It can lower it by a factor of three or four. For unidirectional composite structures, the box-beam shows the greatest effect in comparison with isotropic structures. Looking at the first mode for each, a comparison between .3140 and .0704 gives a 4.46 slower decay rate. For a typical laminated composite lay-up, a comparison with the isotropic case for the Z-section skin-stringer panel shows an effect of anisotropy of only twenty percent (i.e., .1648 versus .1364). For the

TABLE IV-B-3

FIRST FOUR DECAY RATES (γ) FOR VARIOUS BEAMS

Material	Cross Section		
	I-Beam	Box-Beam	Rect.-Beam
Isotropic	0.0703	0.3140	0.9286
	0.5717 ± 1.1627i	0.6459	1.0652 ± 0.5828i
	0.64392	0.7367	1.2348 ± 0.1763i
	0.8925 ± 0.4874i	1.0157 ± 0.4378i	1.8285 ± 0.5674i
Unidirectional Composite	0.0194	0.0704 ± 1.4573i	0.2432
	0.1844	0.1348 ± 0.0711i	0.3018
	0.2857	0.1847	0.4105
	0.3266	0.2299	0.4466
Laminated Composite	0.0255	0.1710 ± 0.6718i	(horizontal laminations)
	0.2667 ± 0.3302i	0.1760 ± 0.2334i	0.3886
	0.4003 ± 0.2419i	0.2024 ± 0.2769i	0.4142
	0.4506	0.3042	0.6130 ± 0.2222i
			0.9063 ± 0.1850i
			(vertical laminations)
			0.7168 ± 0.4839i
			0.7772 ± 0.0464i
			0.8372 ± 0.3634i
			0.8873

TABLE IV-B-4

FIRST FOUR DECAY RATES (γ) FOR SKIN-STRINGER PANELS

Material	Cross Section	
	Z-Section Skin-Stringer	Hat-Section Skin-Stringer
Isotropic	0.1648	0.2269 ± 0.1030i
	0.2284 ± 0.1013i	0.3346
	0.3361	0.4488 ± 0.1676i
	0.4175 ± 0.1867i	0.6055 ± 0.2169i
Laminated Composite	0.1364	0.1203 ± 0.2110i
	0.1550	0.1732
	0.2581 ± 0.0601i	0.1986
	0.3791	0.3101 ± 0.0439i
Isotropic Stringer Only (no skin)	0.1512	
	1.4756 ± 0.8272i	
	1.6351 ± 1.0892i	
	2.9159 ± 1.0703i	

I-beam, however, the laminated composite lay-up decays nearly as slowly as for unidirectional composites; almost three times slower than for isotropic materials.

It should be re-emphasized that the lowest decay rates discussed here are the slowest possible for any boundary condition. A modal superposition could be performed to vary the degree of participation of the first (or any other) mode for any particular boundary conditions.

In summary, a general finite element method for quantifying Saint-Venant's principle for prismatic members has been described. A second-order eigenproblem results, whose eigenvalues are the natural decay rates and whose eigenvectors are the cross-sectional response modes. It should be kept in mind that the resulting decay rates are the natural tendencies of the cross section, independent of the support or boundary conditions used. If one were interested in the stress redistribution due to particular support conditions, a normal finite element analysis or a modal superposition using the method described here, could be performed. The types of results given above can be thought of as indicating general tendencies that may, for example, be of use for preliminary design purposes.

4. Plans for Upcoming Period

Effort will be expended in an attempt to extend the method so as to perform modal superposition to find solutions for specific end boundary conditions. In addition, a

paper is being submitted to the Journal of Applied Mechanics on the material discussed above.

5. References

1. Toupin, R. A., "Saint-Venant's Principle", Archive for Rational Mechanics and Analysis, 18, 1965, pp. 83-96.

2. Knowles, J. K., "On Saint-Venant's Principle in the Two-Dimensional Linear Theory of Elasticity", Archive for Rational Mechanics and Analysis, 21, 1966, pp. 1-22.

3. Horgan, C. O., "On Saint-Venant's Principle in Plane Anisotropic Elasticity", Journal of Elasticity, 2, 1972, pp. 169-180.

4. Horgan, C. P., "Some Remarks on Saint-Venant's Principle for Transversely Isotropic Composites, Journal of Elasticity, 2, 1972, pp. 335-339.

5. Choi, I. and C. O. Horgan, "Saint-Venant's Principle and End Effects in Anisotropic Elasticity", ASME Journal of Applied Mechanics, 44, No. 3, 1977, pp. 424-430.

6. Choi, I. and C. O. Horgan, "Saint-Venant's End Effects for Plane Deformation of Sandwich Strips", International Journal of Solids and Structures, 14, No. 3, 1978, pp. 187-195.

7. Dong, S. B. and D. B. Goetschel, "Edge Effects in Laminated Composite Plates", ASME Journal of Applied Mechanics, 49, March 1982, pp. 129-135.

8. Knowles, J. K. and C. O. Horgan, "On the Exponential Decay of Stresses in Circular Elastic Cylinders Subjected to Axisymmetric Self-Equilibrated End Loads", International Journal of Solids and Structures, 5, 1969, p. 33.

9. Klemm, J. L. and R. W. Little, "The Semi-Infinite Elastic Cylinder Under Self-Equilibrated End Loading", SIAM Journal of Applied Mathematics, 19, 1970, pp. 241-255.

10. Power, L. D. and S. B. Childs, "Axisymmetric Stresses and Displacements in a Finite Circular Bar", International Journal of Engineering Science, 9, 1971, pp. 241-255.

11. Duncan Fama, M. E., "Radial Eigenfunctions for the Elastic Circular Cylinder", Quarterly Journal of Mechanics and Applied Mathematics, 25, 1972, pp. 479-495.

12. Mitra, D. N., "On Axisymmetric Deformations of a Transversely Isotropic Elastic Cylinder of Finite Length", Archiwum Mechaniki Stodowanej, 17, 1965, pp. 739-747.

13. Warren, W. E., A. L. Roark and W. B. Bickford, "End Effect in Semi-infinite Transversely Isotropic Cylinders", AIAA Journal, 5, 1967, pp. 1448-1455.

14. Horgan, C. O., "The Axisymmetric End Problem for Transversely Isotropic Circular Cylinders", International Journal of Solids and Structures, 10, 1974, pp. 837-852.

15. Spilker, R. L. and S. C. Chou, "Edge Effects in Symmetric Composite Laminates: Importance of Satisfying the Traction-Free-Edge Condition", Journal of Composite Materials, 14, 1980, pp. 2-20.

16. Altus, E., A. Rotem and M. Shmueli, "Free Edge Effect in Angle Ply Laminates - A New Three-Dimensional Finite Difference Solution", Journal of Composite Materials, 14, 1980, pp. 21-30.

17. Sandorff, P. E., "Saint-Venant's Effects in an Orthotropic Beam", Journal of Composite Materials, 14, July 1980, pp. 199-212.

PART V

PROCESSING SCIENCE AND TECHNOLOGY

V-A VARIATION OF RESIN PROPERTIES THROUGH THE THICKNESS OF CURED SAMPLES

V-B INITIAL SAILPLANE PROJECT: RP-1

V-C SECOND SAILPLANE PROJECT: RP-2

V-A VARIATION OF RESIN PROPERTIES THROUGH THE THICKNESS OF CURED SAMPLES

Senior Investigator: B. Wunderlich

1. Introduction

It is the purpose of this work to gain knowledge of glassy materials and to study the homogeneity and curing progress of composite materials. We intend to link the glass transition quantitatively with the presence of a given material (through the glass transition temperature T_g and the increase in heat capacity ΔC_p). Superposition of reference materials should enable sample characterization. The limits of this somewhat novel approach are planned to be tested using the equipment and techniques developed in our ATHAS* (Advanced Thermal Analysis) laboratory. The project will have the support of postdoctoral fellow J. Grebowicz and research assistant L. Judovits.

2. Status

This is a new project and was started on May 1, 1983. Earlier work on epoxy model compounds was carried out by graduate student N. Gjaja.

Numerous compounds known under the generic name of epoxy resins have great practical importance in industrial applications. Through many different chemical reactions, epoxy resin molecules can be interconnected into polymeric three-

dimensional networks. There are two major groups of reactions which are capable of crosslinking epoxy resins. Either a crosslinking agent is used where a different molecule is built into the epoxy network connecting two or more epoxy resin molecules, or a crosslinking catalyst is used where the entire resulting network is essentially built out of epoxy molecules mutually interconnected.

It is believed that epoxy crosslinked networks, resulting from certain catalytic reactions, form into a heterogeneous structure. That is, particles of high crosslink density form and grow in the matrix of uncrosslinked or sparsely crosslinked material. As the crosslinking reaction advances, these gel particles become interconnected into a global network, but the intrinsic heterogeneity remains. Further, the gradual decrease in mobility of reacting molecules causes the network built at the end of the reaction to be considerably lower in crosslink density than that which was formed initially.

The two distinctly different crosslink densities have associated with them two respective glass transition temperatures.

Using differential scanning calorimetry (DSC), measurements of heat capacity have been made to provide a basis for accurate study of the glass transition region. Such heat capacity measurements on uncrosslinked, partially crosslinked and fully crosslinked epoxy resins have provided insight into

basic mobility changes of the molecules. Knowledge of heat capacity at the glass transition yields an estimate of mobile units in the molecule. Coupled with information about the coefficient of expansion, compressibility and group and skeletal vibrations, this provides an understanding of the behavior of the epoxy resin molecule.

On this basis, we believe that study of changes in heat capacity, with the advancement of crosslinking, provides a means for characterizing polymeric networks.

Although there is a large body of literature concerning crosslinked epoxy resins, there appears to be no data available on heat capacities of these epoxy materials as such. Studies which have been made are limited to reactions which occur when these formulations are crosslinked to mechanical, thermal and other application oriented properties of resulting networks.

This work is expected to make a significant contribution to a deeper understanding of a large family of materials which are widely used in structural laminates.

There are three other areas of possible advancement from this study, First, the heterogeneous nature of crosslinked resin networks may become better understood. Second, the ability to change the glass transition with advancing crosslinking may add further detail to our knowledge of glass transition phenomena in general. Third, some new details in the technique of using thermal analysis for study of other heterogeneous granular macrostructures may evolve.

3. Progress During Report Period

a. Approach

The earlier work, outlined in Section 2 - Status, was reviewed and will be completed in the next half-year period.

Three uncured samples and two cured samples of epoxy resins were supplied by Dr. R. J. Diefendorf to initiate the planned analyses. The uncured resins were:

1. Fiberite 979,
2. Hercules 1908 and
3. Hercules 3501-6.

The cured resins were:

1. Fiberite 979 and
2. Hercules 3501-6.

The chemical structures of the major constituents of these epoxies are given in Table V-A-1[1,3,4]*. The curing reaction for the Hercules 3501-6 resin is given in Table V-A-2[2].

b. Results

Various DSC scans using the DuPont 990 have been performed in order to establish the glass transition temperatures of the provided epoxies. Only endo- and exothermic peaks were noted for the samples measured. However, macroscopic observation of the uncured samples revealed that, if brought to ambient temperature, the uncured epoxy resin would go from a hard glassy state to a rubbery state. Further scans of the cured Fiberite sample showed an endotherm

*Numbers in brackets in this section refer to the references which are listed on page 147.

TABLE V-A-1

CHEMICAL STRUCTURES OF THE MAJOR CONSTITUENTS OF MATRIX RESINS

Hercules 3501-6 Resin

Prepolymer

MY 720 (N,N,N′,N′ – Tetraglycidyl – 4,4′–methylenebisenzenamine)

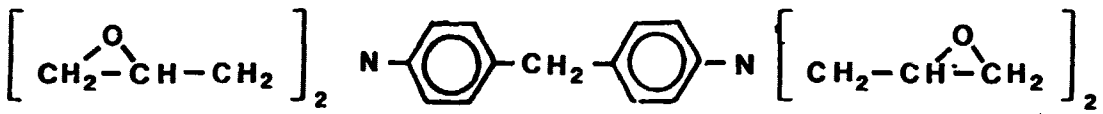

4,4′–Diaminodiphenylsulphone (DDS)

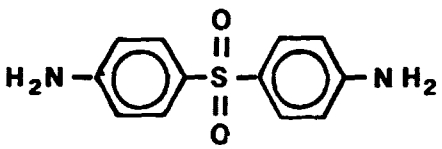

Catalyst

$BF_3 - C_2H_5OH$

Fiberite 979 Resin

Resin, Epoxylated phenol–formaldehyde novalac

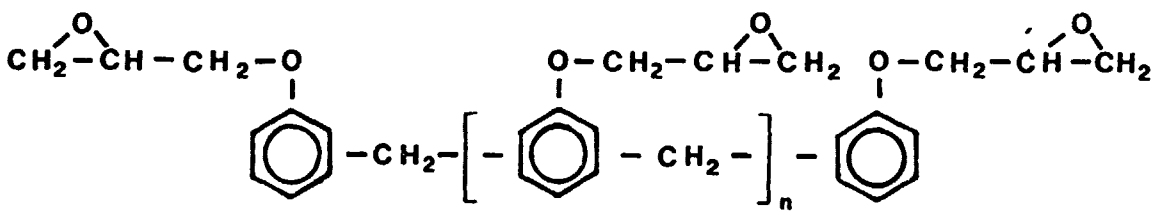

Curing Agent, Dicyandiamide (DICY)

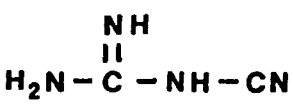

TABLE V-A-2

CURING REACTIONS FOR HERCULES 3501-6 RESIN

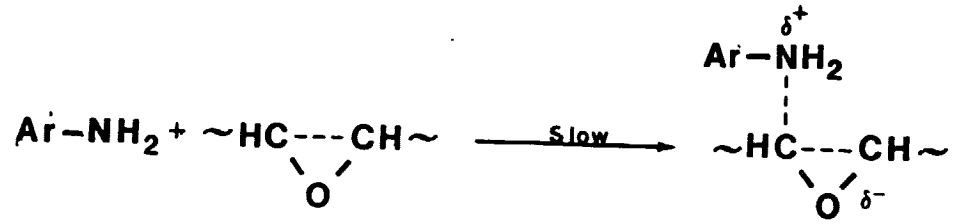

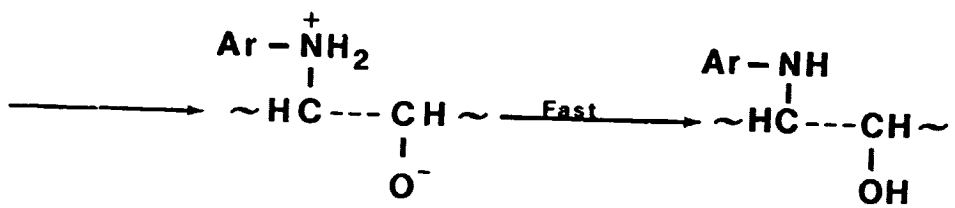

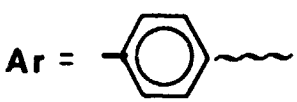

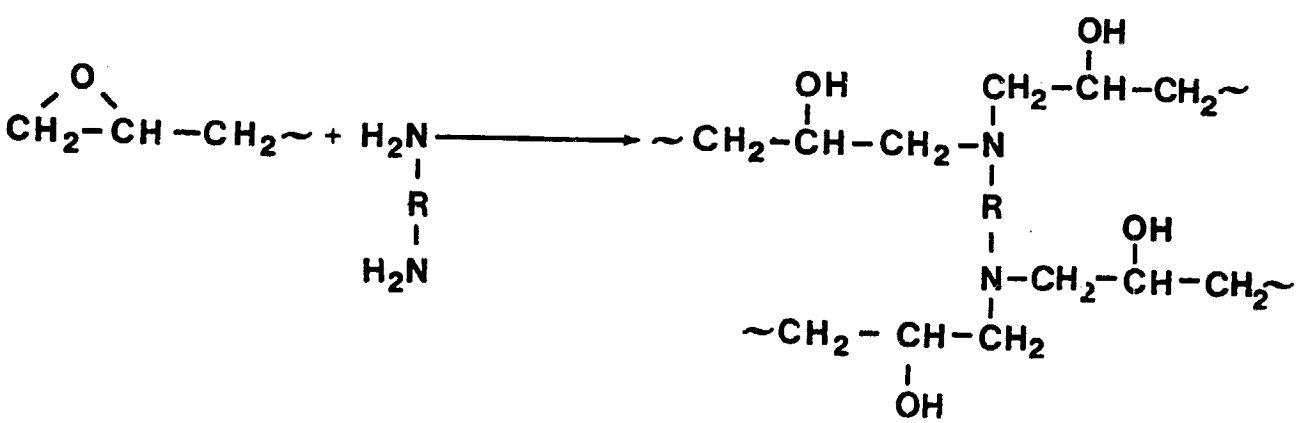

starting at 120°C followed by an exotherm beginning at 160°C. After repeated scans, a glass transition (T_g) of 142°C was clearly seen without the accompanying exotherm. Since curing does not take place below the glass transition temperature[6], the moment the sample is heated above the T_g region curing begins. Thus, the endotherm covers the glass transition of the not fully cured epoxy. This transition region was about 135°C.

4. Plans for Upcoming Period

The work of graduate student N. Gjaja, outlined under Part 3.b., Results, should be completed within the next reporting period. In addition, model substances closer to those used in composite structures are to be developed which, however, do not show the complication of superposition of curing reaction and glass transition. A third approach will be to follow closely the actual use of epoxies in composite formation and to model that process in the DSC equipment.

5. References

1. Allen, J., Personal communication, Fiberite Corporation, 501-559 W. Third Street, Winona, MN 55987, 1983.

2. Badram, B. M., A. A. Yehid and E. M. Abdel-Bary, "The Modification of Epoxidized Linseed Oil with Aromatic Amines", European Polymer Journal, 13, 1977, p. 155.

3. Mohajer, Y., E. Yurgitis, G. Wilkes and J. McGrath, "Physical Aging Studies of Epoxy Resins with Emphasis on Graphite Fiber-Epoxy on Graphite Fiber-Epoxy Composites", Proceedings of the Critical Review: Techniques for the Characterization of Composite Materials, Army Materials and Mechanics Research Center, Watertown, MA 02172, 1982.

4. Diefendorf, R. J., Personal communication, Rensselaer Polytechnic Institute, Troy, NY 12180, 1983.

5. Lee, H. and K. Neville, Handbook of Epoxy Resins, McGraw-Hill, New York, NY, 1967, pp. 5-15.

6. Gillham, J. K., "The Time-Temperature (TTT) State Diagram and Its Role in Determining Structure/Property Relationships in Thermosetting Systems", Org. Coat. Plast. Chem., 44, 1981, p. 185.

7. Savla, M. and I. Skeist, "Epoxy Resins", High Polymers - Vol. XXIX Polymerization Processes, C. E. Schildknecht, Ed., Wiley-Interscience, NY, 1977, p. 582.

8. Odiam. G., Principles of Polymerization, 2nd Edition, Wiley-Interscience, NY, 1981.

V-B INITIAL SAILPLANE PROJECT: THE RP-1

Senior Investigators: F. P. Bundy
R. J. Diefendorf
H. Hagerup
H. Scarton

1. Status

Recognizing that the resins in composite materials can change properties somewhat with aging and exposure to temperature/moisture cycles, the wing/fuselage ensemble structure of the RP-1 glider has been static tested about once a year since its initial fabrication in '79-'80. This initial series of tests consisted of simple vertical bending, and the last of this series was done on August 5, 1981. That test consisted of simple bending using a distributed load up to a maximum of 590 pounds per wing, which corresponds to a little over 4 g's for average pilot weight.

Some changes were made in the wing beam "carry-through" structure of the RP-2 glider, in the summer of 1982, with an eye to making it stronger and more fail-proof. In subsequent tests of the RP-1 glider, the wing-fuselage assembly was subjected not only to simple vertical bending, as in previous years but, in addition, to a bending-torsion test with fore-aft bending components, which would simulate the stresses in a high speed pull-out.

In the simple bending tests, the fuselage was held in a horizontal position and the weights were laid directly over

the wing beam. In the bending/torsion tests, the fuselage was positioned on a ten degree slant (nose low, tail high, inverted) and the weights placed on a line fourteen centimeters aft of the wing beam. Thus, both torsion and fore-aft bending were induced, in addition to vertical bending. These two static tests were survived very successfully.

With the achievement during the summer of 1982 of sustained thermal soaring of the RP-1 on two separate occasions, the first all-composite glider built under this program has been set aside. Some additional flights may be undertaken in the future for demonstration purposes, to stimulate student interest in the program, to maintain an experienced flight crew, to test ideas for further aerodynamic refinement and for their influence on structural life; none, however, were conducted in 1983,

2. Progress During Report Period

In addition to static tests of the complete RP-1 airframe, tests have also been conducted on structural elements of two different kinds, typical of those used on the RP-1 and hidden from view, in the falls of '81, '82. Five of each kind were tested each year.

This kind of test was repeated in September 1983. Configurations of the test specimens are shown, as they were in earlier progress reports, in Figure V-B-1. The results of the latest round of testing are shown with those of the two earlier rounds, in Figure V-B-2.

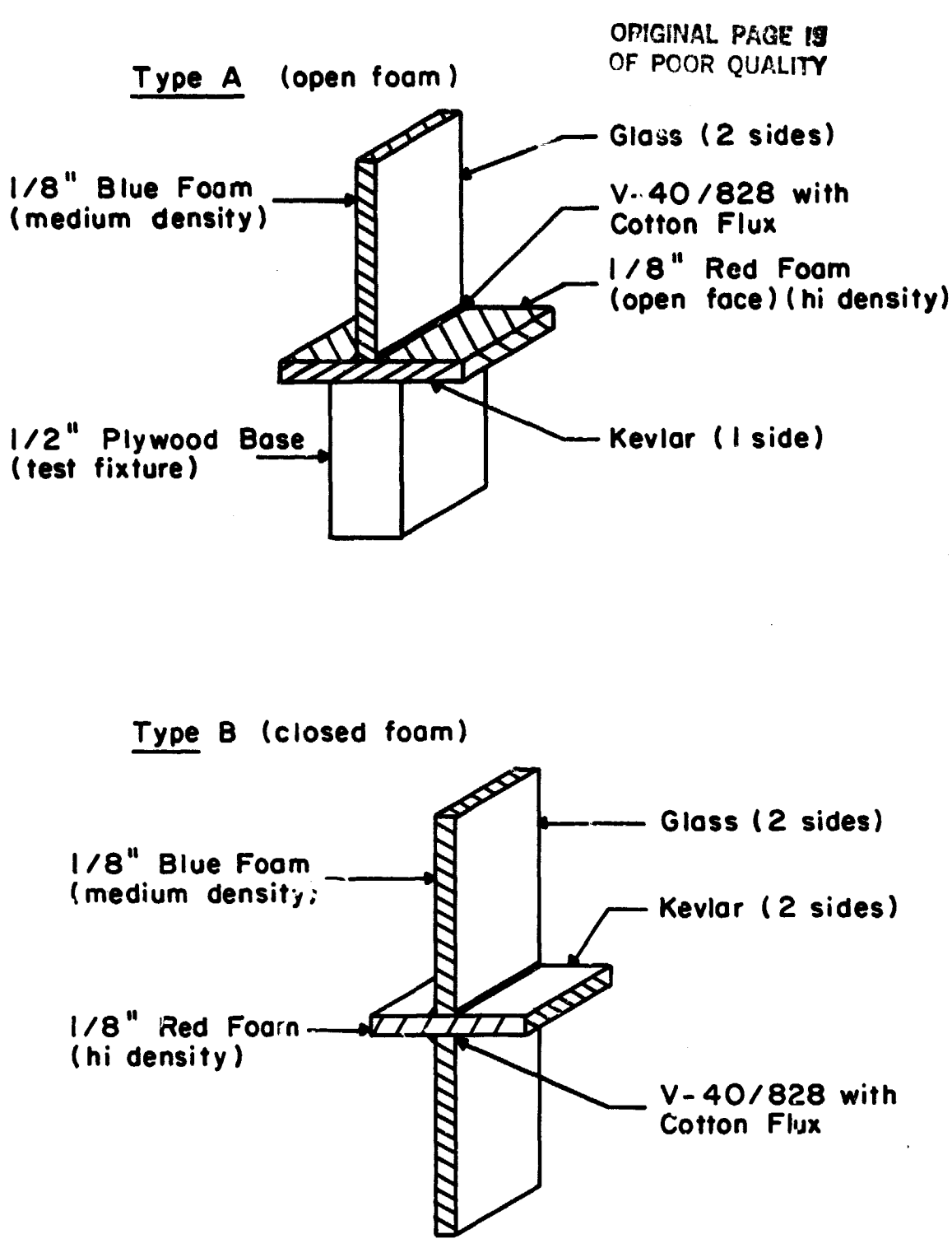

Figure V-B-1. Two Types of Structural Joints Used in the RP-1 (lightly-loaded, low-cost composite structures)

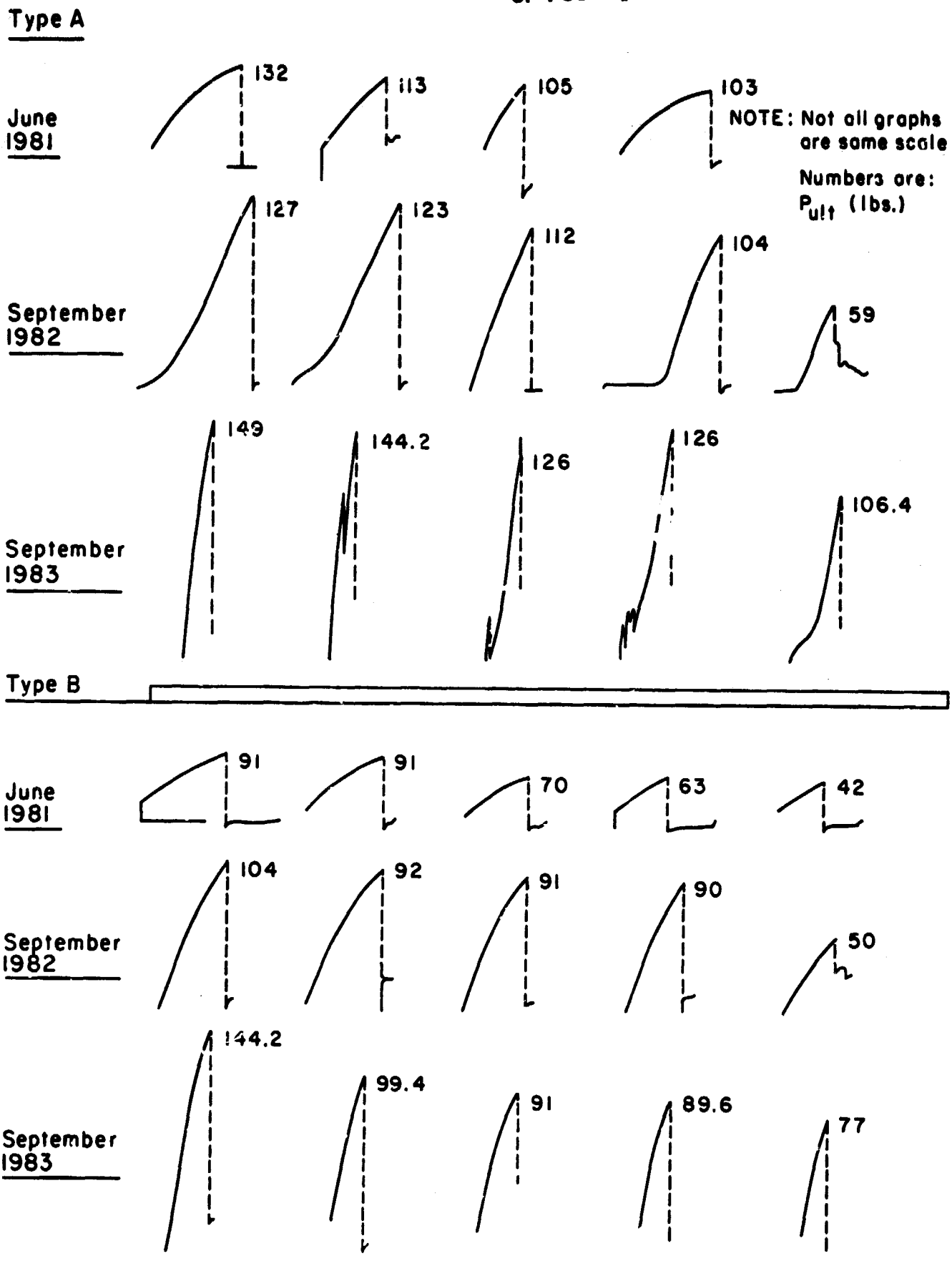

Figure V-B-2. Results of Tensile Tests to Failure of the Structural Joints Shown In Figure V-B-1

It appears that the conclusion reached earlier, namely, "degradation with time is well-within the spread in strength due to fabrication or materials quality", is also supported by the most recent data.

V-C SECOND SAILPLANE PROJECT: THE RP-2

Senior Investigators: F. P. Bundy
R. J. Diefendorf
H. Hagerup
H. Scarton

1. Status

The aircraft, as rebuilt following damage sustained in failures at 95% of combined bending-torsion, design ultimate loading and with structural modifications installed, was made ready for structural proof tests.

The wings were rebuilt using carbon spar cap splicing techniques that were developed in a series of experiments. Structural modifications included an improved wing spar, "carry-through" design which utilized two major shear pins to link the stubs of the port and starboard wing spars. The affected part of the fuselage structure was also rebuilt. This incorporated a much stronger carbon fiber tubular compression strut between the front wing pins, to better resist the forward deflection of the wings. "Window" openings in the "elephant tusk" side beam members of the fuselage structure, through which the wing beam stubs pass to form the "carry-through" linkage, had to be enlarged to accommodate the larger, thicker, female wing stub member. (See earlier progress reports for more graphic descriptions of the aircraft.) The clearances between the male and female members of the "carry-through" were also increased so that the only "leverage contacts" that could occur between them would be

at the two major shear pins. Thus, there could be no local contact forces transmitted to the open end of the female stub.

2. Progress During Report Period

The RP-2 aircraft was assembled in an inverted position, in the CAPGLIDE workroom area, high bay section of the Jonsson Engineering Center on June 21-22, 1983. The fuselage supports were placed at the pilot's seat and the (normally) top face of the "junction box" (into which the tail boom and the wing pins connect). Sand bags were placed on the wing to simulate the aerodynamic lift on the wing in flight. In the simple bending test, the bags were placed directly over the main wing spar, one 10-lb. bag every 10 inches. The span density of loading was tapered off toward the outboard ends to account for chord taper and spanwise load reduction due to induced effects near the wing tips. The pitch attitude was set such that the tail boom was horizontal, which, in the inverted position, corresponds to a $2\frac{1}{2}°$ down pitch of the wing chord (the angle of incidence of the wing relative to the fuselage is set at $+2\frac{1}{2}°$). The physical setup is illustrated in Figure V-C-1.

Arrangements were made for deflection measurements at six positions along the leading edge and six positions along the trailing edge, as shown in Figure V-C-2 - looking down. The structure was monitored using acoustic emission

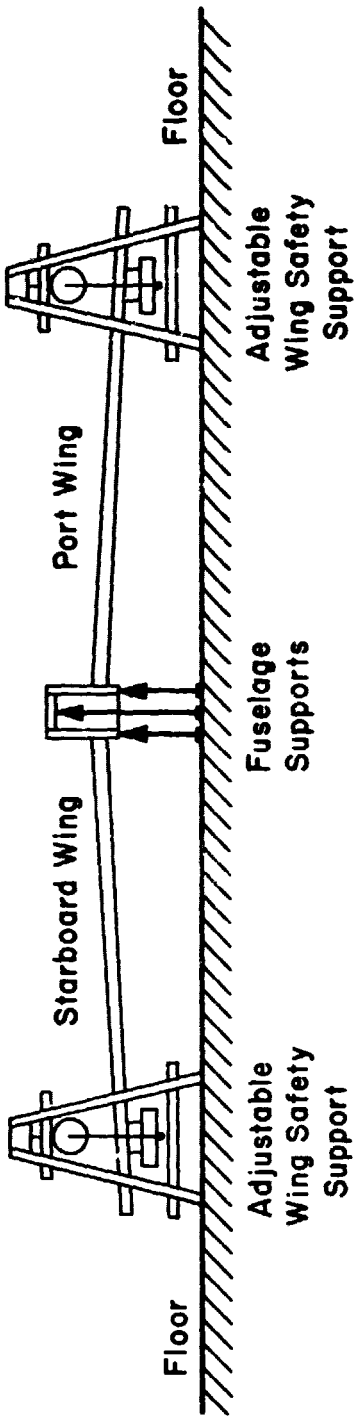

Figure V-C-1. RP-2 Static Test Set-Up (looking from aft forward)

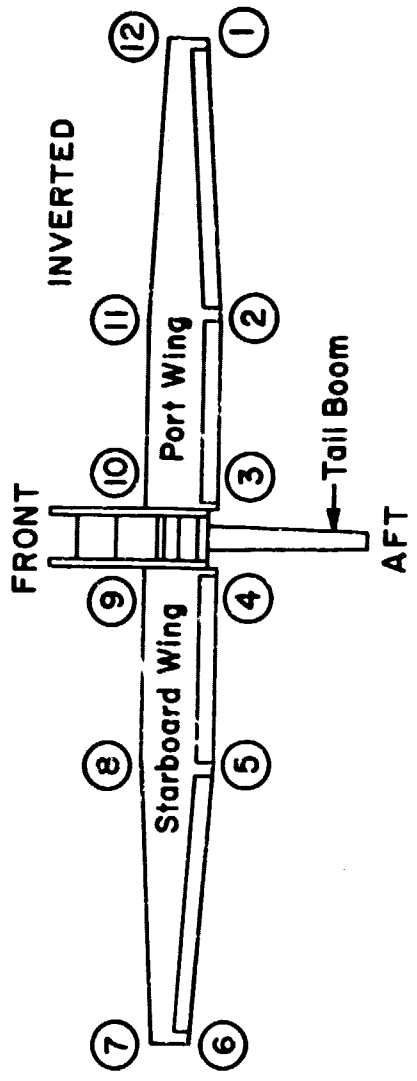

Figure V-C-2. RP-2 Test Set-Up

(Looking down on the inverted assembled wing-fuselage structure. The 12 vertical deflection measurement stations are shown.)

instrumentation for "acoustic events" during the test. This was done by applying microphones to the wing skins at four points at the inboard edges adjacent to the carbon fiber cap strips of the wing beams, top and bottom. To provide their electronic recording system with a "loading signal", strain gauges were bonded to the inside surfaces of the carbon cap strips of the male wing beam stub. The output of these gauges was nearly proportional to the bending moment at the inboard end of the wing. This loading record against time made it possible to correlate any recorded sonic events with the level of loading.

At each loading step, the pullout of the aft wing pins from their receptacles in the fuselage was measured by inserting feeler gauge strips in the gaps. In the simple bending test at the full specified loading, the strain gauge installed on the inside surface of the (normally) upper cap strip read 0.325% strain at the maximum loading, and there were no hints of incipient failure. The wings were unloaded by sand bag layer steps, with deflection readings being made at each step. The strain gauge in question read 0.001% at the unloaded state, which was considered a good return to "zero".

Concerning the torsion test, review of the Air Force pitching moment characteristics and the flight envelope (Figure V-C-3) showed that in upright flight at 79 mph the torsion moment at the wing root about the spar axis would be

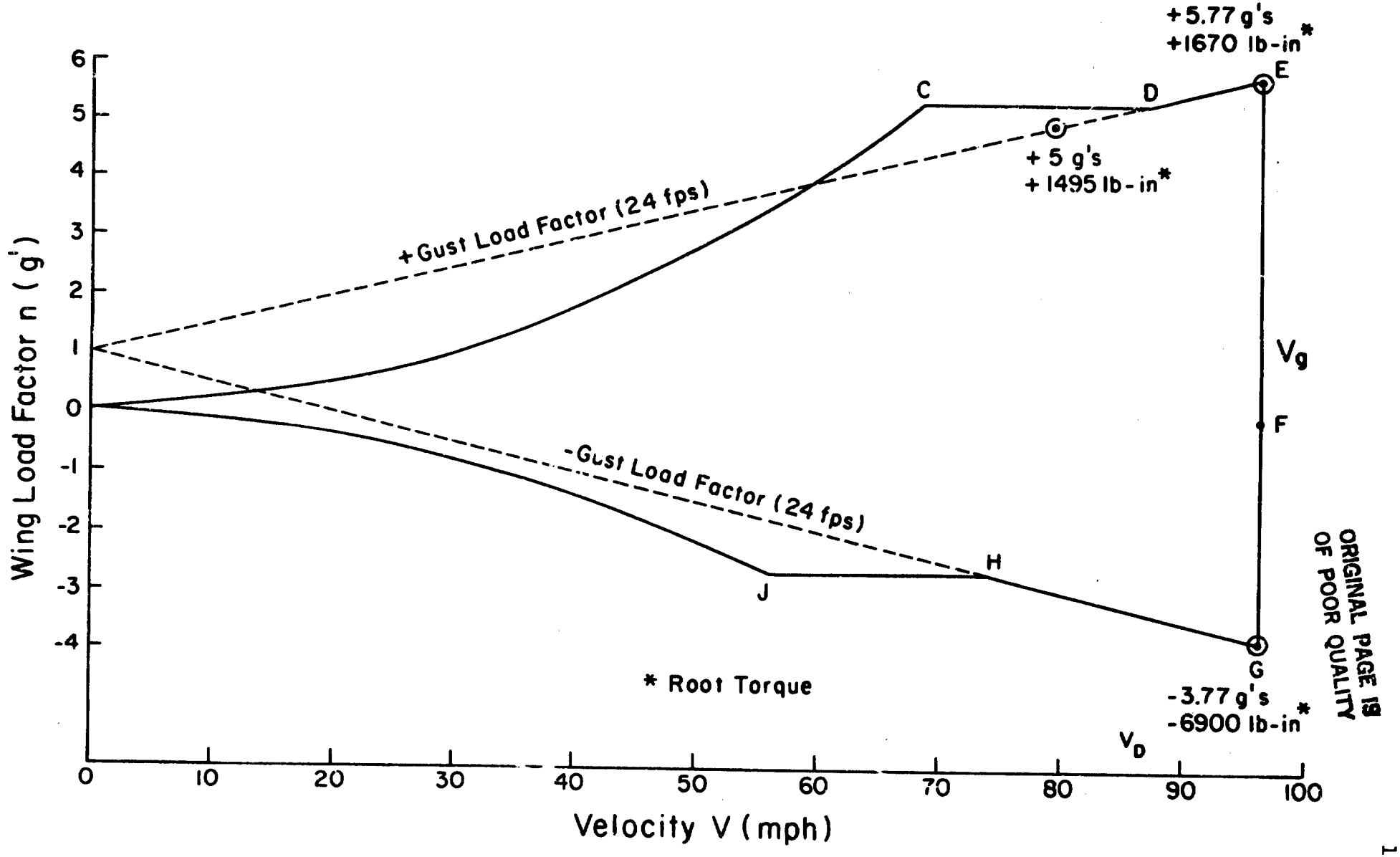

Figure V-C-3. Flight Envelope - RP-2

about 1445 #-in, nose up. This is the net of 3920 #-in due to the lift acting at the quarter chord, hence nose up, and -2475 #-in moment associated with the airfoil's camber which is nose down.

The worst torsion case occurs at the negative g, high-speed corner of the flight envelope (-3.77 g's; 96.2 mph) for which the total torque per wing is predicted to be about -6900 #-in (nose down). This torque could be induced by loading sand bags on the inverted wing aft of the spar with the glider in its inverted position. In an actual flight condition with negative g's, however, the upper wing surface and spar caps would be subjected to tension; in an inverted static test with sand bags aft of the leading edge, spar bending would be in the opposite direction. Since the spar had already been tested to 6 g's in positive simple bending, it was decided to conduct the torsion test to about -7000 #-in, while restraining the wing from the full bending that such loading would produce.

Thus, the test was conducted by placing the sand bags along a line 30 cm (11.81") aft of the spar on the constant chord (inboard) part of the wing. On the tapered (outboard) part of the wing, the sand bags were laid along a line extending from 30 cm aft of the spar at the inboard end to 15 cm aft of the spar at the wing tips. This is illustrated in Figure V-C-4. This arrangement provided a realistic span distribution of the applied torque (as in flight), with about

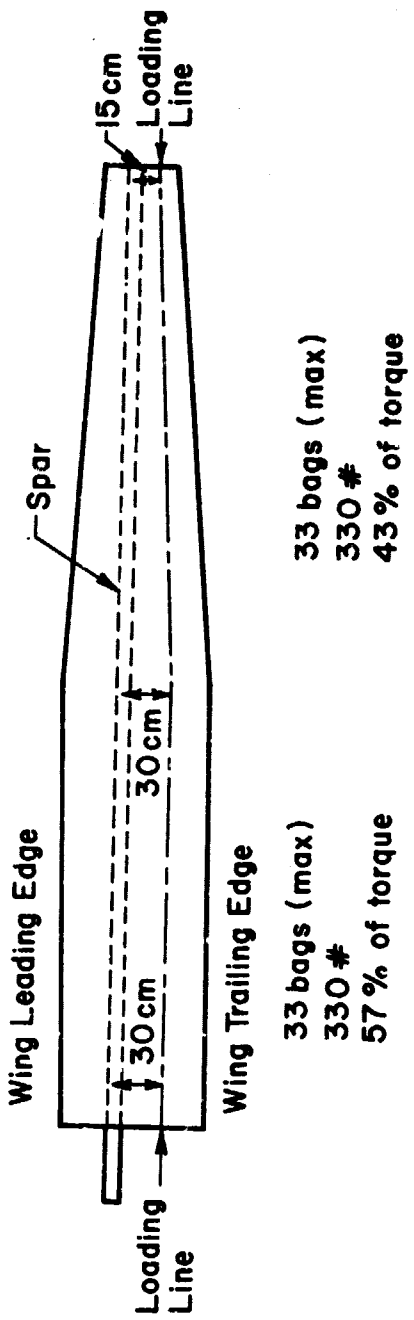

Figure V-C-4. Loading Plan for the RP-2 Torsion Test

57% of the total torque contributed by the constant chord part and 43% by the tapered chord sections. For the first 1.5-g loading of the spar, the wing was allowed to bend slowly. From that loading on, the safety supports, positioned spanwise as shown in Figure V-C-1, and bearing fulcrums of styrofoam backed by wood 2 x 4's, were set so that the styrofcam fulcrums contacted the wing at the chord position of the spar. Similar load-bearing fulcrums were also put under the wing spars at about the one-third span positions. Thus, loadings beyond 1.5 g's produced more torque about the spar but not more bending.

As in the bending tests, vertical deflection measurements re taken at the 12 stations shown in Figure V-C-2. In addition, at the same stations, scales were set up to measure horizontal deflections. At given loading levels readings of vertical and horizontal deflections were made and recorded for the twelve stations. The pull out of the aft wing pins was observed and measured as in the simple bending test, and, again, acoustic emissions were monitored. The structure withstood the torsion test without any indication of overstrain or damage.

The vertical deflections measured in the simple bending test at the various stations and at the different stages of loading are shown graphically in Figure V-C-5. The wing tip deflection at the heaviest loading was a little over 60 cm. This corresponds to a tip-deflection semispan ratio of .09,

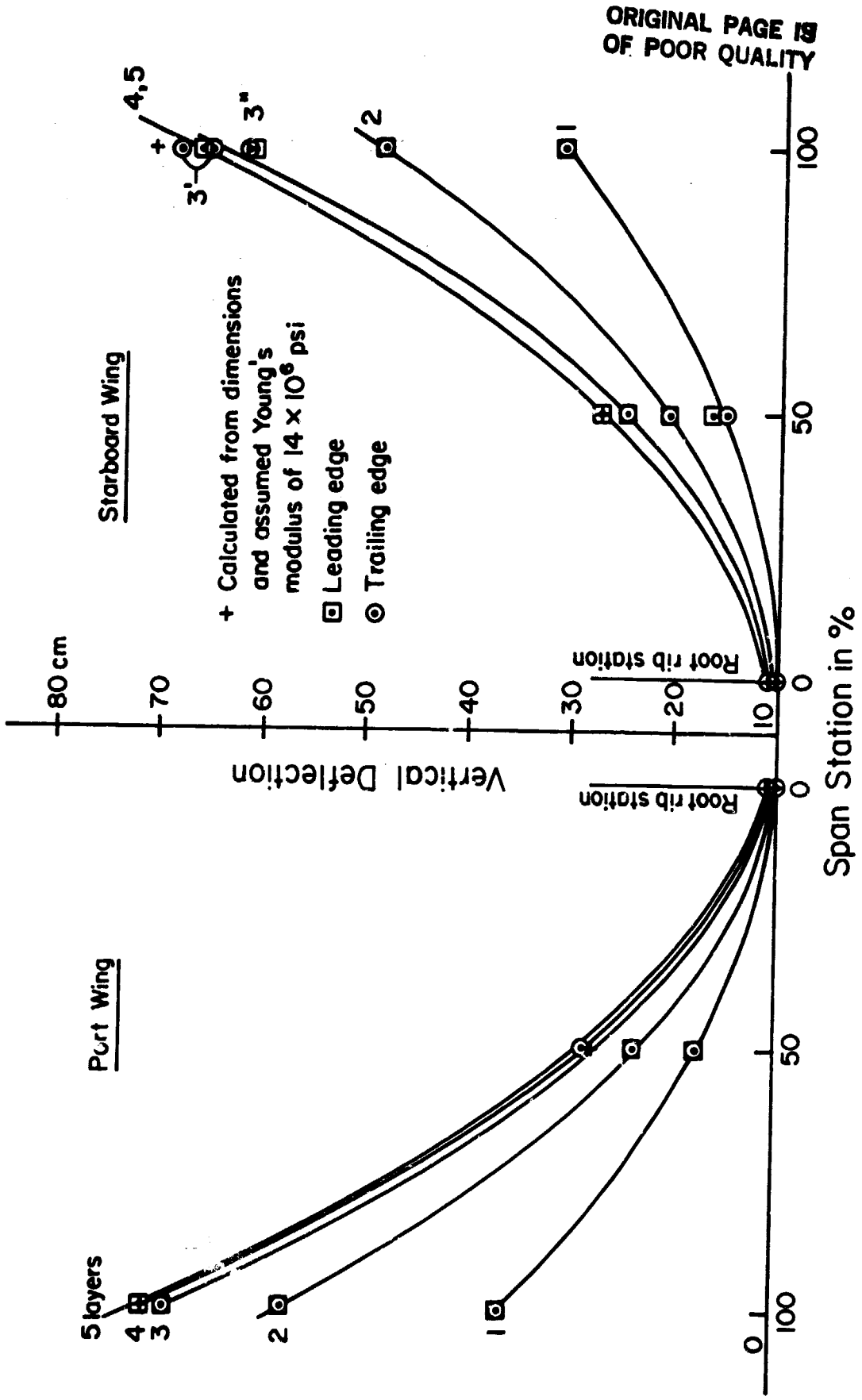

Figure V-C-5. Vertical Deflections Versus Span Position at Different Loadings: RP-2 Simple Wing Bending Test, June 21, 1983

which is quite stiff for a cantilever beam. The data also shows that the inboard ends of the wings moved slightly relative to the laboratory floor (which was the reference). Since the wing pins engaged the fuselage at these inboard measuring stations, this inboard deflection must have been due to compression of the supports under the fuselage. At the heaviest loading it was about 1 cm, or roughly 1.7% of the tip amplitude.

When the wing was unloaded, the inboard station readings returned to the initial values within one or two millimeters, but the outboard station readings indicated some permanent distortion. Figure V-C-6 shows the differences between the initial and the final readings, unloaded. The distribution of the net deflection spanwise suggests two things: (i) that the whole aircraft rolled very slightly (about 0.1°) during the test, and (ii) that there may have been a permanent "set" which, at the wing tips, was about 1 cm. This appears to have been an "additional dihedral" due to distortion in the "carry-through" zone, also amounting to about 0.1°. This is not seen as serious, since this was the first time these wings and "carry-through" linkages had been heavily loaded, and there was no visible or other evidence of difficulty.

The "pull out" of the aft wing pins from the receptacles in the fuselage is plotted in Figure V-C-7 as a function of the loading. The magnitude of the pull out seems to be

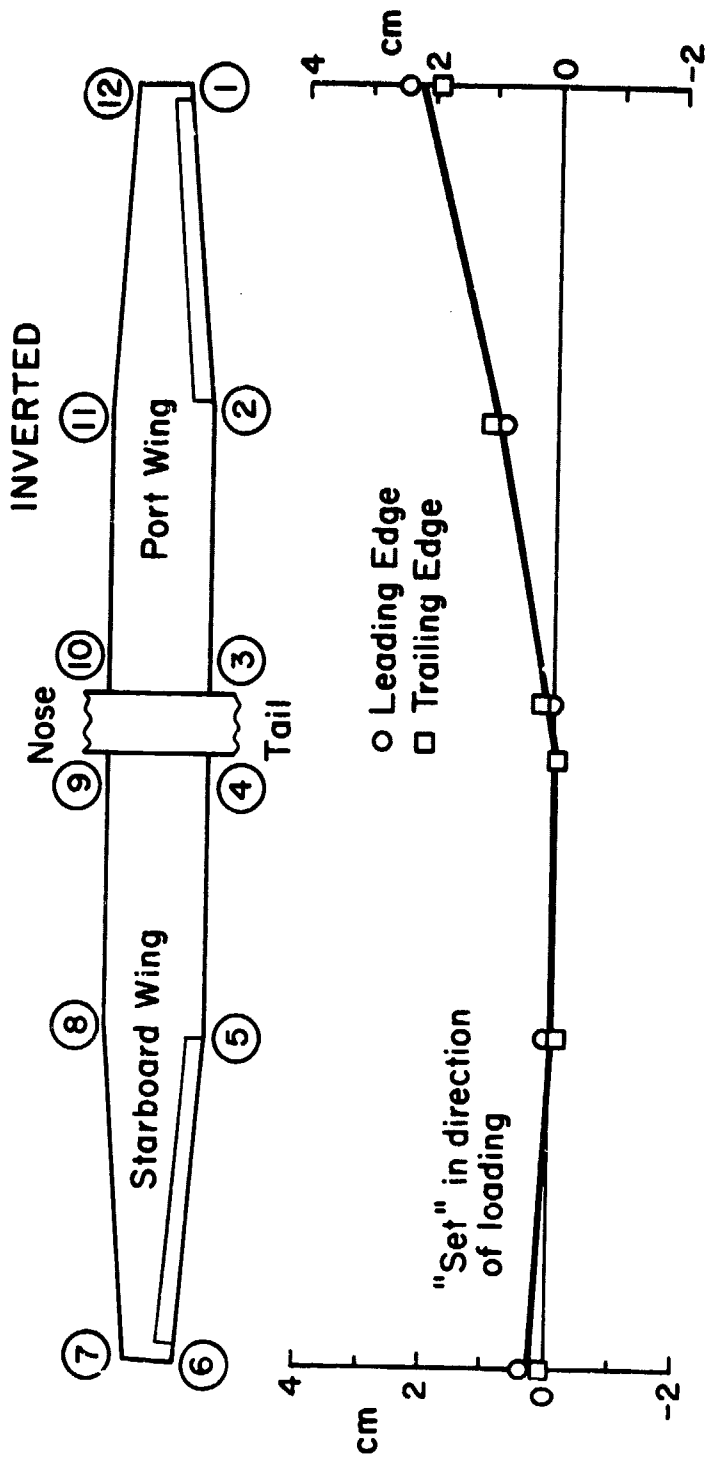

Figure V-C-6. Differences Between Before and After Test Vertical Readings at Zero Load

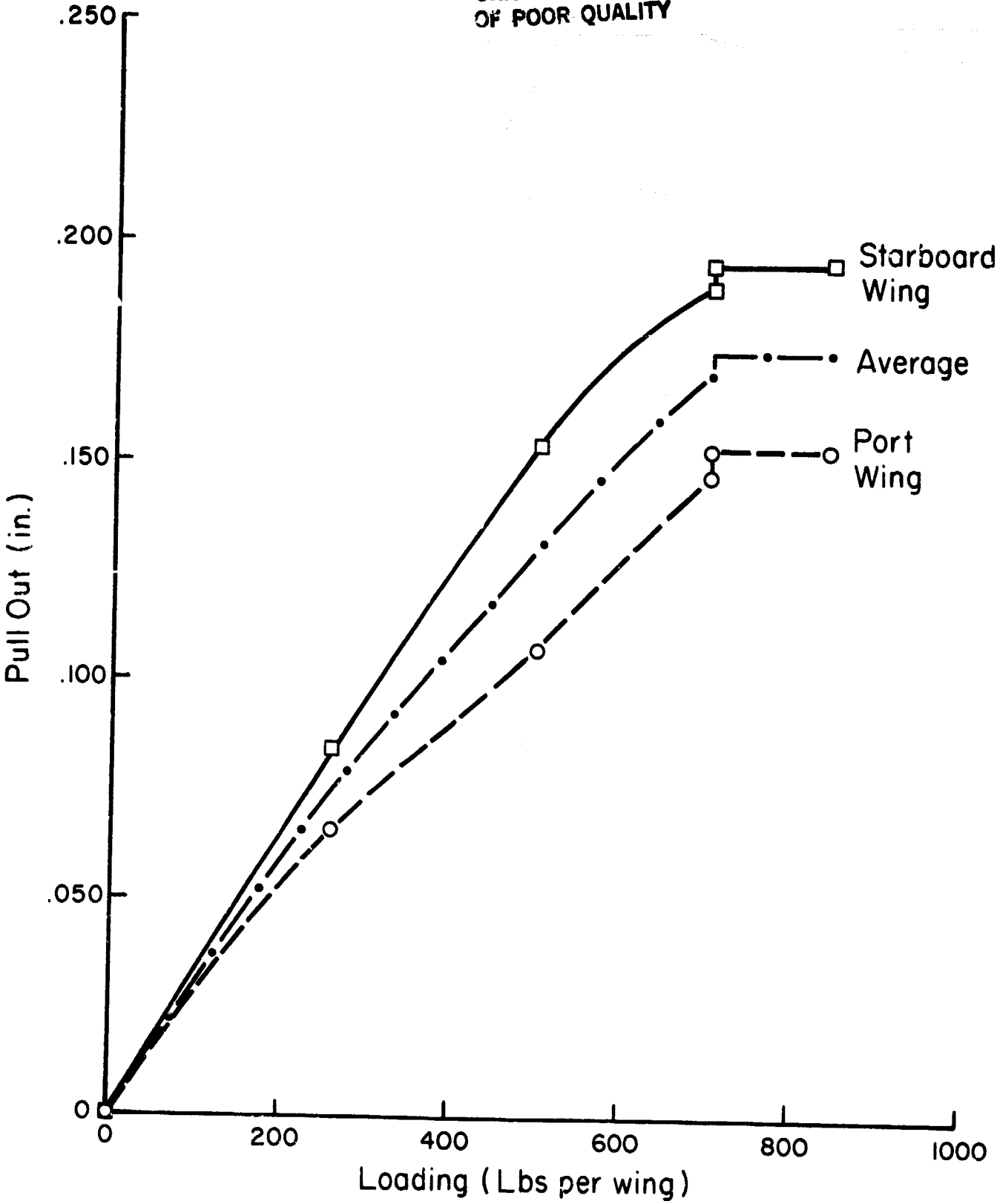

Figure V-C-7. Pull-Out of the Aft Wing Pins from Their Fuselage Receptacles, Versus Loading: RP-2 Simple Wing Bending Test, June 21, 1983

about proportional to the loading up to the 700 pounds per wing value. Additional loading to 850 pounds per wing produced no further gapping. Possibly the pins jambed or locked in the sockets, or clearance in the ball joints "bottomed" and tensile reactions were generated across the fuselage "junction box". The pull out was not measured during unloading, but it was observed that when unloading was complete, the pins were back in their initial positions. This relatively large amount of pull out of the aft pins is a result of the forward thrust component on the wings and suggests that, even with the stronger and stiffer carbon compression strut between the forward pins, the leverage isn't enough to prevent the wing from bending forward an appreciable amount. Possibly the forward inboard wing skins are not stiff and strong enough to prevent the forward bend.

Vertical deflections were observed at the measuring stations during the torsion test, done on June 22, 1983. As stated earlier, the wing was restrained from additional bending after the first layer of sand bags was applied. Consequently, the deflections shown are nearly the same for the first, second and third layers of sand bag loadings. The amount of bending due to the 22 bags per wing (i.e., one layer) is consistent with that observed in the simple bend test at 26 bags per wing.

The observed twist deformations of the wings are summarized in Figure V-C-8. The starboard wing apparently

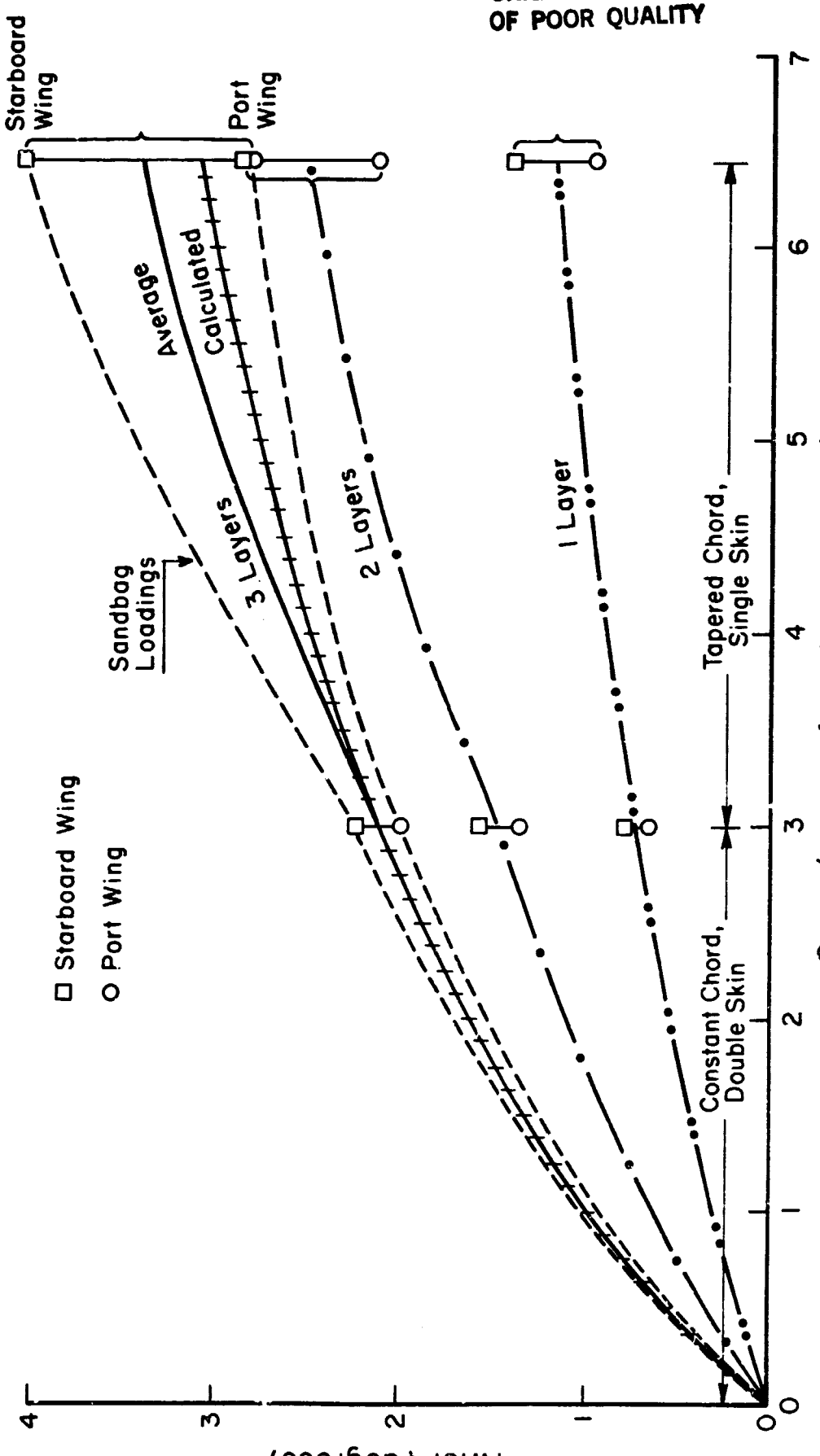

Figure V-C-8. Wing Twist Versus Span: RP-2 Torsion Loading Test

twists more than the left one. Differences in wing twist angle increase as the measurement stations approach the tip. The average of the two wings' torsional deflections are shown for the three layers of loading. The wings appear to have twisted elastically, as the amount of twist increased in near proportion to the applied torque and, upon unloading, returned nearly to the initial angle. These data show that the port wing took on a permanent twist deformation of 0.23°, while the starboard wing "set" by about 0.57°, as measured at the wing tips. If these values for permanent twist "set" are real, the "washout angle" of the wings, built in at $1\frac{1}{2}°$, will now be about 2° (which is still satisfactory). It is possible that some of the difference in response of the two wings may have been due to inaccuracy in placing the support fulcrums exactly under the wing beams, with different errors on the two wings.

The magnitude of the twist may be compared with that based on the torsion measurements made on an 0.8 meter long test section of the wing on September 24-26, 1981. The torsional compliance estimated from those test results was 1.72×10^{-4} deg/#-in/meter. Applying this value to the actual wing geometry and allowing for the outboard tapered section of the wing to have a single layer of Kevlar skin, the calculated twist distribution corresponding to the applied torque came out as shown in Figure V-C-8. It seems, from a comparison with the average of the two wings' torsion

deflections, that the twist response is about what it should be.

The acoustic event instrumentation showed no significant acoustic events except on the tension side of the female wing "carry-through" transition zone (i.e., at the inboard master rib station). A total of 487 events were recorded, with 12 large amplitude events of over 75 db occurring during the simple bending test. No continuous emission was observed at the maximum loading during a short hold period. Although frictional "stick-slip" acoustic events were possible at this position, the observed acoustic events were probably caused by benign adjustments normally encountered for a virgin structure. No high-amplitude acoustic events occurred during the torsion test.

In summary, the June 1983 static tests and subsequent data analysis lead to the following conclusions:

a) The RP-2 air frame structure withstood both the simple bending and the torsion tests without failure and without any visible evidence of damage.

b) In the simple bending test, at 850 pounds per wing loading (approx. 6 g's), the deflection of the wings was very close to that calculated using the loading pattern, the dimensions of the cap strips and a linear modulus of 14×10^6 psi for the carbon fiber cap strips. The magnitude of deflection also agreed closely with those observed in the bending test of October 22, 1981.

c) The calculated strain in the cap strips at the root was .31% as compared to that observed on the strain gauges of .325% at the maximum loading.

d) Upon unloading the wing tips returned to within 1 cm of their initial (virgin) position. This amount of "set" is reasonable after the first major loading cycle of a composite structure.

e) The observed twisting response of the wings in the torsion test was very close to that calculated using the stiffness constant derived from torque tests made in September 1981 on a special 80 cm long test section of the constant chord (95 cm) section of the wing. The starboard wing showed more twist than the port wing. Both wings had about $\frac{1}{2}^{\circ}$ angular "set" after the test.

f) The new carbon fiber tube compression strut between the forward wing pins showed no signs of over stress. However, the rear wing pins pulled out of their bushings nearly 3/16" at the maximum loading in the bending test. This, together with the known strength and rigidity of the carbon compression strut at the forward pins, suggests that the forward inboard wing skin is yielding considerably under the forward bending moment on the wings.

g) The cause of the acoustic event and audible snap, that occurred at 700 lb/wing loading has not been identified. The most probable cause was a partial break of bonding between the tension cap strip and the U-plates added to the

female "carry-through" structure on the port wing. At this point there is an abrupt change of section, which could have caused high local stresses in the bonded joint; it may have been an "accommodation adjustment". At this point, there was a step in the deflection at the starboard wing tip, but it was in the wrong direction to be due to yielding.

h) During the torsion test, the strain gauge on the male spar cap read an unbelievably high value of 0.6 to 0.7%. There were no acoustic events of significance or evidence of overstressed parts. Upon unloading, the gauge returned to a zero reading, and test loads of 30 pounds on the wing tips yielded reasonable readings around .03%. This strange behavior of the strain gauge and the structure is not explained.

3. Plans for Upcoming Period

To remedy the problems seen as associated with the forward bending of the wings, it seems likely that a tension "carry-through" linkage should be installed near the rear wing pins. This arrangement would have a much larger lever arm with respect to the front wing pins than the wing spar "carry-through" structure, and this could much more effectively restrain the forward bending deflections of the wings. Such a structure will be considered and, if practical, designed, fabricated and installed in the RP-2.

After installation, the full, 6-g bending test will be repeated to determine whether the 700 pound/wing snap

phenomenon reoccurs, and whether the wing structure takes on any more "set". The degree to which the "gapping" at the rear root pins occurs will also be assessed. With the successful completion of such a test, the wing/fuselage structure will be considered airworthy.

4. Current Publications or Presentations by Professor Scarton on this Subject

"Acoustic Emission Proof Testing of Composite Sail-Planes", with G. Bobal.

Presented at the 1st International Symposium on Acoustic Emission from Reinforced Plastics, CARP, San Francisco, CA, July 19-21, 1983.

PART VI
TECHNICAL INTERCHANGE

Technical meetings, on- and off-campus, provide important opportunities for interchange of technical information. Because of the large number of composites meetings, a central catalog with upcoming meetings is being maintained and distributed periodically. In this way we help to assure that a Rensselaer faculty/staff member can participate in important meetings. The calendar for this reporting period is shown in Table VI-1. Meetings attended by RPI composites program faculty/staff/students during the reporting period are shown in Table VI-2. Some meetings particularly relevant to composites, held on-campus with special speakers, are listed in Table VI-3. A list of composite-related visits to relevant organizations by RPI faculty/staff/students, with the purpose of each visit outlined, is presented in Table VI-4.

A continuing education special course, an outgrowth of the composite materials and structures program, was presented for graduate engineers in industry and government, for the fourth time: "Advanced Composite Materials and Structures" during the week of July 11-15. The course lasted one week, and the level of the material was again planned to be particularly useful to managers of engineering structures activities who are involved in technical work, but who may not have taken courses for several years. Because of the wide variety of special courses available throughout the United States dealing with this subject matter, only rather

TABLE VI-1

CALENDAR OF COMPOSITES-RELATED MEETINGS

(April 30, 1983 through September 30, 1983)

5/2-4	24th Structures, Structural Dynamics and Materials Conference, Lake Tahoe, NV. Sponsored by AISS/ ASME/ASCE/AHS.
5/8-11	39th Annual Forum and Technical Display, St. Louis, MO. Sponsored by AHS.
5/10-12	Annual Meeting and Technical Display, Long Beach, CA. Sponsored by AIAA.
5/10-12	Conference on Physics of Composite Interfaces, Pasedena, CA. Sponsored by California Institute of Technology.
5/17-19	5th Metal Matrix Composites Materials Conference, Silver Springs, MD. Sponsored by DOD/MMCIAM.
5/19	Spring National Convention, Philadelphia, PA. Sponsored by ASCE.
5/24	4th Engineering Mechanics Division Special Conference, Purdue University, Lafayette, IN. Sponsored by ASCE.
5/24-25	Workshop on Toughening of Composites, Langley Research Center. Sponsored by NASA.
6/1-3	Thermophysics Conference, Montreal, Canada. Sponsored by AIAA.
6/6-8	2nd U.S./Japan Composites Materials Conference, NASA/Langley, VA. Sponsored by NASA and ASTM Coms. E-9 and D-30.
6/6-8	Symposium on Dynamics and Control of Large Structures, Blacksburg, VA. Sponsored by VPI and SU/AIAA.
6/6-11	6th International Symposium on Air Breathing Engines, Paris, France. Sponsored by AIAA.
6/13-15	Conference on Macromolecules, Cleveland, OH. Sponsored by Case Western Reserve University.
6/14-16	Materials and Structures Technical Conference, White Oak, MD. Sponsored by DOD.

TABLE VI-1 continued

6/22	91st Annual Conference, Rochester Institute of Technology, Rochester, NY. Sponsored by ASEE.
6/27-29	19th Joint Propulsion Conference, Seattle, WA. Sponsored by AIAA/SAE/ASME.
6/27-7/1	International Symposium on Plasticity Today, Udine, Italy.
7/12-13	Symposium on Environmental Effects in Fiber Reinforced Plastics, Imperial College, London, England. Sponsored by Aero Department, Imperial College and Royal Aircraft Establishment.
7/18-21	1st International Symposium on Acoustic Emission from Reinforced Composites, San Francisco, CA. Sponsored by Society of Plastics Industry.
7/18-22	16th Biennial Conference on Carbon, San Diego, CA. Sponsored by the American Carbon Society.
7/25-27	Lighter-Than-Air Systems Conference, Anaheim, CA. AIAA.
8/22-26	Gordon Conference on Thermosets, New Hampton, NH.
8/23-26	International Conference on Structural Mechanics in Reactor Technology, Chicago, IL.
9/7	Forum of Flexible Spacecraft Dynamics, Massachusetts Institute of Technology, Cambridge, MA. Sponsored by AFOSR.
9/14-15	Testing, Evaluation and Quality Control of Composites, Surrey, England. Sponsored by Surrey University.
9/26	Symposium on Solid Modeling by Computers, Detroit, MI. Sponsored by General Motors Research Labs.

TABLE VI-2

COMPOSITES-RELATED TECHNICAL MEETINGS ATTENDED OFF-CAMPUS

(April 30, 1982 through September 30, 1983)

5/2-4 24th Structures, Dynamics and Materials Conference (Prof. Loewy), Lake Tahoe, NV.

Professor Loewy presented the paper: "Effect of Shaft Flexibility on the Structural Dynamics of Bladed Drive Assemblies".

5/10-12 Conference on the Physics of Composite Interfaces (Prof. Diefendorf), California Institute of Technology, Pasedena, CA.

Professor Diefendorf presented the paper: "The Physical Chemistry of Fiber/Matrix Interactions in Composite Materials".

5/19 ASCE Spring National Convention (Prof. Shephard), Philadelphia, PA.

Professor Shephard Chaired a Session: "Computer Graphics Application and Design".

5/24 4th Engineering Mechanics Division Special Conference (Prof. Shephard), Purdue University, Layfayette, IN.

Professor Shephard presented the paper: "Computer Graphics in the Development of an Automatic Three-Dimensional Mesh Generator"

6/6-9 ASTM/NASA 2nd US/Japan Conference on Composite Materials (Prof. Diefendorf), Langley Research Center.

6/13-15 Cleveland Conference on Macromolecules (Prof. Sternstein), Case Western Reserve University, Cleveland, OH.

Professor Sternstein presented the paper: "Mechanical Characterization of Neat Resins and Composites".

6/22 ASEE 91st Annual Conference (Prof. Shephard), Rochester Institute of Technology, Rochester, NY.

Professor Shephard presented the paper: "RPI's Industrial Associates Program in Computer Graphics and CAD/CAM".

TABLE VI-2 continued

6/27-7/1 International Symposium on Plasticity Today (Prof. Krempl), Udine, Italy.

Professor Krempl presented the Topical Paper: "Inelastic Work and Thermo Mechanical Coupling in Viscoplasticity".

7/18-22 American Carbon Society 16th Biennial Conference on Carbon (Prof. Diefendorf), San Diego, CA.

Professor Diefendorf made 13 presentations related to pitch precursor carbon fibers and carbon fiber composites, plus a Plenary Lecture, "The Physical Chemistry of Pitch Mesophase Formation".

8/18-21 1st International Symposium on Acoustic Emission from Reinforced Composites (Prof. Scarton), San Francisco, CA.

Professor Scarton presented the paper: "Acoustic Emission Proof Testing of Composite Sail-Planes", with G. Bobal.

8/22-26 Gordon Conference on Thermosets (Prof. Sternstein), New Hampton, NH.

Professor Sternstein gave a Lecture: "Inhomogeneous Swelling Theory and Applications".

8/23-26 International Conference on Structural Mechanics in Reactor Technology (Prof. Krempl), Chicago, IL.

Professor Krempl was a Session Chairman.

9/7 AFOSR Forum of Flexible Spacecraft Dynamics (Prof. Loewy), Massachusetts Institute of Technology, Cambridge, MA.

9/26 General Motors Research Labs. Symposium on Solid Modeling by Composites (Prof. Shephard), Detroit, MI.

Professor Shephard presented the paper: "Finite Element Mesh Generation for Use with Solid Modeling and Adaptive Analysis", with M. A. Yerry.

TABLE VI-3

COMPOSITES-RELATED MEETINGS/TALKS HELD AT RPI

(April 30, 1983 through September 30, 1983)

Topic	Date	Speaker(s)
Steering Committee Meeting "Toughness and Damage Tolerance of Composites", Sponsor: NASA/Langley	7/26-28	Host: Prof. S. Sternstein, RPI
Directions Currently being Taken by the CICG Finite Element Group (Albany-Hilton)	8/18	Workshop Coordinator: Prof. M. Shephard, RPI
Tomographic Evaluation of Internal Damage in Plastically Deformed Solids	9/1	Dr. A. Sawczuk Polish Academy of Sciences, Warsaw, Poland and University of Aix-Marseille III, France
The Constitutive Law in Thermoplasticity - Theoretical Considerations and Experimental Results	9/20	Prof. Dr. Ing. Th. Lehmann Ruhr-Univerität Boehum, West Germany
Mechanics of Brittle, Plastic Materials	9/22	Prof. Zenon Mróz Polish Academy of Sciences, Warsaw, Poland

TABLE VI-4

COMPOSITES-RELATED VISITS TO RELEVANT ORGANIZATIONS

by RPI Faculty/Staff/Students

(April 30, 1983 through September 30, 1983)

Visited	Date	By	Purpose
Owens-Corning Research, OH	7/7	Prof. S. S. Sternstein	Presented a lecture, "Mechanical Properties of Composites"
Boeing Vertol Company Essington, PA	7/29	Prof. R. G. Loewy	Progress report on a contract to study tension-compression fatigue in Gr/E, G/E and K/E tubes and tapered members
W. R. Grace Co. Columbia, MD	9/2	Prof. R. J. Diefendorf	Presented a lecture, "Ceramic Matrix Composites"
McDonnell-Douglas Company St. Louis, MO	9/15	Prof. R. J. Diefendorf	Presented a lecture, "The Effects of the Physical Chemistry of Fiber/Matrix Interfaces or the Toughness of Composites"

unique aspects justify additional offerings in these areas. Our programs were planned from the outset to be unusual in the respect that "hands-on" experiences were inherent and required for completion of each course. These aspects have continued to develop and such development was evident in our fourth-year offering. Use of personal computers, application of optimization programs using computer graphics, lay-up and cure of a simple part in graphite epoxy and testing tensile, shear and compressions coupons to failure were all part of the course.

It was gratifying to note that government research laboratories; the Army, Navy and Air Force; both large and small industrial firms and other universities were represented among those who took the course, and that their post-course questionnaires were, once again, overwhelmingly favorable.

Faculty-staff and attendees for the courses were as follows:

Composite Materials and Structures

July 11-15, 1983

Program Director:

R. G. Loewy
Institute Professor
Rensselaer Polytechnic Institute

Faculty:

R. Judd Diefendorf
Professor, Materials Eng.
Rensselaer Polytechnic Inst.

H. Gunther Helwig
Design Specialist
Composites Group
Dornier System Gmb H

S. Leigh Phoenix
Associate Professor
Mechanical and Aeronautical
Engineering
Cornell University

Stephen W. Tsai
Chief, Mechanics and Surface Interactions Branch
Air Force Materials Lab.
Wright-Patterson AFB

Dick H. Wilkins
Sr. Eng. Specialist
General Dynamics
Fort Worth

Students:

Les Bevans
Design Engineer
Sundstrand Corp.
4747 Harrison Avenue
Rockland, IL 61125

Michael Carroll
Sr. Engineer
Harris Corp.
Div. GASD
P. O. Box 37
Milbourne, FL 32901

Michael P. Clark
Mechanical Engineer
GTE Products Corp.
520 Winter Street
Waltham, MA 02254

Major Mark H. Davis
Assistant Professor
Dept. of Mechanics
W. S. Military Academy
West Point, NY 10996

John Emmel
Engineer II
Northrop Corp.
8900 E. Washington Blvd.
Pico Rivera, CA 90660

Captain Joseph W. Hager
Assistant Professor
U. S. Air Force Academy/DFEM
Dept. of Eng. Mechanics
Colorado Springs, CO 80840

James E. Kozicki
Member Eng. Staff
RCA Amer. Com., Inc.
400 College Road East
Princeton, NJ 08540

Luis J. Lozano
Quality Assurance Manager
Anaconda Metal Hose
698 South Main Street
Waterbury, CT 06706

Thomas J. Mallets
Project Manager
AF Logistics Command
Process Eng. & Tech. Div.
AFLC/MAXT
Wright-Patterson AFB
OH 45433

William B. Matkin
Mechanical Engineer
DRSMI-RLC
Commander, U. S. Army
Missile Command
ATTN: DRSMI-RLC, W. B.
Matkin, Redstone Arsenal
AL 35898

John T. McVickar
Principal Engineer
Measurement Analysis Corp.
23852 Madison Street
Torrance, CA 90505

Glenn O'Hara
Mechanical Engineer
U. S. Army Watervliet
Arsenal
ATTN: SARWV-PTT
Watervliet, NY 12189

S. Philip Oyoung
Analytical Engineer
Sundstrand Corp.
4747 Harrison Avenue
Rockford, IL 61125

Joseph Perez
Director, Tech. Services
SICMA America Inc
6926 NW 46th Street
Miami, FL 33166

George Pflegl
Mechanical Engineer
U. S. Army Watervliet
Arsenal
ATTN: SARWV-PTT
Watervliet, NY 12189

Richard Polanic
Development Engineer
Goodyear Aerospace
ATTN: 392-WFL
1210 Massillon Road
Akron, OH 44315

Craig Rix
Research Analyst
Lockheed
P. O. Box 551
Burbank, CA 91520

Mohammed A. Sattar
Sr. Analytical Engineer
Pratt & Whitney Aircraft
400 Main Street
M. S. 165-13
East Hartford, CT 06108

Peter M. Switchenko
Engineer
General Electric Company
Aircraft Engine Bus. Group
MO 14508 1000 Western Av.
Lynn, MA 01910

Thomas Talboys, PE
President
Talboys Engineering Corp.
1 Palisade Avenue
Emerson, NJ 07630

Terry L. Vandiver
Mechanical Engineer
DRSMI-RLC
Commander, U. S. Army
Missle Command
ATTN: DRSMI-RLC, W. B.
Matkin, Redstone Arsenal
AL 35898

For the last several years, as the diversity of the research conducted within this program has increased, once-a-week luncheon programs have been held to insure information transfer among the faculty and graduate students involved (listed in Part VII - Personnel of this report). These meetings are held continuously when classes are in session and are known as "Brown Bag Lunches" (BBL's), since attendees bring their own. Each BBL is an opportunity for graduate students and faculty to present briefly plans for, problems encountered in and recent results from their indi-

individual projects. These sessions also are occasions for brief administrative reports, usually on the part of one of the Co-Principal Investigators, and for brief reports on what transpired at off-campus meetings attended by one of the participants (as listed in Tables VI-2 and VI-4 of this report). Visitors from off campus, who are at RPI during a BBL day are often invited to "sit in". A calendar of internal, oral progress reports as they were given during the last reporting period at BBL's is listed in Table VI-5.

TABLE VI-5

COMPOSITE MATERIALS AND STRUCTURES PROGRAM

BROWN BAG LUNCH (BBL) SCHEDULE

(April 30, 1983 through September 30, 1983)

Date	Topic	Responsible Faculty
4/15	Administrative Report	J. Diefendorf
	Generic Structural Components	D. Goetschel
	Free Edge Failures of Laminates	S. Sham
4/22	Report on AGARD Meeting	R. Loewy
	Resin-Fiber Interface Research	J. Diefendorf
4/29	Administrative Report	R. Loewy
	Composites Fatigue Research	E. Krempl
	Computer Aided Design and Analysis	M. Shephard
5/6	Report on 24th SDM Conference	R. Loewy
	Matrix Characterization and Environmental Effects	S. Sternstein
9/16	Administrative Report	R. Loewy
	Report on Vertol Research	R. Loewy
9/23	Administrative Report	J. Diefendorf
	Generic Structural Components	D. Goetschel
	Computer Aided Design and Analysis	M. Shephard
9/30	Administrative Report	R. Loewy
	Fabrication Technology Experiments	F. Bundy H. Hagerup V. Paederlt
	Static Test Review	H. Scarton

PART VII

PERSONNEL

AUTHOR INDEX

PERSONNEL

Co-Principal Investigators

Ansell, George S., Ph.D.	Dean, School of Engineering
Loewy, Robert G., Ph.D.	Institute Professor
Wiberley, Stephen E., Ph.D.	Professor of Chemistry

Senior Investigators

Brunelle, E. J., Jr., Sc.D. (Aeroelastic and structural design and analysis, applied mechanics of composite structures)*	Associate Professor of Aeronautical Engineering
Bundy, F. P., Ph.D. (Physical chemistry and structures testing)*	Research Professor of Materials Engineering
Diefendorf[i], R. J., Ph.D. (Fabrication, resin matrix, fiber behavior, interfaces)*	Professor of Materials Engineering
Feeser[i], L. J., Ph.D. (Computer applications and graphics, computer-aided design, optimization)*	Professor of Civil Engineering
Goetschel, D. B., Ph.D. (Structural analysis design and testing)*	Assistant Professor of Mechanical Engineering
Hagerup, H. J., Ph.D. (Aerodynamics, configuration, pilot accomodation, flight testing)*	Associate Professor of Aeronautical Engineering
Krempl, E., Dr.Ing. (Fatigue studies, failure criteria)*	Professor of Mechanics and Director of Cyclic Strain Laboratory
Scarton, H., Ph.D. (Acoustic emission NDE)*	Associate Professor of Mechanical Engineering and Mechanics

---

*Fields of Speciality

[i]Member of Budget Committee together with Co-Principal Investigators

Senior Investigators

Sham, T-L., Ph.D. (Fracture mechanics, composites)*	Assistant Professor of Mechanical Engineering
Shephard, M. S., Ph.D. (Computer graphics, finite element methods)*	Associate Director, Center for Interactive Computer Graphics and Assistant Professor of Civil Engineering
Sternstein[i], S. S., Ph.D. (Failure analysis, matrix behavior, moisture effects)*	William Weightman Walker Professor of Polymer Engineering
Wunderlich, B., Ph.D. (Processing science, constituent material characteristics)*	Professor of Chemistry

Research Staff

Manager & Master Technician, Composites Laboratory

Paedelt, Volker

Visiting Scholar

Brouer, R., B.S., Free University of Brussels

Graduate Assistants

Anderson, Stephen, B.S.	Judovits, Lawrence, B.S.
Baxter, Scott, B.S.	Liu, Shiann-hsing, M.S.
Bertolazzi, Andrew, B.S.	Sing, Sachchica, B.Tech.
Burd, Gary, B.S.	Srinivasan, Krishna, B.S.
Cackett, Matthew, B.S.	Uzoh, Cyprian, B.S.
Chen, Kuong-jung, B.S.	Yang, I-Horng, M.S.
DeMint, Thomas, B.S.	Yang, Philip, M.S.
Father, Philip, B.S.	Yehia, Nabil, M.S.
Helmer, James, B.S.	Yurgartis, Steven, M.S.
Hu, Tsay-hsin, M.S.	

*Fields of Speciality

[i]Member of Budget Committee together with Co-Principal Investigators

Undergraduate Assistants - Seniors

Blasioli, Lou Ann
Casabella, Susan
Halicki, Paul
Keavney, Thomas
Lopez, Matthew
Martin, Randall
McCaffrey, Micheal
Robertson, Scott
Simmons, Michael
Symmes, Jeffrey
Tomlin, Rogers
Younes, Mona

Undergraduate Assistants - Juniors

Bacich, Linda
De La Fuente, Horacio
Jun, Wan Ki
Karkow, Jon
Marquis, Carl
Pickett, David
Safran, Paul
Sawyer, Christina

Undergraduate Assistants - Sophomores

Barnett, John

AUTHOR INDEX

	Page(s)
Brunelle, E. J., Jr.	85
Bundy, F. P.	149 154
Diefendorf, R. J.	9 149 154
Goetschel, D. B.	93 119
Hagerup, H. J.	149 154
Krempl, E.	33
Scarton, H. A.	149 154
Sham, T. L.	79
Shephard, M. S.	61
Sternstein, S. S.	35 51
Wunderlich, B.	141